THESIS

REDOX-SENSITIVE TRACE ELEMENTS DOCUMENT CHEMICAL DEPOSITIONAL ENVIRONMENT AND POST-DEPOSITIONAL OXIDATION OF THE EDIACARAN BIRI FORMATION, SOUTHERN NORWAY

Submitted by

Nathan J Marolf

Department of Geosciences

In partial fulfillment of the requirements

For the Degree of Master of Science

Colorado State University

Fort Collins, Colorado

Summer 2014

Master's Committee:

Advisor: Judith Hannah

Holly Stein
Greg Butters

ABSTRACT

REDOX-SENSITIVE TRACE ELEMENTS DOCUMENT CHEMICAL DEPOSITIONAL ENVIRONMENT AND POST-DEPOSITIONAL OXIDATION OF THE EDIACARAN BIRI FORMATION, SOUTHERN NORWAY

The Ediacaran Biri Formation comprises carbonate and silisiclastic facies including a ~ 70 m thick organic-rich shale facies exposed 9 km west of Biri, Norway in a steep bedrock stream channel at Djupdalsbekken. This outcrop is overlain by ~ 30 m of coarse-clasitic conglomeritic facies of the Ring Formation, deposited in the southern and western portion of the Hedmark basin as prograding subaerial and submarine delta fans. Concentrations and distributions of some redox-sensitive trace elements, specifically molybdenum and uranium, within the Biri Formation shale indicate deposition under sub-oxic to anoxic conditions. Pyrite framboid size distribution corroborates trace element evidence and suggests that sulfidic conditions existed within the sediment with a chemocline at or near the sediment-water interface.

An attempt to date the Biri Formation shale by Hannah et al. (2007) found disturbed Re-Os isotope systematics from samples in the first 8 meters of the exposure, while data obtained from samples further down section were undisturbed. Here, an attempt to understand these disturbed and undisturbed sections using redox-sensitive trace element chemistry suggests the disturbed data was a result of post-depositional re-oxygenation within the upper few meters of the Biri shale. This is indicated by concentration peaks in trace element profiles that result from remobilization and subsequent re-fixation of these elements at different locations in the shale. A well constrained hypothesis constructed using uranium and molybdenum as proxies for rhenium shows that rhenium was likely remobilized after deposition of the Biri Formation and either subsequently re-deposited, or flushed out of the system. In

this scenario, the post-depositional remobilization of rhenium (and most likely osmium also) resulted in disturbed Re-Os isotope systematics described by Hannah et al. (2007).

Trace element geochemistry, petrographic, and $\delta^{13}C$ and $\delta^{18}O$ stable isotope evidence document post-depositional re-oxygenation of the Biri Formation shale. Re-oxygenation occurred either synchronous to deposition of the overlying Ring Formation or during a later event, the Caledonian orogeny ($\sim$ 440 Ma) being the most likely candidate. While the geochemical evidence does not preclude one time period or the other, disturbed Re-Os isotope systematics and resulting dates given by Hannah et al. (2007) can only be supported by re-oxygenation of the Biri Formation shale during the Caledonian orogeny.

ACKNOWLEDGEMENTS

I would foremost like to thank my advisor, Judy Hannah, for her unending support during this project, and for the continued learning opportunities she provided me during my graduate work. Her sincere, thoughtful and patient guidance through countless discussions, in the office and in the field, made a lasting impact on me and will not be forgotten. Thanks go to Holly Stein for her encouragement during this project and model of enthusiasm for the geosciences. Thanks also go to Greg Butters for his willingness to serve on my committee and for providing useful insight and feedback. I would like to thank the AIRIE staff, including Aaron Zimmerman, Svetoslav Georgiev and Gang Yang for their thoughtful conversation and willingness to teach me during this project. I would also like to thank the Geoscience faculty at CSU, specifically Jerry Magloughlin and Sally Sutton for their desire to teach, and for the many informative and thoughtful discussions I had with them, in and out of the classroom. Thanks also go to my fellow graduate student office mates who continually made my time at CSU enjoyable.

Finally, I would like to thank my father and mother for getting me out on the rocks so early and often in my life, and for my father's model of a man who loves God and His creation and gave me so many opportunities to enjoy it all. And last, but most of all, I want to thank my wife for her continued love and encouragement during my graduate work, and for her amazing strength to be a wonderful wife, mother and professional all at the same time. I could not have done this without her support.

TABLE OF CONTENTS

LIST OF FIGURES

LIST OF TABLES

CHAPTER 1: INTRODUCTION

The systems governing major and trace element chemistry in sedimentary environments are notably complex and vary from one depositional setting to the next. During sedimentation, conditions that control chemical behavior may continue to change as the environment within the water column, sediment and at the sediment-water interface evolve. Trace element depletion or enrichment may be achieved in the sediment depending on factors including redox potential and sedimentation rate. If conditions remain unchanged, trace element enrichment can serve as a tool to understand the paleoenvironmental and paleoredox conditions at the time of sedimentation and early diagenesis. However, post-depositional processes can modify the concentration, distribution and speciation of trace elements in such a way that they do not reflect the original depositional setting (Schultz, 1989; Leventhal, 1998; Tuttle et al., 2003). Trace elements sensitive to the redox conditions at the time of deposition are particularly prone to modification via post-depositional processes. Trace elements occur in various phases within the sediment: adsorbed onto mineral or organic surfaces, as organometallic complexes or in solid solution in pyrite, phosphate and sulfate, metal sulfides, or as insoluble oxides and oxyhydroxides (Tribovillard et al., 2006). Their post-depositional behavior is thus dependent on the pH and Eh conditions within the sediment environment. Trace elements that are immobile under reducing conditions may be mobilized upon re-oxidation and subsequently re-deposited or flushed out of the sediment entirely. As a result, their usefulness as paleoredox indicators and assumed inferences to paleoenvironmental conditions may be limited and ultimately problematic (Vine and Tourtelot, 1970, Crusius et al., 1996; Tribovillard et al., 2006).

Recognition of these post-depositional changes is implicitly important for Re-Os isotopic studies. Acquiring Re-Os data sets is costly and labor intensive and recognizing processes that disturb the Re-Os chronometer is critical to its use (e.g. Georgiev et al., 2012). Understanding systematic variations in the

distribution of redox-sensitive elements provides the opportunity to properly interpret conditions at the time of deposition. Correlation of those variations with disturbed and undisturbed Re-Os isotope systematics likewise affords the opportunity to define geochemical parameters that may limit the usefulness of Re-Os geochronology.

The Biri Formation consists of organic-rich shale and carbonate facies deposited in an intracratonic rift basin along the northwestern margin of the Baltoscandian craton. It varies in lithology and thickness throughout its exposures in the Osen-Røa nappe complex within the Caledonides of southern Norway. Nine km west of Biri, Norway, at the Djupdalsbekken locality, $\sim$ 70 m of carbonate-rich and organic-rich black shale is exposed along a steep bedrock stream channel. Here, a detailed petrographic and trace-element chemistry study is done to understand the chemical depositional environment and post-depositional redox conditions in the Biri shale. An attempt is made to correlate the post-depositional mobility of redox-sensitive elements with disturbed and undisturbed Re-Os isotope systematics of the section.

CHAPTER 2: GEOLOGIC SETTING

Deposition of the Biri Formation occurred during the Neoproterozoic Ediacaran Period (635-541 Ma; Gradstein et al., 2012), indicated by the presence of acritarchs (Vidal and Nystuen, 1990). The Ediacaran is characterized by significant marine geochemical changes including negative C-isotope excursions, rising $^{87}Sr/^{86}Sr$ values, and an increase in deep-marine oxygenation (Narbone et al., 2012). Abundant and diverse microfossils throughout the Ediacaran and a unique assemblage of marine soft-bodied animals near its end (579 Ma) are hallmarks of the period. Glacial tillite attributed to the middle Ediacaran Gaskiers Glaciation (584-582 Ma) (Bowring et al., 2002; Hoffman and LI, 2009) marks the last known record of the Neoproterozoic glacial events.

During the late Proterozoic (middle Cryogenian: 800-635 Ma), crustal extension along the north-western side of Baltoscandia (Figure 1) resulted in numerous intracratonic rift basins of the Mesoproterozoic granitic basement (Figure 2) (Nystuen, 1982). Infilling of these western rift basins occurred through the Ediacaran period and is thought to be coeval with the opening of the Iapetus (proto-Atlantic) ocean, commencing with the break-up of Rodinia (Nystuen, 1982; Nystuen et. al., 2008). These basins filled with both marine and terrigenous sediments, and were likely connected to the open ocean during the majority, if not all, of their infill history (Bjørlykke et al., 1976; Nystuen, 2008).

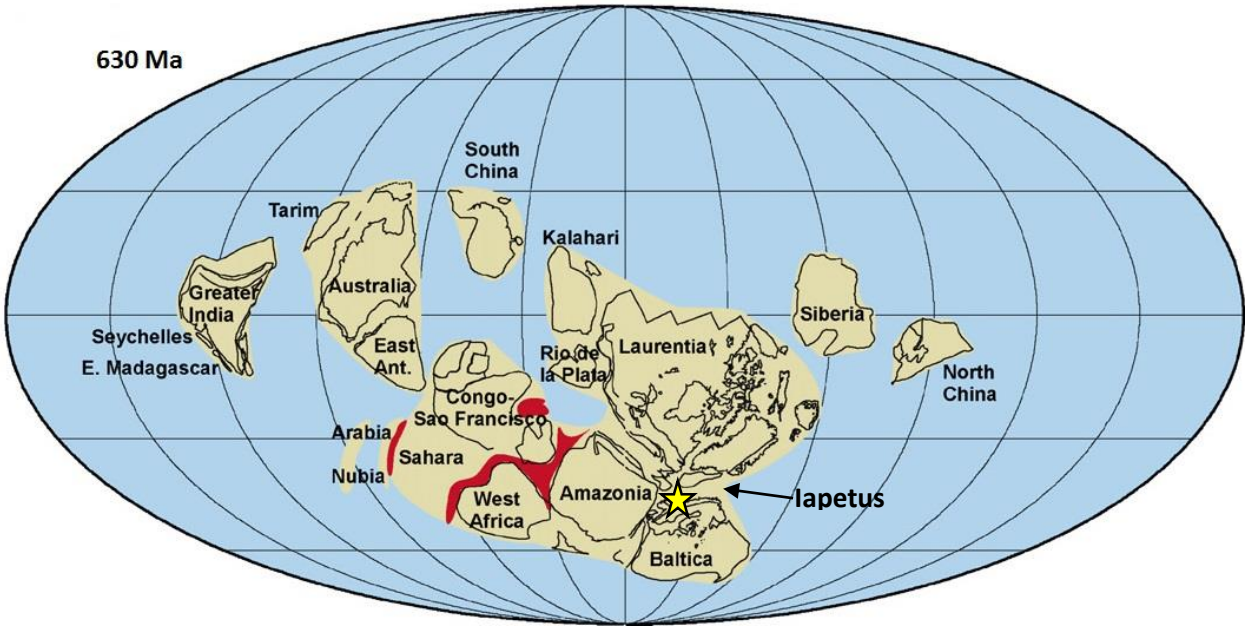

Figure 1. *Approximate location of Baltica, Laurentia, and the Iapetus (proto-Atlantic) seaway at 630 Ma. From Li et al. (2008). Location of the Hedmark Basin indicated by the yellow star.*

Tectonic events during the Paleozoic reversed the previous rifting and initiated the closure of the Iapetus seaway. The resulting collision of Baltica and Laurentia is referred to as the Caledonian orogeny. This mountain building event was accompanied by large-scale thrust faulting which formed the allocthonous terranes found in western Scandinavia (Figure 3) (Roberts, 2003). Around 440 Ma, the Hedmark group sedimentary rocks were thrust an estimated 135 - 150 km southeast as part of the Osen-Røa Nappe Complex within the lower-most allocthon (Nystuen, 1987). Estimated thrust distances using the balanced cross-section method and hanging wall and footwall cut-offs give similar distances, while restoration of a hanging wall ramp by Kumpulainen & Nystuen (1985) indicates 230 km of displacement for the southern margin of the Hedmark basin. Extensive mapping of the region in southern Norway reveals a series of broad synclines and anticlines as well as localized minor folds and imbrications within the thrust (Sæther and Nystuen, 1981).

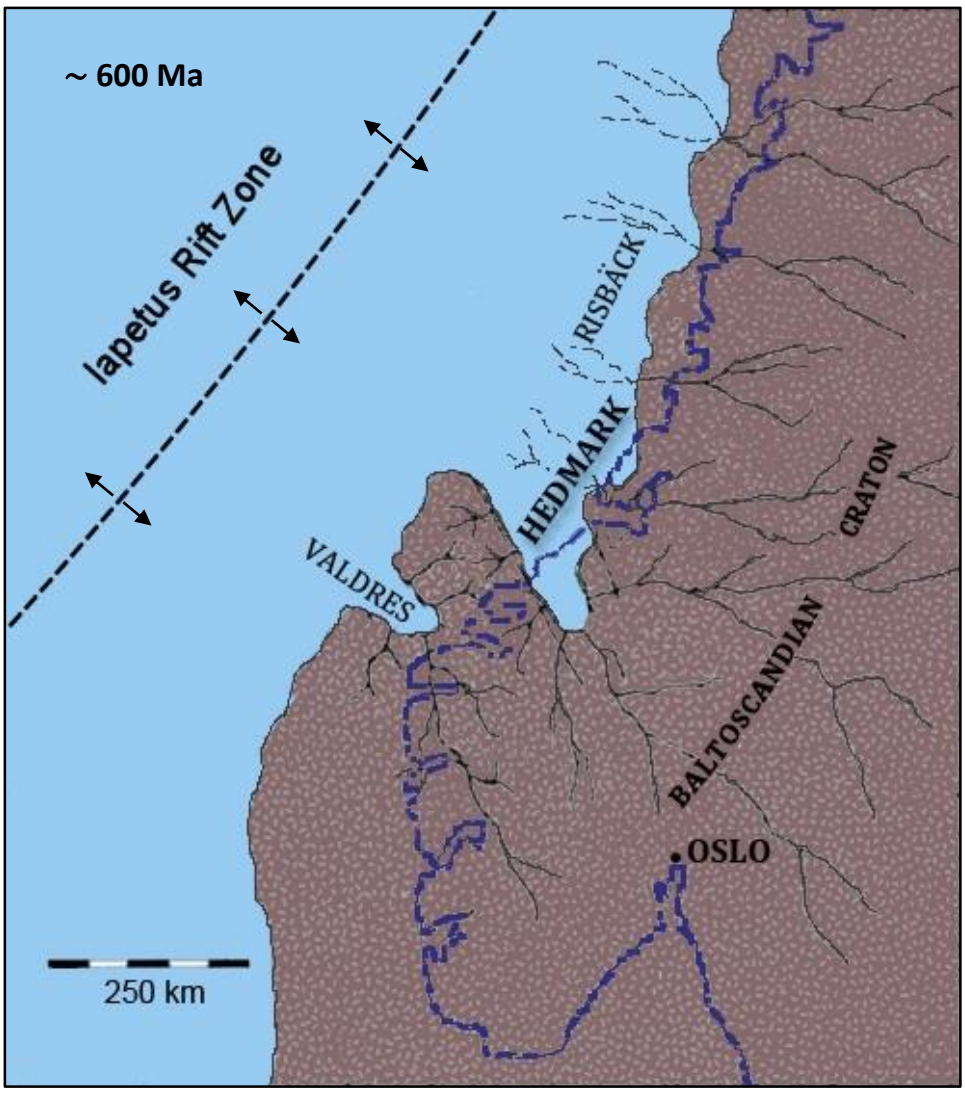

Figure 2. *An illustration showing the relative location of intracratonic rift basins along the northwestern margin of Baltica during the opening of the Iapetus seaway. Outline of present-day Norway in blue, location of Oslo shown. After Nystuen (1982).*

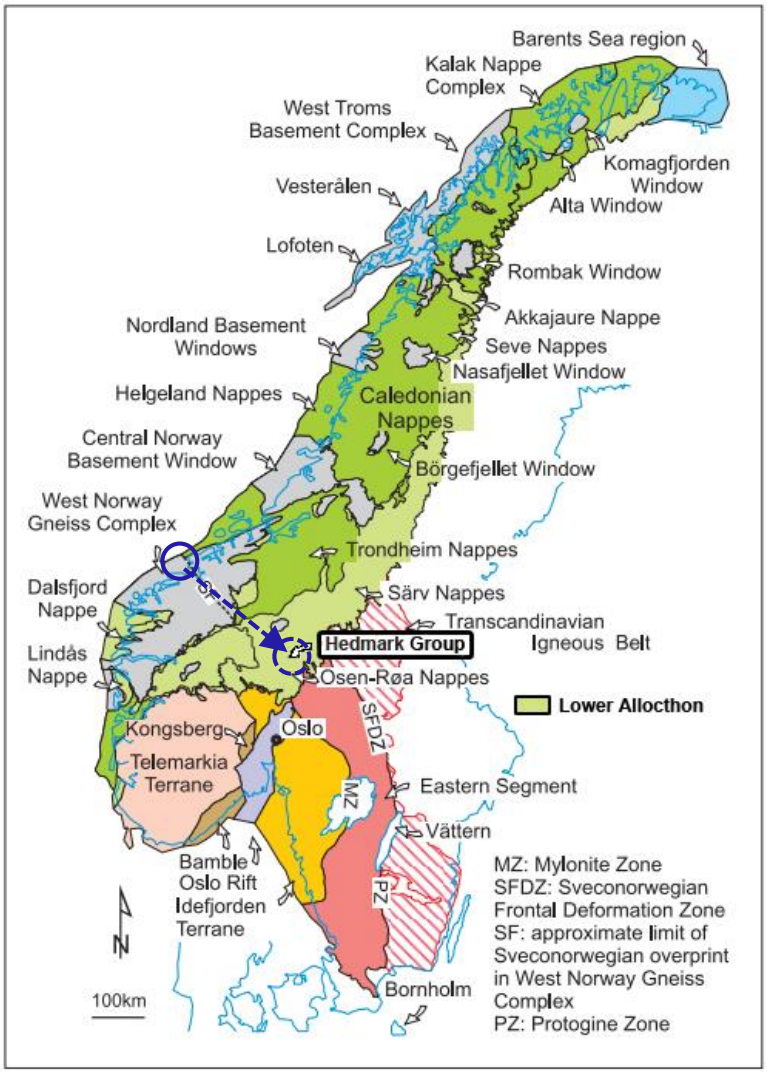

Figure 3. *Map showing the allocthonous terranes that form the Scandinavian Caledonide region. Approximate Location of Hedmark Group rocks within the lower allocthon and illustration of the estimated thrust distance during the Caledonian orogeny. After Bingen and Solli (2009).*

2.1 STRATIGRAPHY OF THE HEDMARK GROUP SEDIMENTS

The Precambrian Hedmark group sequence consists of at least 6 km of sediment that accumulated in the Hedmark basin. The presence of acritarchs indicate deposition of marine shales during late Cryogenian to early Ediacaran time (Bjørlykke et al., 1976; Nystuen, 2008). Inferences from palinspastic restoration and facies trends show that the Hedmark rift basin was 2-300 km wide with an equivalent length, and the main axis of the basin trended in the NNW-SSE direction. Various

depositional environments yielded varying types and amounts of sediment with considerable lateral variation. Much of the variation was due to the syndepositional Imsdalen Fault which forms a structural boundary between the eastern and western part of the Hedmark Basin. The Imsdalen Fault shows significant normal and strike-slip components, along with reactivation during the Caledonian orogeny (Nystuen, 2008). The lateral variation occurs exclusively below the Moelv Tillite and is illustrated by the distribution of lithofacies within the Brottum Formation in the west and the Rendalen Formation in the east (Figure 4).

The more than 4000 m Brøttum Formation forms the basinal sequence of the Hedmark group in the west and consists of deep-marine sandstone turbidites, black shales and conglomerate beds (Nystuen, 1982). In the east, at more than 2500 m, the Rendalen Formation dominates, consisting of alluvial conglomerates and fluvial sandstone members. In the north, the shallow-marine Atna Quartzite is also laterally equivalent to the Brøttum Formation.

Both the Brøttum and Rendalen formations are succeeded by the limestones and shales of the Biri formation which represent a transgressive sea-level rise known as the Biri transgression. The early Biri transgression was interrupted by basin emergence and erosion developed as the conglomeritic facies of the Biskopåsen Formation in the west and the Osdalen Conglomerate in the east, each containing clasts of both Biri Formation shales and Atna Quartzite. Both also contain clasts of tholeittic basalt representing a phase of basalt volcanism that occurred at the end of the Brottum and Rendalen deposition and is preserved in the Svarttjørnkampen Basalt in the northern part of the basin. The following marine transgression deposited Biri Formation shales and carbonate facies (Sæther and Nystuen, 1981; Nystuen, 1987). The fine-grained sandstones and coarse arkoses of the Ring Formation overlie the Biri Formation and occur as localized, prograding marine fan deltas around the basin margin (Bjørlykke et al., 1976; Nystuen, 1987). Overlying the Ring Formation in the south and the Biri in the north are the glacial Moelv tillite and glacial-marine Ekre shale; the Moelv tillite sits unconformably

above the Ring and Biri Formations. As a poorly sorted, polymict conglomerate, it has long been interpreted as being glacially derived (Holtedahl, 1922; Bjørlykke, 1976). The Vangsås formation is the youngest unit in the Hedmark group and consists of the Vardal Sandstone and Ringsaker quartzite members.

In some areas, the stratigraphy of the Hedmark basin shows numerous chronostratigraphically equivalent facies of the above formations (Figure 4). In the Bjørånes district, time equivalent sediments of the Brottum formation and Biri formation are both developed as shale and are indistinguishable. The Bjørånes shale member at this location includes shale beds that are likely time-equivalent with deposition of Biri, Ring, and Biskopåsen Formations (Bjørlykke et al., 1976).

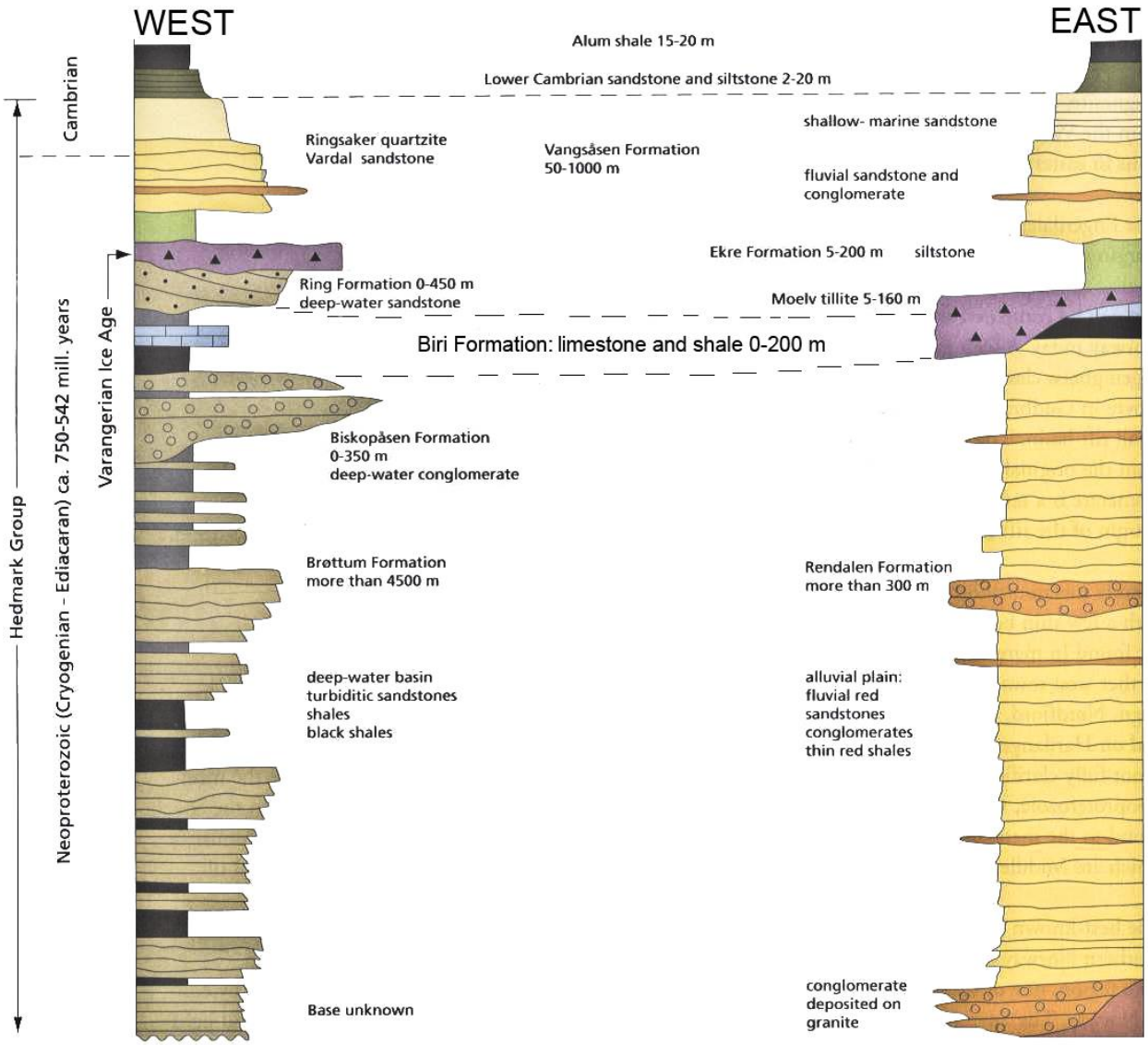

Figure 4. *Stratigraphic columns representative of the eastern and western Hedmark Group sediments. The syndepositional Imsdalen fault divides the basin between east and west and caused differential chronostratigraphic facies development. The Moelv tillite lies unconformably on the Biri Formation in the east while the Ring Formation seperates the Biri and Moelv in the west. Section after Nystuen (2008).*

2.2 THE BIRI FORMATION

The Biri Formation consists of shallow-marine limestones and organic-rich shales deposited during a marine transgression (the Biri transgression) of the Baltoscandian craton during the Ediacaran Period (Nystuen, 1982). Within the Hedmark rift basin, deposition of carbonate occurred around the margin, while organic-rich muds were deposited in deeper shelf, slope and basin regions. Much, if not at

all, of the upper members of the Hedmark group sediments, including some parts of the Biri formation, are thought to have been formed via turbidity currents and other types of submarine gravity flows (Nystuen, 1987). Localized subbasins in the Bjørånes district and at Øvre Rendal have been identified based on outcrop patterns where it is thought that deposition of the Biri Formation coincided with localized, tectonically-controlled, high-rate subsidence (Sæther and Nystuen, 1981).

The numerous and varied lithofacies of the Biri formation have been extensively mapped throughout southern Norway. Carbonate-dominated facies include oolitic limestones, intraformational limestone breccia, organic-rich massive limestones, micritic limestone, oolitic limestone, dolomite, intratidal to supratidal flat-pebble conglomerates, and platform carbonates with algal structures. Silisiclastic facies include calcareous sandstone, calcareous mudstone and calcareous laminated siltstone, as well as fine-grained sandstones and laminated black shale (Vidal and Nystuen, 1990). Carbonate-rich sandstone and shale have been interpreted as slope deposits and black shale as distal, deep-basin mud deposits (Nystuen, 1982). The wide variation in lithofacies represents deposition under shifting sea levels during the tectonically active period of rifting within the intracratonic Hedmark basin (Nystuen, 1987). These facies variations occur within limited distances of one another and represent a complex depositional setting where carbonate shelf facies transition quickly into basinal facies. Because continuous, outcropping sections are few and structural relationships within the eastern fold and thrust belt of the Osen-Røa Nappe are complex, a detailed stratigraphy and paleoenvironment reconstructions of the Biri Formation are difficult, if not impossible (Bjørlykke et al., 1976; Nystuen, 1982; Tucker, 1983).

The study presented here focuses on samples taken from the upper shale member of the Biri Formation at the Djupdalsbekken locality (Figure 5). Samples taken at Øvre Rendal are also included for reference and discussion on depositional setting. References to the “Biri shale” from here forward are meant to indicate the black shales of the Biri Formation at Djupdalsbekken.

Figure 5. *Outcrop locations within the study area. The defined map extents represent the majority of the area in which Hedmark Group sediments are found.*

At the Djupdalsbekken locality 9 km west of the town of Biri (described by A. Bjørlykke (1979) and Tucker (1983)), the Biri Formation is exposed along a steep bedrock stream channel. The exposure includes lower carbonate-rich facies that grade upward into a 70 m section of black shale that is overlain by 30 m of the Ring Formation (Figure 6 and Figure 7). Just below the contact with the Ring Formation, the organic-rich shale coarsens upward into a roughly 5-cm-thick siltstone. This siltstone is interpreted as early distal deposits of prograding conglomeritic fan deltas of the Ring formation that ultimately covered both marginal carbonate facies and deeper-water shale facies (Bjørlykke et al., 1976). Marginal oolitic carbonate facies down section were deposited under shallow waters (a few meters) in low, intertidal to shallow subtidal zones (Tucker, 1985). In the studied section presented here, the Biri limestones and shales at Djupdalsbekken are steeply dipping and include minor structural features and calcite veins that vary in distribution, frequency and orientation throughout the exposure. Carbonate content is on average 30 wt % in the middle to lower part of the exposure and decreases toward the top of the section and contact with the Ring Formation. Bjørlykke et al. (1976) suggest that carbonate content in the black shale varies to the degree the basin was supplied with carbonate mud from the shelf. Just under the contact with the overlying Ring Formation, the last 0.5 m of shale is a dolomitic mudstone with $\sim$ 70 wt % CO_3, likely deposited under shallowing shelf conditions during the regression that occurred prior to deposition of the overlying coarse clastic, deltaic Ring Formation and Moelv tillite. Development of strong cleavage occurs in weaker shales toward the top of the section while carbonate-rich units are better indurated and show more widely spaced cleavage. Pictures from of ultra-thin, 15 µm thin sections using light microscopy are given in Appendix III. The thin sections offer a detailed look at the petrology of the outcrop at Djupdalsbekken and cover the range of collected hand samples within the upper, shale-dominated member of the Biri Formation.

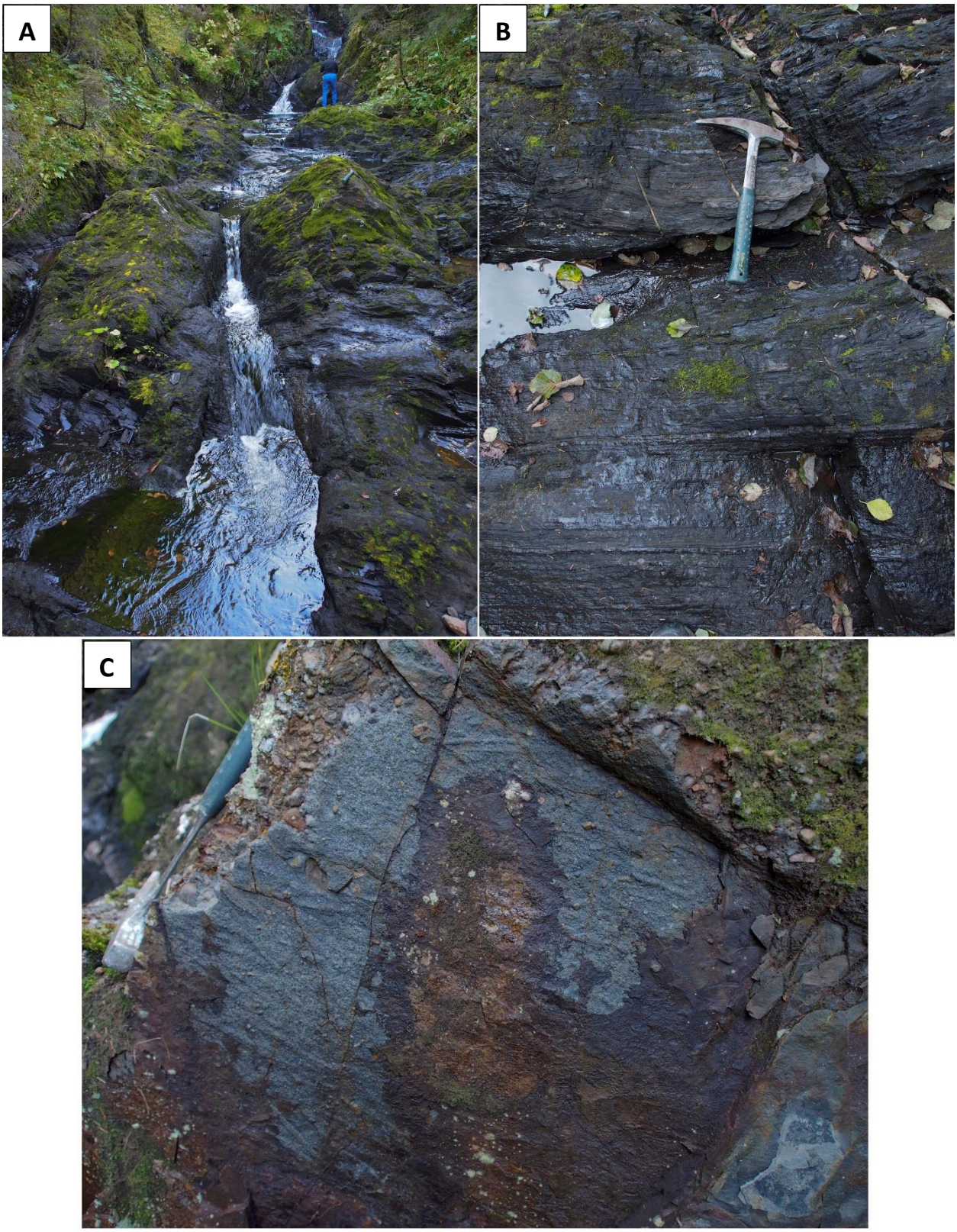

Figure 6. *The Biri Formation outcrop at Djupdalsbekken. A). Judy Hannah standing at the contact with the Ring Formation. B.) A representative section of Biri shale. C.) The contact with the Ring Formation - load casts are visible, as well as the siltstone at bottom right.*

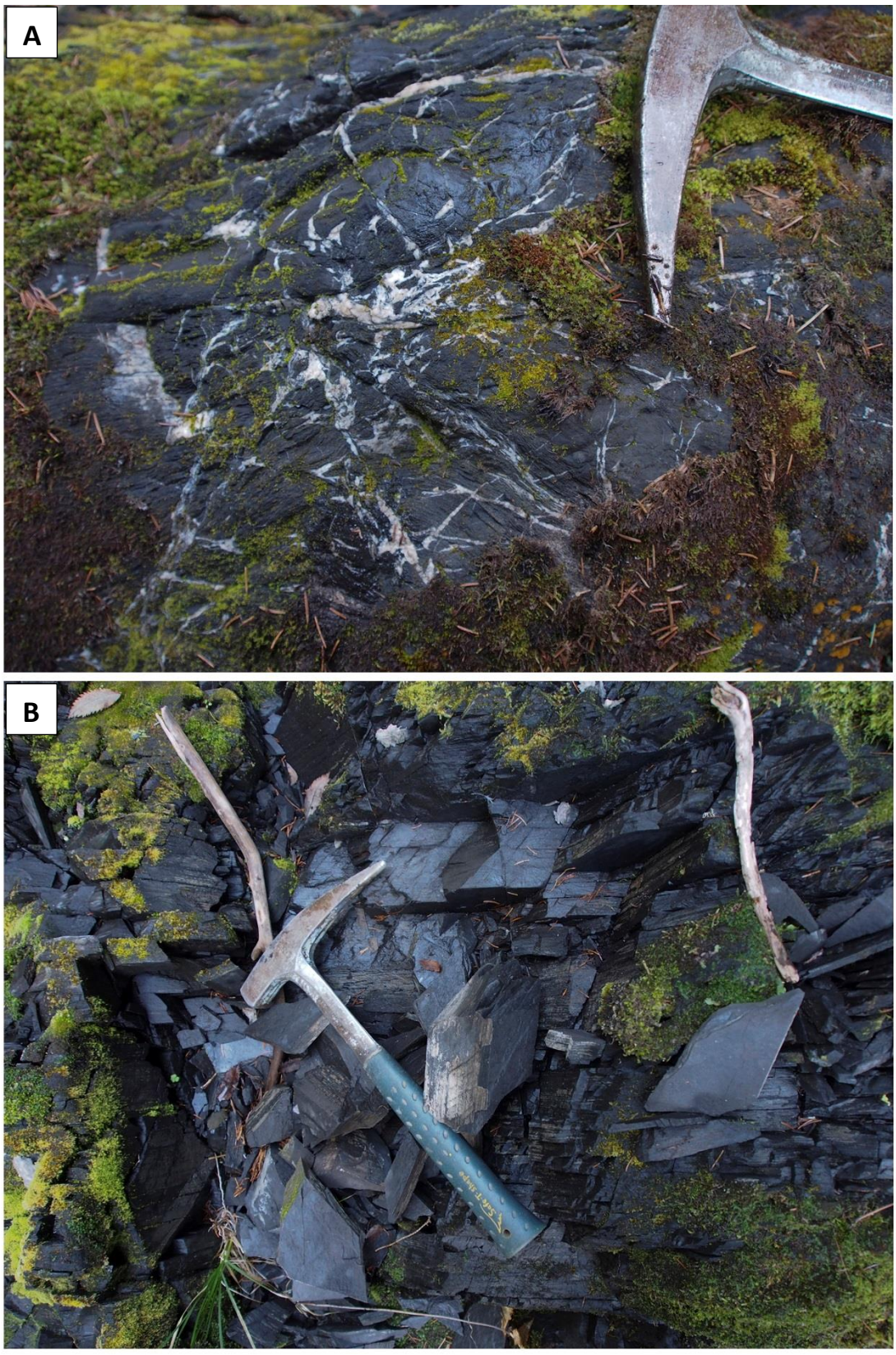

***Figure 7**. A.) A section of the Biri Fm with abundant veining (calcite). B.) Fissile shale near the top.*

CHAPTER 3: METHODS

3.1 SAMPLE COLLECTION

Thirty-one samples were obtained from outcrop west of Biri, Norway at the Djupdalsbekken locality (Figure 5) where the Biri Formation is exposed along a steep bedrock stream channel (Hannah et al., 2007). Beginning at the contact with the overlying Ring conglomerate, samples were taken along intervals down the stream channel with increasing distance between sample locations: Three sample locations in the first meter, two in the second meter, and one or less between meter 3 and the last sample at meter 47. In some cases, multiple samples were taken at or very near to one sampling location. Samples were collected by Judy Hannah, Holly Stein and Bernard Bingen. Initial field work in 2006 and also in 2009 was supported by the Geological Society of Norway (NGU – Trondheim). Continued funding for this thesis was provided by the CHRONOS project (H. Stein and J. Hannah, PIs).

3.2 SAMPLE PREPARATION

Samples were prepared for geochemical analysis by obtaining a 5 to 6 gram subsample of the pieces collected from outcrop. Five to 6 gram subsamples were obtained by either selecting broken pieces of more fissile samples, or by cutting suitable sections from indurated samples. Care was taken to choose representative samples where variation occurred, and to select samples that showed no weathering surfaces. In some cases, surfaces that showed visible weathering were cut away to expose fresh rock.

The subset of 31 samples were subsequently powdered using a ceramic ball mill. More fissile samples with small fragments were placed directly into the ball mill and powdered, while better indurated samples were first wrapped in layers of paper and crushed using a hammer and steel plate. Care was taken to remove any visible paper fragments from the samples prepared in this way. Samples were powdered using a Spex SamplePrep Mixer/Mill 8000M with a ceramic grinding jar. After

powdering, the grinding jar was rinsed with water, dried, and placed back in the mill with pure quartz sand. The powdered sand was removed and the grinding jar again rinsed and finally washed with ethanol and allowed to dry.

3.3 MAJOR AND TRACE ELEMENTS

Abundances of major and trace elements for the complete set of 31 samples were acquired commercially from Actlabs using the Ultratrace 6 method. Powdered, 0.25 g sample amounts were used for whole rock (WR), mulit-acid (HF, $HClO_4$, HNO_3 and HCl) digestion, followed by inductively coupled plasma atomic emission spectrometry (ICP-AES) and inductively coupled plasma mass spectrometry (ICP-MS) analysis. Elemental abundances were determined using a Varian ICP and a Perkin Elmer Sciex ELAN ICP-MS.

3.4 TOC AND ROCK-EVAL PYROLYSIS

Data for the complete set of 31 samples was acquired from Geomark Rock Source. TOC data were obtained with a LECO 230 instrument on decarbonated samples. Samples were treated with concentrated HCL for at least two hours and dried at 110 C. Standards with known carbon contents were run as unknowns every 10 samples for calibration. The acceptable standard deviation for TOC is 10% from an established value. Rock Eval pyrolysis data was obtained by a Rock Eval II instrument using approximately 100 mg of sample. Calibration against a known standard was done every 10 samples. Acceptable standard deviation from an established value is 10% for S1 and S2 peaks, and 20% for S3 peaks.

3.5 CARBON, OXYGEN AND SULFUR ISOTOPES

Measurement of stable isotopes was done at Iso-Analytical, UK. For inorganic carbon (carbonate) and oxygen analyses, powders were oven-dried for 24 hours, flushed with 99.995% helium and reacted in phosphoric acid overnight. Analysis was by Continuous Flow – Isotope Ratio Mass

Spectrometry (CF-IRMS). Liberated CO_2 was sampled into a continuous flow of He and resolved on a packed column gas chromatograph linked to a Europa Scientific 20-20 IRMS. Sulfur-34 and organic carbon-13 were analyzed by Elemental Analyser - Isotope Ratio Mass Spectrometry (EA-IRMS). Samples for sulfur analysis were placed in a furnace and combusted in the presence of oxygen. Combusted gases were then swept over combustion catalysts where SO_2 was resolved from N_2 and CO_2 on a packed GC column at 45°C and S isotope species subsequently measured by IRMS. Organic carbon 13 samples were acidified with 2M hydrochloric acid for 24 hours after which the acid was decanted upon centrifugation. Sample fractions were oven dried at 60°C, loaded into a Europa Scientific Roboprep-CN module and subsequently combusted in a furnace at a temperature near 1700 C. Combusted gases were variously removed by catalysis, N_2 was separated from CO_2 by a packed column gas chromatograph at 100°C and the remaining CO_2 analyzed by a Europa Scientific 20-20 IRMS.

Stable isotope ratios are reported as the per mil (‰) difference between the measured isotope ratio in the sample and the isotope ratio in the standard using the standard delta (δ) notation. The standard is the Vienna Pee Dee Belemnite (V-PDB) for carbon and oxygen, and the Vienna Canyon Diablo Troilite (V-CDT) for sulfur. Analytical precision (1σ standard deviation) from multiple analyses using International standard IAEA-SO-5 and laboratory standard IA-R061 traceable to NBS-127 was 0.23 ‰ for $\delta^{34}S$ (n=8); 0.07 ‰ for $\delta^{13}C_{org}$ (n = 8) using laboratory standard IA-R001 traceable to international standard IAEA-CH-6; 0.04 ‰ for $\delta^{13}C_{inorg}$ (n = 9), and 0.15 ‰ for $\delta^{18}O$ (n = 9) using international standards NBS-18, NBS-19. Samples with duplicates are reported as the average value of the two measurements.

3.6 RHENIUM AND OSMIUM

Re and Os data were collected at Colorado State University in the AIRIE Program using procedures outlined by Georgiev et al. (2011).

3.7 THIN SECTIONS

Thin sections chips were cut from indurated samples, while more fissile samples chosen for thin section were carefully stacked and taped together. No more than 2 pieces were stacked together. Polished, ultra-thin 15 µm sections were obtained from Applied Petrographic Services. Petrography was done on a Lecia DM 2500P petrographic microscope using a Clemex C mount camera to take digital photographs. Scanning Electron Microscope (SEM) images and data were taken on a JEOL JSM-6500F with a Noran System Six EDS at Colorado State University. Petrographic images of representative samples from the section are presented in Appendix III.

3.8 NORMALIZING DATA

Trace element sources

Determining the source of trace elements, whether detrital, hydrogenous or biogenic is critical to evaluation of TEs as indicators of paleoenvironmental conditions. Only those TEs derived from the hydrogenous fraction (derived from seawater) are useful as these indicators. A measure of TE values in the sediment vis-à-vis crustal values gives a relative degree of enrichment of TEs that reflect values of hydrogenous-derived TEs and thus paleoenvironmental conditions. The most common method used to isolate the hydrogenous fraction from the detrital component is to normalize the whole rock data to an assumed marker of the detrital component. Al, Ti and Th are generally assumed to reflect the aluminosilicate (detrital) component in the sediment and in most cases Al is used as the marker of the detrital component (Calvert and Pederson, 1993; Morford et al., 2001; Algeo and Maynard, 2004), though thorium is used as well (Thompson et al., 1998; Schroder and Grotzinger, 2007). This process assumes that Al, Ti, or Th are representative of the siliciclastic component which does not contain any TEs derived from seawater. However, Van der Weijden, (2002) showed the potential problems associated with this normalization technique (discussed in section 5.2), while Xu et al. (2012) suggest that the best method to isolate the detrital and hydrogenous TE fractions is through analytical

techniques. To the extent possible, TE data should be combined with other approaches to help resolve the ambiguities created by the multiple, sometimes indistinguishable TE sources.

Variable carbonate content

The CO_3 content of the Biri shale is relatively constant but becomes highly variable near the top of the section. Because of this variability, the TE signature is unclear due to TE dilution that is dependent on the CO_3 content of each sample. Because CO_3 excludes almost all TEs from its lattice structure (notable exceptions, e.g. Mn, Ba), the resulting concentration of any TE is limited to the amount of the sample that is not CO_3. For example, if a sample contains 50% CO_3, TE concentrations are indicative of only 50% of the sample size. Thus, comparison of TE concentrations between samples becomes impossible. Normalizing to CO_3 content may help to some extent, but the variable enrichment or depletion of any TE in a sample is dependent on more factors than CO_3 content. Again, for example, TE concentration at 35 m depth may reflect a period of hydrothermal input, while TE concentrations at 5 m do not. Correction for the dilution that occurs from CO_3 content enables us to find the hydrothermal variable that otherwise would have been hidden because the samples contained different amounts of CO_3. Select major and trace element data taken from the results of XRF done at the NGU, Trondheim, were normalized to account for variable carbonate content, particularly near the top of the measured section. Elemental concentrations were calculated from XRF results presented as oxides (Appendix I). Evolved gases were assumed to be 100 % CO_2 and wt % CO_3 was back calculated from the total evolved gases. A total $CaCO_3$ content was calculated by adding the Ca, Mg and CO_3 content together. Afterward, the total siliciclastic (non-carbonate) content for each sample was calculated as follows:

$$(100 - (Ca+Mg)CO_{3(\text{total sample})})/100 = \%\ \text{Siliciclastic}_{(\text{total sample})}$$

Finally, the concentrations of select major and trace elements were individually calculated based on the non-carbonate fraction by dividing the original element concentration by the non-carbonate % of each

sample. This procedure yields a well constrained estimate of the elemental concentration bound in the non-carbonate portion of each sample.

CHAPTER 4: GEOCHEMICAL BACKGROUND

4.1 DEPOSITION OF ORGANIC-RICH SHALE

Shale accounts for nearly 70% of all sedimentary rock and is defined by a composition of fine-grain (< 0.1 mm) clastic fragments and high abundance of clay minerals (Schieber and Zimmerle, 1998). Shale-forming sediment is deposited in a wide variety of slow-moving water environments that range from fluvial systems, lakes, and continental slopes to deep marine basins (Bohacs, 1998).

A significant portion of shales, termed “black”, are derived from organic-rich sediment. They typically contain greater than 1% organic carbon (Tourtelot, 1979) and have high concentrations of trace elements (TE). It has historically been understood that the muddy, organic-rich sediment constituting black shale accumulated only in relatively slow-moving to stagnant deep marine basins. A contemporary understanding, however, places their deposition not only in stratified, anoxic and/or euxinic deep basins like the Black Sea, but also in zones of coastal upwelling similar to the Gulf of California where, if the right conditions are met, organic-rich sediment can be deposited and preserved in shallow waters (Wignall, 1991) and under oxic conditions as well (Quinby-Hunt et al., 1989). Work done by Schieber (1994) shows hummocky cross-stratification, erosional surfaces and low-angled cross bedding in Devonian black shale; he argues against a slow, stagnant environment in favor of a shallow, highly bio-productive environment. Ripple migration in shales were observed by Schieber and Southard (2009), and MacQuaker et al. (2010) show evidence for organic-rich shale deposition not as continuous rain of fine-grained particles in stagnant environment, but by “advective sediment transport processes”. Bohacs (1998) demonstrates that the greatest amount of organic carbon enrichment occurs in a lower-slope depositional environment, but notes that no simple relationship exists between depositional environment and organic content.

4.2 SYSTEMATICS OF TRACE ELEMENT ENRICHMENT IN BLACK SHALE

Sediment enrichments in trace elements (TEs) that vary based on paleoenvironmental conditions can serve as proxies for understanding the paleodepositional and paleoredox setting, as well as paleoclimate and other factors (Vine and Tourtelot, 1970). Elements found in marine water are derived from terrestrial sources, biogenous plankton remains, and/or thermal water sources within the marine basin (Leventhal, 1998; Brumsack, 2006; Tribovillard et al., 2006). TEs present in seawater are either adsorbed onto particles or occur in soluble form. Biotic and abiotic processes remove the dissolved TEs from the water column where abiotic processes dominate under anoxic conditions. Oxygen concentrations are categorized as oxic (> 2.0 ml O_2/L), dysoxic or suboxic (~ 0.2 – 2.0 ml O_2/L), anoxic – nonsulfidic (< 0.2 ml O_2/L, 0 ml H_2S/L), and anoxic – sulfidic or euxinic (0 ml O_2/L, > 0ml H_2S/L) (Wignall, 1994; Algeo and Tribovillard, 2009).

In black shale, most TE enrichments occur at the sediment-water interface and in the upper layer of sediment under anoxic conditions. Enrichment of TEs and their distribution in amount and type is dependent on a number of factors that will be discussed below. Cruse and Lyons (2004) note that TE enrichment variability in laterally continuous mid-Continent Pennsylvanian shale was dependent on geographic location. Although Brumsack (2006) showed little difference in trace element enrichment between coastal upwelling zones and deep euxinic basins, some differences (higher or lower enrichment values of certain TEs) do exist, and variation within each setting is controlled by localized geographic differences: sediment influx, type and degree of sulfidization, and redox threshold factors.

The relative abundance of TEs in sediment is controlled sedimentation rate, terrigenous flux, biogenic flux, hydrothermal input, diagenesis and ultimately, weathering (Schultz, 1989; Leventhal, 1998; Schieber and Zimmerle, 1998). The complex interplay of these variables makes a straightforward interpretation paleo-conditions difficult. During deposition, individual elements may not show any well-developed redox-controlled separation within the sediment even though contemporaneously measured

sections show decreasing Eh profiles with depth (Thompson et al., 1993). Thompson et al. suggest, among many possibilities, that changing redox conditions as accumulated sediment is buried may overprint earlier diagenetic conditions, homogenizing the TEs.

TEs that are enriched in organic carbon-rich sediments generally form three groups: Stable sulfide forming TEs, redox-sensitive TEs, and TEs involved in the biological cycle. Organic matter and pyrite are commonly the main hosts for these elements (Brumsack, 2006; Georgiev et al., 2012). TEs occur in various phases within the sediment: adsorbed onto mineral or organic surfaces, as organometallic complexes, in solid solution in pyrite, phosphate and sulfate, metal sulfides, or as insoluble oxides and oxyhydroxides (Morse, 1994; Tribovillard et al., 2006). As a result, their depositional behavior depends on pH and Eh conditions of the sediment environment. Trace elements that undergo pyritization include As, Hg, Mo, Co, Cu, Mn, Ni, Pb, Cd, Cr, and Zn, in order of decreasing degree of pyritization (Huerta-Diaz and Morse, 1992). Eventual incorporation into the sediment is common if conditions remain reducing.

Most TEs that are sensitive to redox conditions are more soluble under oxidizing conditions and less soluble under reducing conditions. In sedimentary facies that are oxygen-depleted, the result is authigenic enrichment of these TE (Tribovillard et al., 2006). Redox potential in the upper most layer of sediment is controlled by the amount of available oxygen, whether or not euxinic conditions exist, and also by the "rain rate" of organic matter in the depositional setting (Morford and Emerson, 1999). Any dissolved hydrogen sulfide can combine with trace metals, reducing them to form metal sulfides. The presence and amount of dissolved sulfide in pore waters and the water column is dependent on bacterial production (sulfate-reducing bacteria) and the amount of H_2S loss through pyrite formation (Wilde et al., 2003). Anoxic conditions preserve the organic matter and newly formed metal sulfides.

Elemental enrichment is dependent on these conditions and processes in combination with the presence of organic matter in the water column and sediment. Some TEs show a strong covariance with

the Total Organic Carbon (TOC), while others are more moderately or weakly associated with TOC (Algeo and Maynard, 2004). In conjunction, the amount and degree to which TOC is preserved in the sediment is dependent on the amount of organic material produced in the photic zone or brought in as terrigenous sediment, and that which survives oxidation as it travels through the water column. Short residence time in the oxic water column and low concentration or complete absence of oxygen in the water column causes a greater amount of TOC to be preserved (Brumsack, 1989).

As long as conditions in the burial environment remain reducing, TEs that are co-precipitated with iron sulfides generally remain immobile. Such is the case with Mo, V, Cd, Ni, Co, Cu, Zn, and Pb (Tribovillard et al., 2006). In the case of Zn, Pb, and Cd, if these elements form soluble complexes with reduced sulfur species, their mobility in anoxic sediments increases and they may subsequently diffuse through the sediments (Huerta-Diaz and Morse, 1992). For most other redox-sensitive and sulfur-bound TEs, as diagenesis occurs and oxidizing agents within the sediment become exhausted by oxidation reactions or by bacterial organic matter oxidation, conditions in the sediment become permanently reducing and TEs remain immobile (Tribovillard et al., 2006). Notable exceptions to this general rule are Mn and Fe-oxides that accumulate at the sediment water interface as particulate oxides. As the oxides are buried in reducing conditions, Mn^{2+} and Fe^{2+} are released and migrate through the sediment.

Mn-oxides may have played an important role in the behavior of TEs in the Biri Formation. In the uppermost layers of the Biri shale at Djupdalsbekken, very negative $\delta^{13}C_{inorg}$ values provide evidence that some C_{org} was oxidized and subsequently included in the CO_3 found in the samples taken from those horizons (see Appendix II, Table 12). However, optical microscopy shows intact pyrite framboids in each thin section, and sulfur concentration is consistent throughout the section. Because pyrite is more reactive than OM during oxidation, the TEs bound to the OM are released upon oxidation only after all of the pyrite is depleted (Georgiev et al., 2012). There is evidence, however, that oxidation of the C_{org} did not occur by O_2, but by MnO_2 reduction. This evidence is discussed in section 6.5 below.

CHAPTER 5: RECONSTRUCTING THE CHEMICAL DEPOSITIONAL ENVIRONMENT OF THE BIRI SHALE

The geochemical signature in black shale results from the input of major and TEs from three main sources, commonly called fractions: Detrital, authigenic and biogenic. Each fraction contains a suite of elements that indicates or signals the degree to which each source contributed to the amount of accumulated sediment. As a result, certain elements serve as primary indicators of each source. Elements delivered to the sediment within the detrital fraction are derived from terrigenous sources and include Ti, Zr, Th, Cr, Co and Al. The biogenic fraction is composed of elements involved in biogeochemical cycles delivered to the sediment with organic matter, carbonate and silica and includes Zn, Ca, Cu, Ni, P and Ba as indicators. The authigenic fraction is derived from seawater and contained primarily within insoluble oxyhydroxides, sulfides and organic matter, of which the primary indicators are V, Mo and U. Due to their differential behavior in varying redox conditions, redox-sensitive TEs are routinely used as proxies to identify sedimentary conditions during deposition of organic-rich sediment.

Vanadium, Uranium and Molybdenum are the three most widely used and agreed-upon TEs that show value as indicators of paleo-depositional redox (Emerson and Huested, 1991; Tribovillard et al., 2006). Other TEs are used as well: Rhenium (Crusius et al., 1996; Morford and Emmerson, 1999), Zinc (Algeo and Maynard, 2004) Ni and Pb (Cruse and Lyons, 2004) in addition to V, U and Mo (see Tribovillard, 2006 and references therein). Examples of element ratios include Ni/Co, V/Cr, Mo/Al (Jones and Manning, 1994; Rimmer, 2004; Riquier, 2006; Ross and Bustin, 2009); Mo/U (Tribovillard et al., 2009; Tripathy et al., 2014); and V/Mo (Piper and Calvert, 2009). Also used are trace element Enrichment Factors (EF) (Algeo et al., 2003; Brumsack, 2006; Riquier, 2006; Ross and Bustin, 2009) that describe the degree to which an element is enriched compared to an average shale, usually the values presented in Wedepohl (1971) as World Shale Average from accumulated data in the literature, or from the Post Archean Average Shale (PAAS) values presented in Taylor and McLennan (1995). Here an

overview of the most commonly used TEs and TE ratios is given, with a discussion of their application to the purposes of the current project.

Table 1. *Geochemical data for selected trace elements.*

Element	Source	Residence Time in seawater (k.y.)	Main species in oxic Seawater	Main species in reducing conditions	Average Crustal abundance	Average Shale (ppm)	Average Biri value (ppm)**	Average Biri value Al-norm (ppm)**
V	Rivers	50	HVO_4^{2-} and H_2VO_4	VO^{2-}, $VO(OH)^{3-}$, $VO(OH)_2$ V_2O_3, $V(OH)_3$	170	130	80	13.014
Mo	Rivers	800	MoO_4^{2-}	$MoO_xS_{(4-x)}^{-2}$ (x= 0-3) MoS_4^{-2}	1.5	1.3	4.6	0.742
U	Rivers	400	$UO_2(CO_3)_3^{4-}$	UO_2, U_3O_7, U_3O_8	2.8	3	6.5	1.048
Re	Rivers	130	ReO_4^-	See Text				
Ni	Hydrothermal	6	$NiCl^+$, $NiCO_3$, Ni^{2+}	NiS	44	68	23.5	3.937
Co	Hydrothermal	0.34	Co^{2+}	CoS	17	19	13.4	2.128
Cr	Hydrothermal	8	CrO_4^{2-} + $Cr(OH)^{2+}$, $Cr(OH)_3^0$	$Cr(OH)^{2+}$, $Cr(OH)_3$, $(Cr,Fe)(OH)_3$	83	90	29	4.8
Cu	Hydrothermal	5	$CuCl^+$	CuS, CuS_2	25	45	27.4	4.398
Mn	Hydrothermal	0.06	MnO_2, Mn^{2+}		600	850	420*	64.194*

Wedepohl (1971); Colodner et al. (1993) - Re source; Emerson and Heusted, (1996) - Mo residence time; Morford and Emerson (1999); McLennan (2001); Miller et al. (2011) - Re residence time; Tribovillard et al. (2006);
*Mn average does not include two samples with heavy enrichment in Mn. All samples avg = 569 | 151.945 (Al-Norm)
**See appendix for complete data tables.

5.1 REDOX SENSITIVE TRACE ELEMENTS VALUABLE FOR THE PRESENT STUDY

The geochemical qualities of U, Mo, Re and V make them good proxies for sedimentary redox conditions. U, Mo and Re behave conservatively (are unreactive) in oxygenated seawater (Emerson and Huested, 1991; Morford and Emerson, 1999) and Vanadium behaves in a nearly conservative manner (Collier, 1984). All undergo reduction to a lower valency, and become reactive or insoluble in anoxic conditions. (Calvert and Pederson, 1993). Their geochemical behavior is detailed below, followed by a presentation of their application to the study of the Biri shale. Samples collected at the Djupdalsbekken outcrop are relatively homogenous except for the first three samples. Sample 1 is a fine siltstone while

samples 2 and 3 are highly enriched in CO_3 content (avg ~ 70%). For this reason, geochemical data from these samples are excluded from the following discussion and data presentation.

Vanadium

Vanadium is delivered to the ocean via continental run-off and from hydrothermal fluids associated with submarine volcanism. In oxic ocean waters vanadium exists as the vanadate oxyanions HVO_4^{2-} and H_2VO_4, reduced to the vanadyl anion $V(IV)O^{2+}$ in anoxic conditions. In the presence of H_2S (euxinic conditions) vanadium can be reduced further to V(III) (Morford and Emerson, 1999) where it may complex with geoporphyrins or precipitate as V_2O_3, a solid oxide, or a hydroxide $V(OH)_3$ phase (Breit and Wanty, 1991; Tribovillard et al., 2006). Enrichment in black shale over marine concentrations occurs under suboxic to anoxic conditions (Piper and Calvert, 2009) and is correlated to organic content through adsorption on to settling organic matter in the water column. However, adsorption of vanadyl onto insoluble oxides and hydroxides is considered to be a stronger, more prevalent mechanism of removal to the sediment than formation of a complex with organic ligands (Breit and Wanty, 1991).

Molybdenum

Molybdenum exists as molybdate (MoO_4^{2-}) in oxic marine waters and has the highest (salinity normalized) seawater concentration (100 nmol/kg) of the TEs discussed here due to its low reactivity (Collier, 1985). Mo is taken up by Fe-sulfides and readily co-precipitates with Mn-oxyhydroxides in the form of ferromanganese crusts and Mn nodules in oxic marine environments (Scott and Lyons, 2012). Mn-Fe redox cycling can play an important role in Mo enrichment: Mn-Fe oxyhydroxides in the water column can adsorb molybdate anions which are subsequently released under reducing condition into the sediment where they can be scavenged and sequestered. Understanding of the geochemical mechanism by which it is removed from seawater and enriched in sediment under reducing conditions is incomplete but has evolved significantly in recent years (see Emerson and Huested, 1991; Helz et al., 1996; Erickson and Helz, 2000; Vorlicek et al., 2002; Algeo and Lyons, 2006; Helz et al., 2011). More than one model has been used to understand concentrations of Mo in sediment (Tribovillard et al., 2006 and

references therein). Helz et al. (1996) put forth the idea of a geochemical switch by which molybdate is converted to a form that is readily taken up in the sediment under anoxic and sulfidic conditions. In the model, molybdate is converted to thiomolybdates via dissolved sulfide above a critical H_2S concentration threshold value. Erickson and Helz (2000) proposed an intermediate transition step through oxythiomolybdates ($MoO_xS_{(4-x)}^{-2}$ (x= 0-3)) on the way to the highly particle-reactive (easily scavenged) species, MoS_4^{2-}. The total reaction can be written:

$$MoO_4^{2-} + 4H_2S_{(aq)} \leftrightarrow MoS_4^{2-} + 4H_20 \text{ (Tissot et al., 2012)}$$

This geochemical switch model is widely accepted (Tribovillard, 2006; Helz et al., 2011; Scott and Lyons, 2012), and Helz et al. 2011 argue for the importance of iron sulfide minerals in the scavenging and sequestration process of Mo in the sediment via this method. Scavenging can also occur by formation of bonds with sulfur-rich organic molecules (Tribovillard et al., 2004), and correlation with TOC is significant in most cases where Mo is enriched in black shale (Algeo and Lyons, 2006, Algeo et al., 2007).

Uranium

Uranium takes the primary form U(VI) in oxygenated ocean waters where uranyl ions bind with carbonate ions to form $UO_2(CO_3)_3^{4-}$. This form is stable and soluble in oxic ocean water with a relatively long residence time (450 k.y.) and importantly, is not involved in Mn-Fe redox cycling in the water column (Algeo and Tribovillard 2009). Authigenic enrichment in reducing sediment is achieved almost exclusively through diffusion across the sediment-water interface (Klinkhammer and Palmer, 1991). Microbially mediated pathways that reduce U(VI) to U(IV) are thought to play an important role in U accumulation in reducing sediment. The degree of enrichment is controlled by either bottom water oxygen concentrations, the rain rate of organic carbon through the water column, or some combination of both (McManus et al., 2005). A strong correlation of U enrichment with organic carbon flux to the sediment is seen where oxygen concentrations overlying the sediment are less than 150 μM. Where

overlying water [O_2] are greater than 150 µM, no such relationship exists between accumulation of authigenic U and the burial rate of organic carbon, suggesting that the generally linear relationship between U enrichment and organic carbon may be a result of unassociated factors (Morford et al., 2009a). Once reduced, U takes the form UO_2, U_3O_7 or U_3O_8 in the sediment (Algeo and Tribovillard, 2009).

Rhenium

Although Rhenium is not used as much as are V, Mo and U, its low crustal abundance and high degree of enrichment in reducing sediments make it an ideal candidate for detecting redox conditions in ancient sedimentary basins. Re occurs predominately as perrhenate (ReO_4^-) in oxygenated ocean waters with a residence time calculated to be as long as 130 k.y. (Miller et al., 2011), and is reduced to an Re(IV) oxide or sulfide in anoxic environments (Helz and Dolor, 2012). Removal of Re from pore waters under anoxic and or euxinc conditions is well established (Colodner et al., 1993; Chappaz et al., 2008; Morford et al., 2012 and references therein) and substantial enrichment in suboxic conditions (limited O_2 or H_2S) was noted by Crusius et al. (1996). The precise mechanism by which removal from pore water and enrichment occurs is, however, at the time of writing still unknown (Dolor et al., 2009; Helz and Dolor, 2012).

Rhenium behavior closely resembles that of Mo in seawater and in reducing sediment so comparisons are common in attempt to understand Re sequestration (e.g. Koide et al., 1986). Two important differences exist: Re removal to the sediment is entirely abiotic (Dolor et al., 2009; Morford et al., 2009b), and Re is unresponsive to Mn-oxyhydroxide scavenging, unlike Mo. Helz and Dolor (2012) hypothesize that Re is in some way coprecipitated with Mo in an Fe-Mo-S phase, which helps explain why Mo and Re concentration profiles in the Black Sea mimic one another, but doesn't explain systems in which enrichment of Re exists without Mo. Re is hosted predominately by organic matter in the sediment (Jaffe et al., 2002) where enrichment over crustal values can be on the order of 1000 times.

Notably, ^{187}Re decays radioactively to ^{187}Os with a half-life of 41.6 billion years, providing a long-lived geochronometer that is useful for placing precise dates on organic-rich black shale deposition (Hannah and Stein, 2013), provided the Re-Os isotope system remains closed with no disturbance by post-depositional oxidation and remobilization (Georgiev et al., 2012).

5.2 A MULTI-PROXY APPROACH TO CHEMICAL DEPOSITIONAL ENVIRONMENT RECONSTRUCTION

Most authors attempting to reconstruct the paleoredox conditions in ancient sediment recommend a multi-proxy approach (see McManus et al., 2005; Tribovillard et al., 2006; Scott and Lyons, 2012). This is because no one proxy can offer definitive evidence of paleoredox conditions, and also because trace element values may vary geographically and through geologic time based on a multitude of variables (e.g. lower Mo values in the Proterozoic, Scott et al. (2008)). The following is an attempt to decipher depositional redox conditions in the Biri shale based on a systematic, geochemical multi-proxy approach complemented by petrographic results.

A first step is to identify which of the TEs in the Biri shale are authigenic - the degree to which they are derived from seawater and thus useful as indicators of paleoredox conditions. Figure 8 shows correlation of select major and TEs with aluminum, an indicator of the detrital component. Strong correlation with Al is a signal that the element is contained in the detrital fraction, generally siliciclastic detritus delivered in the form of insoluble clay minerals (aluminosilicates). A good example of an element held almost exclusively in the detrital fraction is thorium. As a result, excellent correlation of Th with Al should be expected, and such is the case in the Biri shale with data showing a Pearson's r Al - Th value of 0.944.

The data show that V, Co and Cu have strong correlation with Al (r^2 values > 0.70), moderate to low correlation of Zn, Cd and Ni (r^2 values 0.41– 0.57), and little or no correlation of U, Mo, Mn, and Cr (r^2 values < 0.22) with Al. Among the most important redox indicators, strong correlation with Al suggests that vanadium in the Biri shale is either entirely or almost entirely of detrital origin, limiting its

Major Element		Trace Element	
Na	0.570	V	0.848
Mg	0.799	U	0.370
P	0.288	Mo	0.307
S	0.750	Mn	0.433
K	0.682	Co	0.842
Ca	-0.622	Cr	0.469
Fe	0.884	Zn	0.642
Ti	0.781	Cd	0.757
		Ni	0.682
		Cu	0.901
		Th	0.944

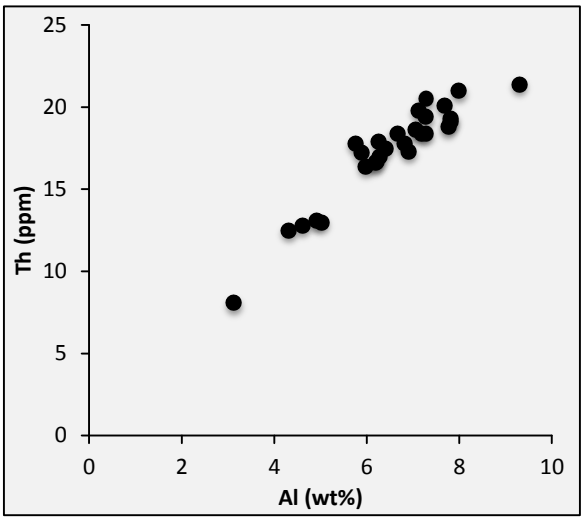

Figure 8. *Table of Pearson's r values for correlation of select major and trace elements with Al (n = 28). Chart at right illustrates the strong correlation of Al and Th, both indicators of the detrital component of the sediment.*

use as a paleoredox indicator. Meunier (1994) report substitution of V for Al in clay minerals at the octahedral site, which may account for the good association of V with Al content in the Biri shale. On the other hand, Mo has no correlation with Al ($r^2 = 0.09$) showing its usefulness as a redox proxy (Figure 9).

It is possible to make a distinction between correlations with Al, versus using Al-normalized data to interpret redox conditions. On the one hand, correlation of individual elements with an indicator of the detrital fraction like Al or Th may provide a useful tool in determining whether or not the given element is reliable as a redox proxy. On the other hand, normalizing the data to Al or Th can prove problematic according to Van der Weijden (2002) who clearly illustrated problems associated with normalizing geochemical data to a supposed indicator of detrital input. Normalized values may give (false) correlation between otherwise uncorrelated elements, correlation coefficients may be enhance or become distorted, or even change signs (negative to positive correlation or vice-versa). These problems become prominent when the coefficient of variation (standard deviation divided by the mean) of the divisor, in this case, aluminum, is high, especially in relation to the coefficient of variation of other TEs. When the coefficient of variation is low, then problems associated with normalization are minimized. If such is the case however, normalization is unnecessary in the first place. Coefficients of

variation for Al and select TEs are provided in Table 2, and the results show that the coefficient of variation for Al is small in relation to other TEs in the Biri shale, especially those of interest as paleoredox proxies. As a result, Al-normalization of the geochemical data is unnecessary. The data presented here are unmodified except in the case of determining Enrichment Factors (EF) where normalizing the data to Al is done in order to compare relative enrichments of TE data in the Biri with the World Shale Average given in Wedepohl (1971).

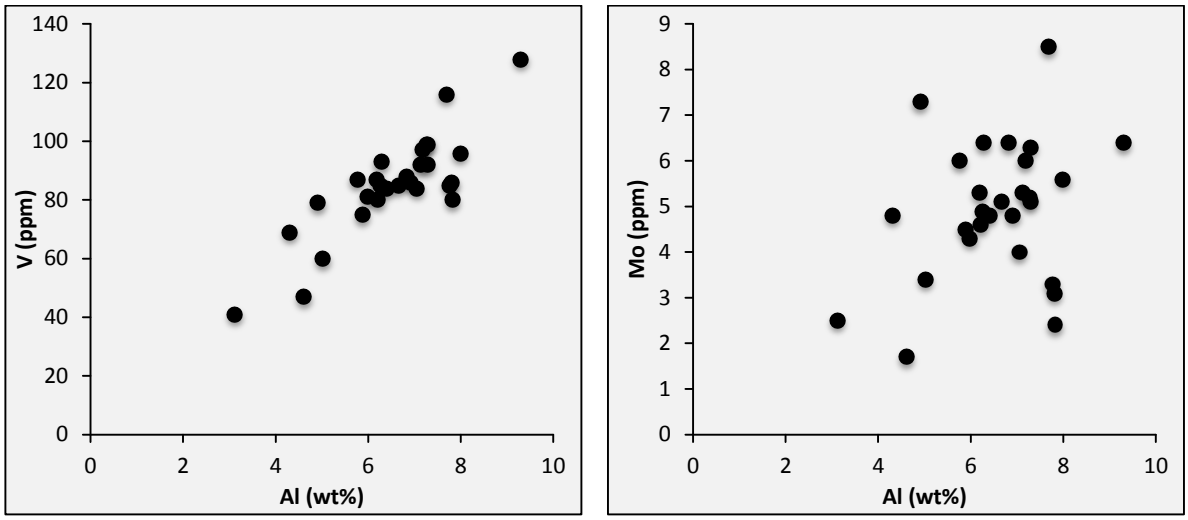

Figure 9. *V - Al cross-plot and Mo - Al cross-plot showing good (V) and poor (Mo) correlation with Al.*

Table 2. *Coefficient of Variation for Al and select TEs*

Al	V	U	Mo	Mn	Zn	Ni	Cu	Co	Cr	Pb	Th
0.19	0.21	0.29	0.30	0.42	0.25	0.35	0.21	0.21	0.34	0.51	0.17

Another way to get at the usefulness of any element as a paleoredox indicator is to estimate the amount of an element associated with the lithogenous fraction against the hydrogenous-associated amount. This can be done by plotting the trace element against Al_20_3 and drawing a line from the origin through the samples with the smallest concentration of the trace element, shown in Figure 10 (Piper et al., 2007; Piper and Calvert, 2009). Data plotting above this line represents the marine contribution, data plotting below the line represent the lithogenous fraction. Plotting the TE: Al_20_3 ratio of an average shale

value (WSA, in this case), acts as a check on the accuracy of the method: The slope of the line drawn from the origin through the samples with lowest TE amounts should match the ratio of TE: Al_20_3 in the world shale average within a small margin of error. Piper and Calvert (2009) report slopes for Ni, V and Mo within 10% of the WSA). In the instance of V, for example, the slope of the line drawn through the samples with the lowest concentration is calculated to be m = 0.13. The ratio of V: Al_20_3 in the WSA (Wedepohl, 1971) is also 0.13 (V = 130 ppm, Al_2O_3 = 16.7 wt %). Thus, any data plotting above the line with m = 0.13 is inferred to be marine-derived and marine concentrations can be estimated by measuring the displacement above the line with slope of 0.13. The results correlate well with correlation coefficient calculations in Table 2 and plotted in Figure 9, re-affirming that V is almost entirely derived from the lithogenous fraction, while Mo shows the opposite result.

Thus, the use of bulk-concentrations of individual trace elements, or ratios of TEs as redox indicators is problematic. This is true in cases exemplified by V where concentration in the sediment is due to the lithogenous fraction. The plot of Th versus Al_20_3 corroborates previous data showing Th partitioned almost exclusively in the detrital fraction, while the plot of U versus Al_20_3 suggest that at least some small portion of the U concentration is due to a lithogenous fraction while the majority is hydrogenous. Of note is the discrepancy with the WSA U/Al_20_3 ratio of 0.22 (3.7 ppm/16.7 wt. %) and the calculated slope of the line through samples with the least U content, calculated to be $\sim$ 0.48. A similar difference occurs with Th between calculated slope and the WSA ratio. Discrepancies between these values may be attributed to factors including samples size and the high degree of variability between two different depositional settings both in place and time, a significant problem associated with comparison to one standard such as the WSA.

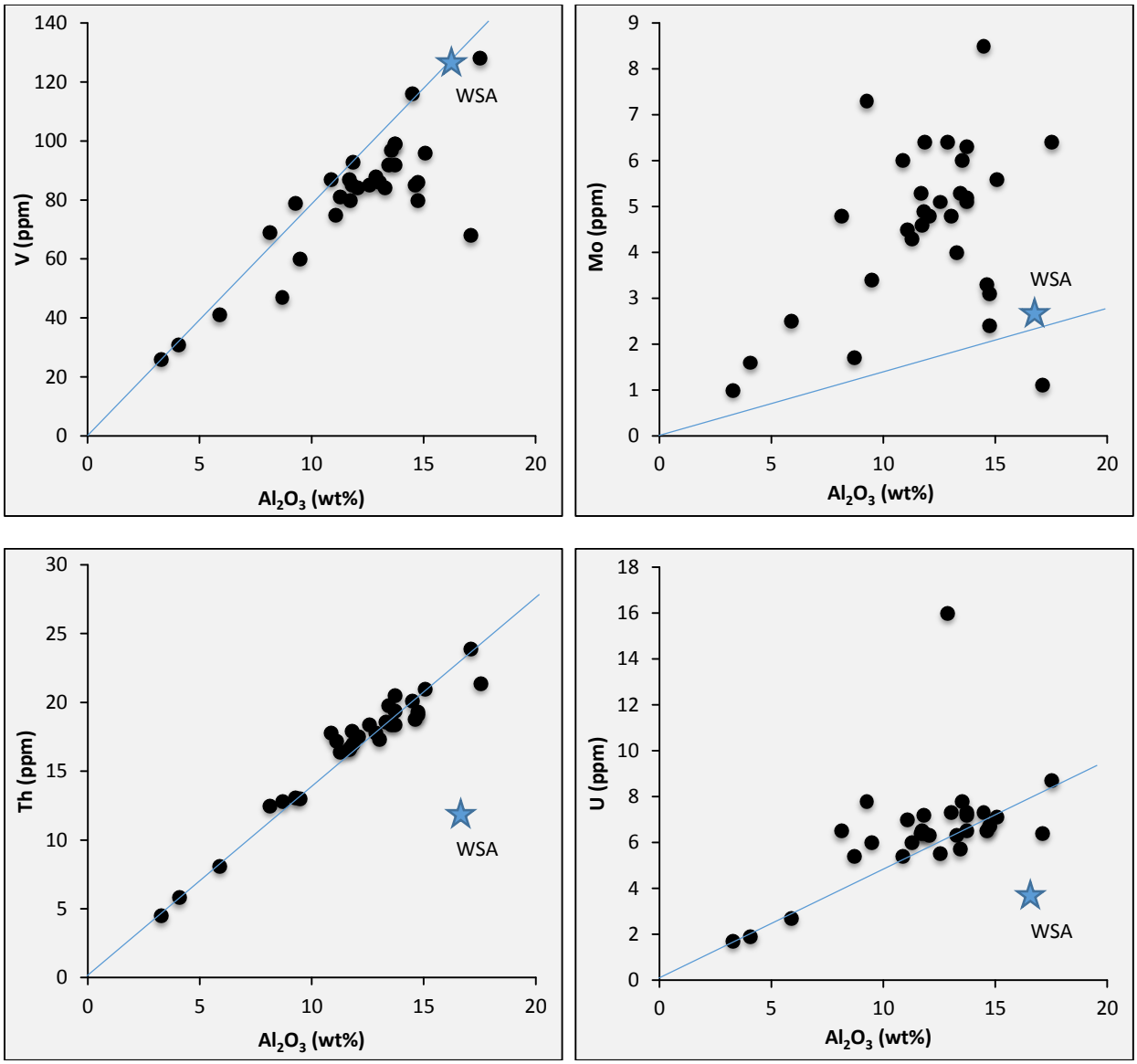

Figure 10. *Cross-plots of selected trace elements with Al_2O_3. See text for description for slope of the line and WSA placement.*

5.3 TRACE ELEMENTS AND TRACE ELEMENT RATIOS

In addition to V, U, Mo and Re, the trace elements Ni, Cu, Zn, Cd, Co, Cr and their ratios, e.g. Ni/Co, V/Cr Mo/Al have been used to deduce paleoredox conditions (Jones and Manning, 1994; Rimmer, 2004; Riquier, 2006) along with V/Mo (Piper & Calvert 2009). Both Ni and Cu are considered valuable as indicators of organic matter flux to the sediment as long as the flux is significant enough to

scavenge them and conditions allow for sequestration, generally in the form of sulfide minerals once released during OM oxidation (Tribovillard et al., 2006). Cr and Co concentrations are regarded as a signal of the detrital fraction and are not influenced by prevailing redox conditions in the water column or sediment (Ross and Bustin, 2009). Both Zn and Cd have relatively short ocean residence times (~ 50 k.y.) due to their nutrient-like behavior (Morford and Emerson, 1999). Both are associated with organic matter (OM) and are released to pore water upon OM decay where they are taken up by sulfides under reducing conditions (Tribovillard et al., 2006).

TE ratios V/Cr, Ni/Co, U/Th cannot be used independently of one another or other redox proxies (Jones and Wignall, 1994), and as Piper and Calvert (2009) show, they become useless when based on bulk TE concentrations since only enrichments of individual TEs above their lithogenous contribution are useful as paleoredox proxies. Such is the case with V: because it shows so little enrichment above the lithogenous fraction, its bulk concentration isn't useful. Similarly, Ni and Co are differentially held in the lithogenous fraction and biogenous fraction, and therefore bulk concentration do not provide accurate information of bottom water redox (Piper and Calvert, 2009) (see also Xu et al., 2012).

Because of differences in the mechanisms and thus conditions of removal to the sediment between V (suboxic to anoxic) and Mo (only under anoxic to euxinic) the V/Mo ratio can suggest depositional redox conditions (Piper and Calvert 2009). Bulk-sediment ratios of V/Mo in the Biri shale are ~ 16 (avg V = 80 ppm, U = 4.9 ppm) without differentiation between marine and lithogenous fractions. The method given in Piper and Calvert (2009) yields an average marine-derived V value of 10 ppm and an average Mo value of 4.6 ppm, and subsequent V/Mo of 2.1. This significantly different value corresponds to data given in Piper and Calvert (2009) for the Black Sea (1.5) and Cariaco Basin (0.65) and seawater-derived value of less than 1. According to Piper and Calvert (2009), values of V/Mo between 2 and 10 indicate oxic to suboxic bottom water conditions while values less than 2 indicate oxic conditions. Although this is an estimation, Biri V/Mo values (2.1) based on a very small marine-derived V

concentration indicate deposition under oxic to suboxic conditions that don't correspond well to the results from other paleoredox proxies discussed here. The two values (16 versus 2.1) based on different concentrations are indicative of some of the larger problems associated with using a single indicator to identify paleoredox conditions.

5.4 TOTOAL ORGANIC CARBON AND TRACE ELEMENT CORRELATION

Recall that the Biri shale was caught up, along with the rest of the Hedmark basin sediments, in the Osen Røa thrust sheet as part of the Caledonian orogeny. It is either prior to or during the orogenic event that the Biri shale became thermally mature, reaching temperatures near 180 C, based on the color of acritarchs (Tucker, 1983). Rock Eval data for the Biri shale indicate an average TOC of 0.70% with a range between 0.22% and 1.04%. Mongenot et al. (1996) report little to no effect on the concentration of trace elements in thermally mature organic rich shale, nor do Ross and Bustin (2009). It is thus presumed that the chemical signal has likewise been preserved in the Biri shale. In addition, Raiswell and Berner (1987) report an average TOC loss of 40% of type II and III kerogens in thermally mature organic rich shale of Devonian age or later. Due to the low TOC values in the Biri shale, determining the kerogen type is not possible, though sources of Proterozoic kerogen during Biri shale deposition are limited to type I and II since type III and IV kerogens are derived from vascular plants which did not arise until the Paleozoic. None-the-less, organic carbon loss can be inferred as a result of maturation of the Biri shale and TOC values may have originally been greater, but likely no more than 2% - 3%. TOC data from Biri shale samples taken near Øvre Rendal show TOC values averaging 3%, and Tucker (1983) report similar values (0.5% - 3.4%) from multiple locations throughout Hedmark basin, taken from organic rich limestone facies.

Correlation between TOC and TEs is used as an indicator of paleoredox conditions by numerous authors (e.g. Cruse and Lyons, 2004; Algeo & Lyons, 2006; Tribovillard et al., 2006; Algeo et al., 2007; Tribovillard et al., 2008; Ross and Bustin, 2009). Tribovillard et al. (2006) discuss how TOC- element

covariation may be related to depositional redox conditions, of which a brief synopsis is given here. No correlation of TOC with TEs indicates that the TEs were, for the most part, deposited with the detrital fraction under oxic-dysoxic conditions. Anoxic but not sulfidic conditions favor strong TOC- trace element covariation because trace element removal to the sediment is governed by the amount of suitable organic substrates available in the water column. Euxinic conditions favor weak correlation with TOC since TEs are reduced to their lowest valence state and are coprecipitated directly from the water column with oxyhydroxides and insoluble metal sulfides. Euxinic conditions usually result in strong enrichments of V, U and Mo with weak correlation to TOC.

Table 3. *Correlation coefficient (Pearson's r) between TOC and selected major and trace elements.*

Al	S	V	U	Mo	Mn	Zn	Ni	Cu	Co	Cr	Pb
0.50	0.51	0.70	0.23	0.60	0.10	0.29	0.35	0.58	0.48	0.37	0.55

Biri shale data show weak to no correlation between TOC and V, U, and Mo: (r^2) = 0.48, 0.05 and 0.37 respectively. Trace element – TOC correlation data from the Biri shale is given in Table 3 and illustrated in Figure 11. Among the possible reasons for poor correlation, the uniformly low TOC concentration is perhaps the best. Uniform data make statistical correlation difficult; samples from the Biri Formation show little variation throughout the section (COV = 0.207). Low TOC can be indicative of an intermittently anoxic or suboxic depositional environment and Algeo et al. (2007) also suggest poor correlation may be due to differential loss of TOC and Mo (specifically) during diagenesis and subsequent generation and migration of hydrocarbons upon thermal maturity.

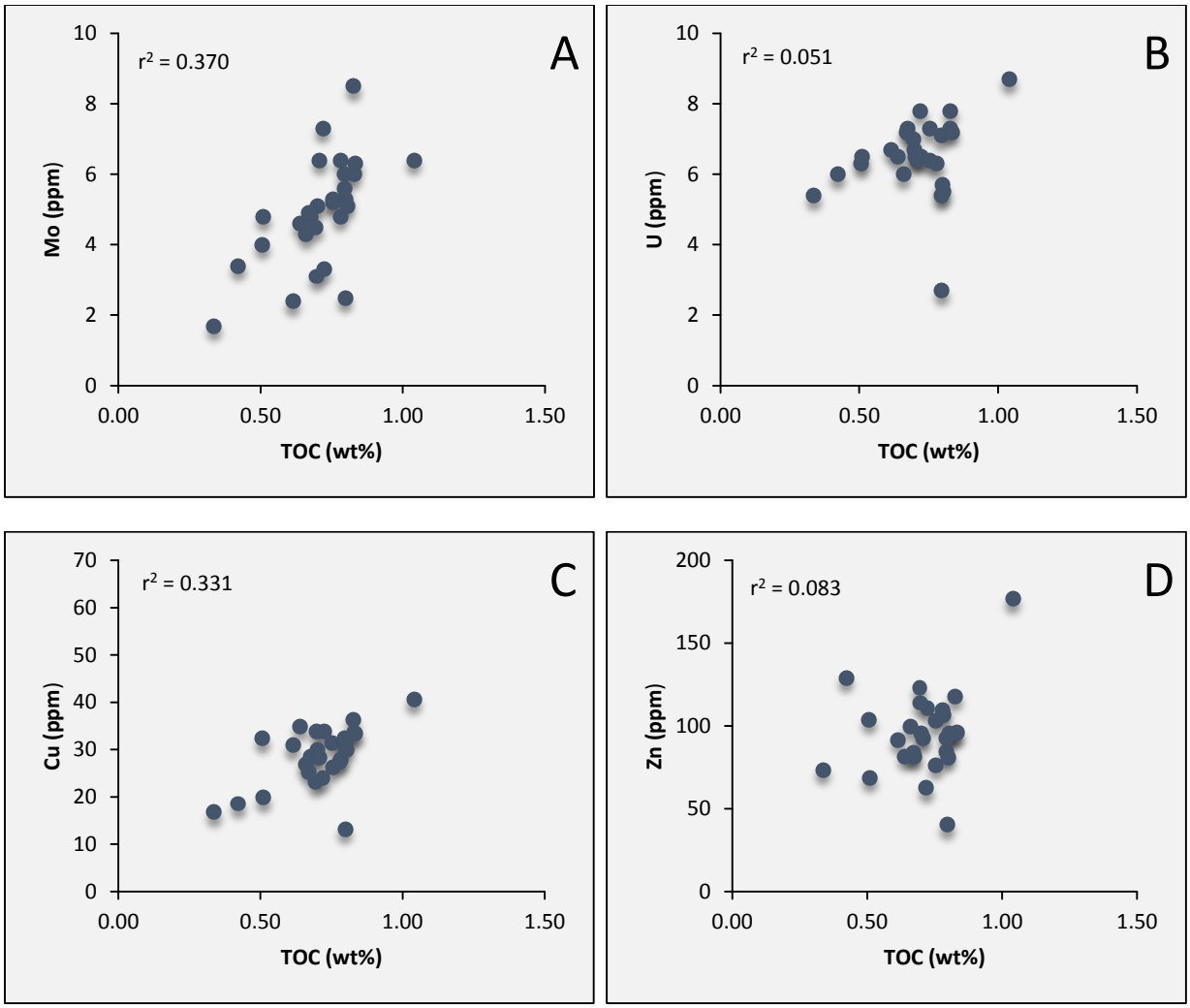

Figure 11. *Cross-plots of Mo, U, Cu and Zn with TOC*

5.5 ENRICHMENT FACTORS

An additional proxy for paleoredox conditions is the relative enrichment of a given element over world average values tabulated from multiple shale data sets. Enrichment factors (EF) here are calculated based on the average shale data gathered in Wedepohl (1971) and are given as:

$$EF_{element} = (element/Al)_{sample}/(element/Al)_{average\ shale}$$

where the average shale composition is derived from normal, oxic marine basins. Enrichments of U, Mo and Pb are modest (> 2), enrichments of Zn, Pb and Co are negligible, and V, Cu, Ni, Mn and Cr show depletion compared to average shale.

Table 4. Average TOC and Enrichment Factors for Biri shale trace elements.

	TOC	U	Mo	V	Zn	Co	Cu	Ni	Mn	Pb	Cr	Mo/U
AVG	0.678	2.55	2.52	0.89	1.38	1.00	0.86	0.49	0.68	1.65	0.46	1.05

U, Mo, Zn, and Pb have EFs > 1. Riquier et al. (2006) suggest that slight enrichment or depletion like those found in the Biri shale must be treated delicately because in such cases, enrichment of TEs isn't as unambiguous as it may be when EFs are orders of magnitude greater. Since the coefficient of variation for Al is small in Biri samples, reported EFs in the Biri are interpreted as realistic enrichments or depletions due to depositional redox conditions or other factors. Furthermore, for these purposes and the purpose of understanding post-depositional mobility discussed below, interpreting the relative amount of enrichment over the stratigraphic interval helps eliminate any bias that may be introduced as a result of normalization (Riquier et al., 2006).

V, Cu, Ni, Mn and Cr have EFs < 1. Elements showing depletion compared to average shale may be explained by depletion of these elements in the source terrain from which they are derived and relatively short marine residence times (except for Vanadium). Not only are these elements depleted compared to average shale (Figure 12), they are depleted compared to average crustal values. Sediments deposited in the Hedmark basin were most likely derived from Mesoproterozoic felsic granitic gneisses. As a result, some elements that were delivered to the Hedmark basin via riverine flux may have been depleted relative to global Neoproterozoic marine values, but short residence times may not have allowed for equilibrium mixing with marine water resulting in depleted EF values.

The modest enrichments of U and Mo can be interpreted to represent conditions during the time of deposition that favored removal to the sediment in relatively small quantities that were neither oxidizing nor extremely reducing (euxinic). The most likely conditions that resulted in these modest enrichments are described here, in consideration of the Mo/U ratio.

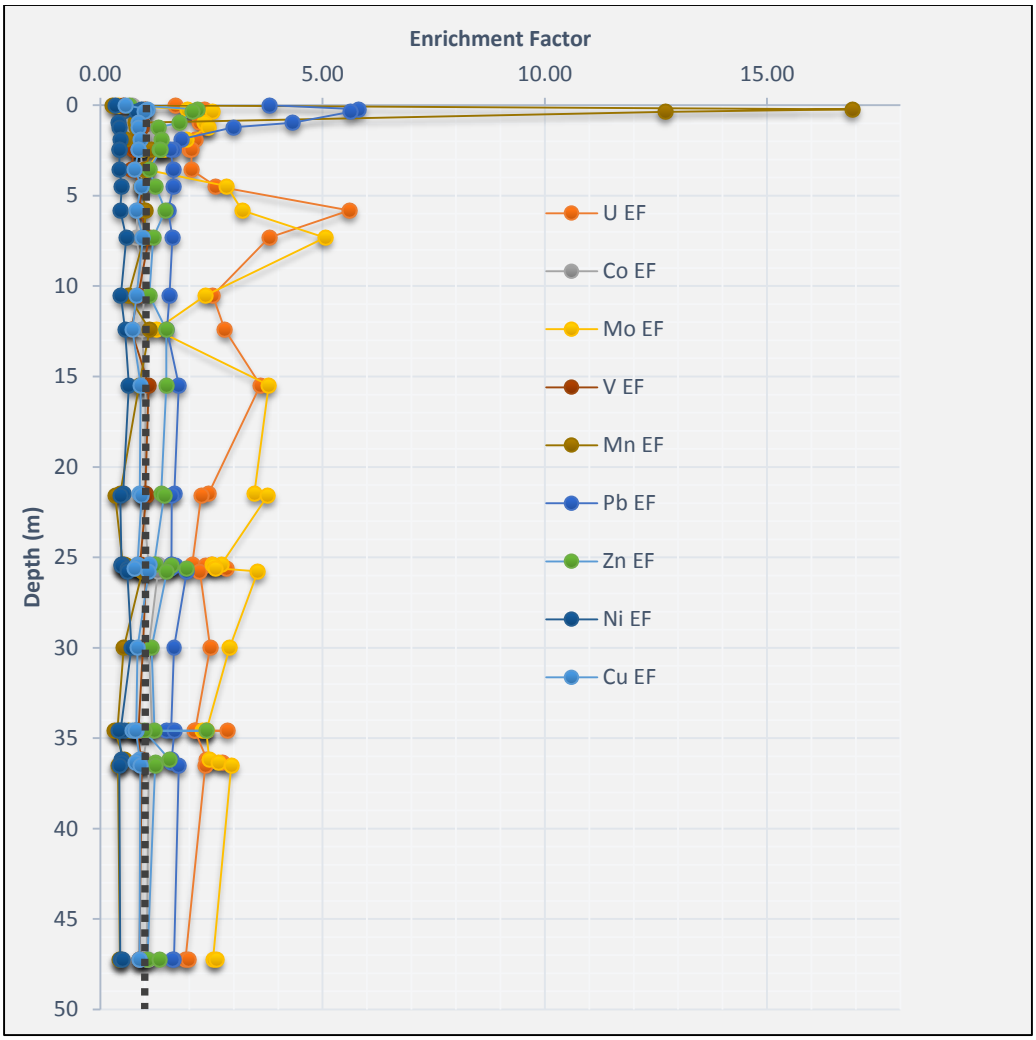

Figure 12. *Enrichment factors for selected trace elements plotted vs. depth. Black dashed line represents an enrichment factor of 1. Values above 1 are enriched compared to the World Shale Average (Wedpohl, 1971).*

5.6 USING THE ENRICHEMENT FACTOR MO/U RATIO

The ratio, EF_{Mo}/EF_{U}, has been used by Algeo and Tribovillard (2009) and Tripathy et al. (2014) based on the assumption that redox conditions will differentially pull down Mo and U according to the degree of anoxia or euxinia in the depositional setting. U is preferentially removed (compared to Mo) from seawater where low oxygen conditions prevail in bottom waters. Where euxinic conditions prevail, Mo is more effectively removed and fixed in the sediment as a result of the molybdate-thiomolybdate switch described above. Thus, under suboxic/anoxic but not sulfidic conditions, the Mo/U ratio will be

lower than those deposited under euxinic conditions. The modern marine ocean EF Mo/U value is 7.5 (Tribovillard et al., 2009 and references therein).

The EF ratio of Mo/U for Biri shales is ~ 1, indicative of preferential U removal over that of Mo in suboxic to anoxic bottom water conditions. Figure 13 illustrates this preferential removal mechanism and corresponds to the Biri EF Mo/U ratio of 1 as illustrated in Figure 14.

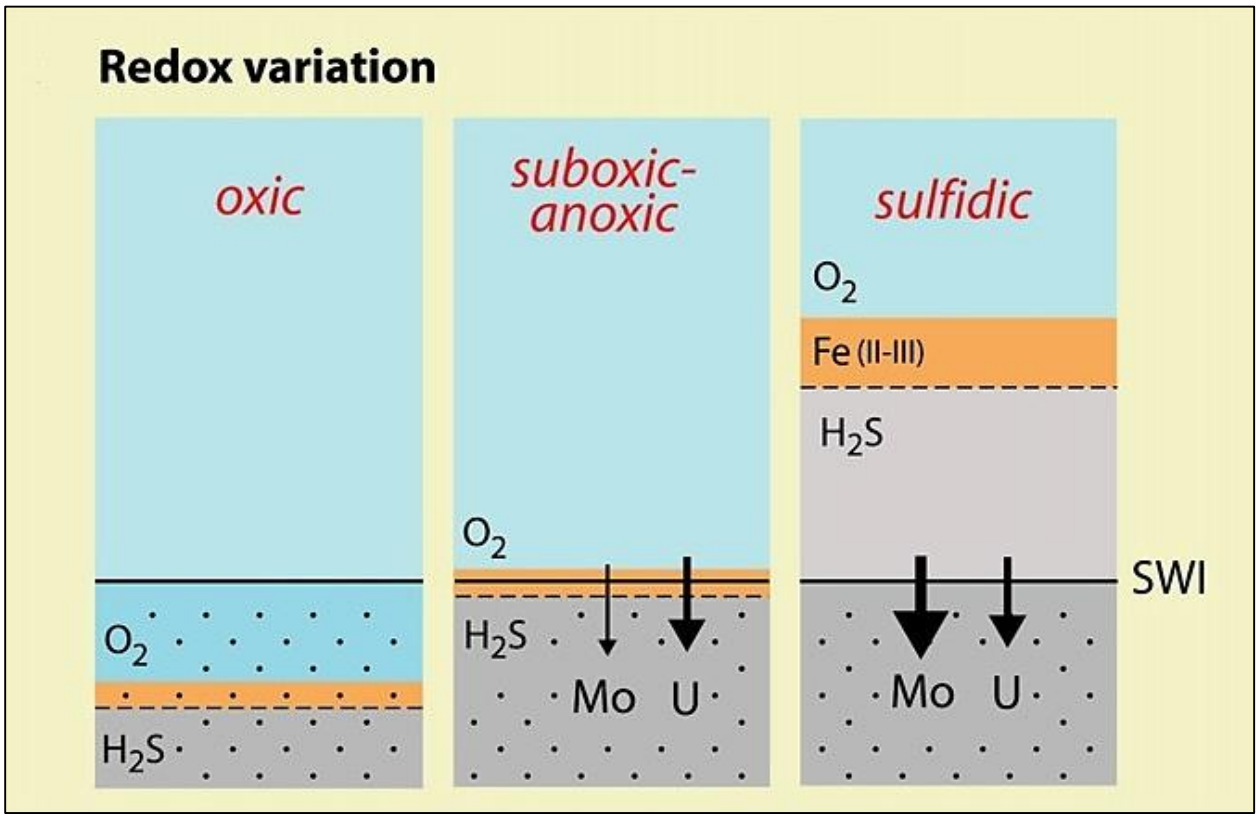

Figure 13. *Illustration demonstrating the degree to which Mo and U are differentially removed and sequestered in the sediment under different redox conditions. From Algeo and Tribovillard (2009).*

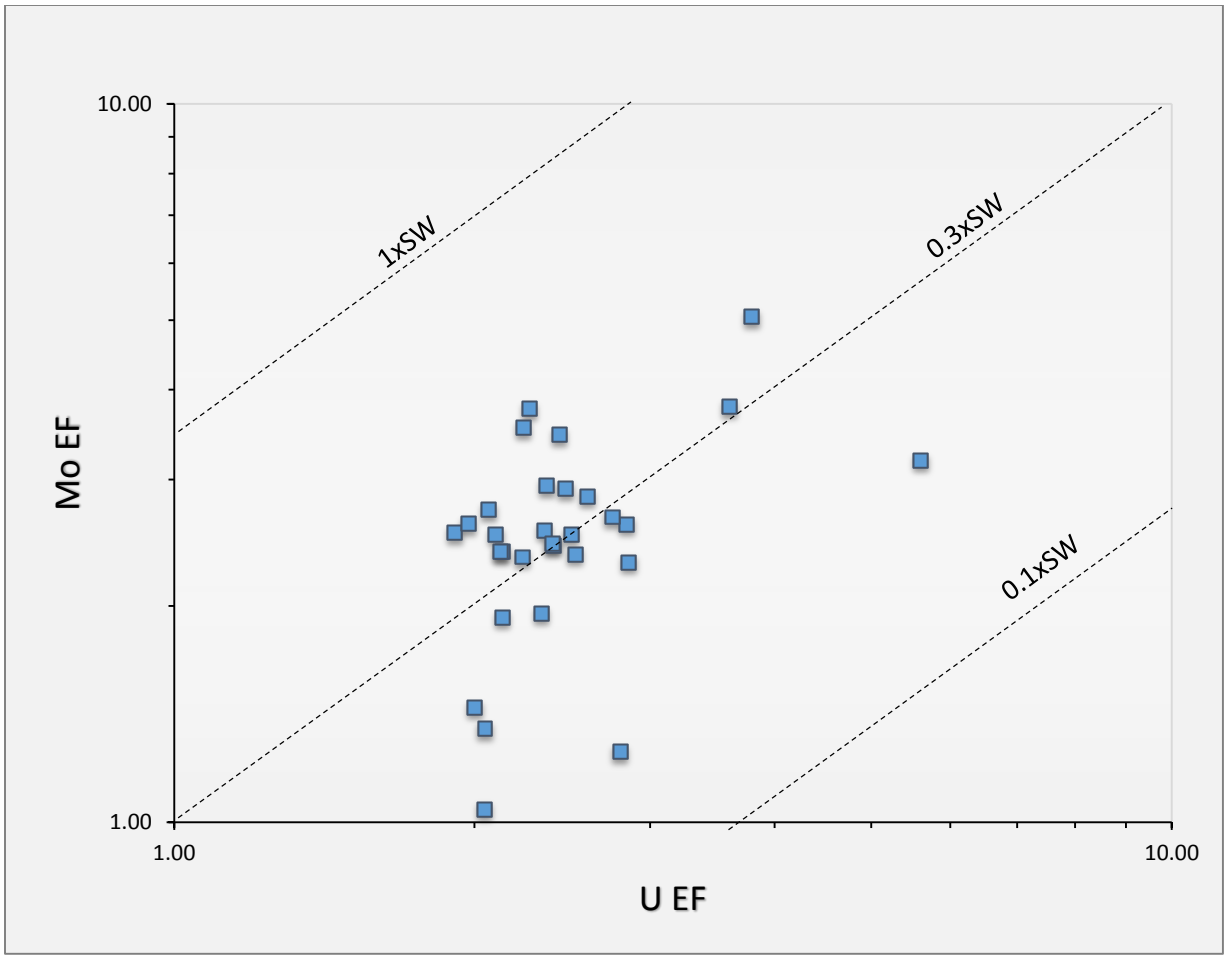

Figure 14. *Mo Enrichment Factor/U Enrichment Factor cross-plot showing the relationship of Biri values to that of modern sweater (1xSW).*

Besides the variables described above, sedimentation rate may also play a role in the variable depletion and modest enrichments of TEs. If sedimentation is slow and conditions are right for enrichment, the resulting condensed section can be significantly enriched in TEs. However, if sedimentation rate is relatively fast, TEs may be relatively diluted in the resulting host sediment, which may be the case for the Biri shale. One last consideration that must be taken into account is the relatively high carbonate content of the Biri shale discussed above. Biri shale contains on average ~ 30% carbonate, with values ranging from 5% to as high as 78%. Compared to a siliciclastic-dominated shale, carbonate mud-derived sedimentary rocks with high carbonate content are depleted in most trace elements.

5.7 EVIDENCE FROM PYRITE

Pyrite (FeS_2) is common in organic rich sediment and is a sink for redox sensitive TEs like U and As that are co-precipitated with or adsorbed on to Fe sulfides (Huerta-Diaz and Morse, 1992). The presence of pyrite is used often as an indicator of paleoredox conditions during deposition of oxygen-deficient ancient black shale and modern sediment. The most common uses involve determining the size and shape of pyrite through microscopy, and determining the amount of Fe within the sediment that has been incorporated into pyrite, known as the degree of pyritization (DOP) (Berner, 1970). Calculated DOP values derived from the ratio of pyrite Fe to total reactive Fe can be used to infer the redox conditions during deposition: values indicative of sediment euxinia (> 0.75), dysoxic (0.46 – 0.75) and oxic (< 0.46) (Raiswell and Buckley, 1988) are normally employed.

Pyrite morphology is used to indicate depositional redox through analysis of the size, shape, texture and distribution of accumulated pyrite. Pyrite occurs predominantly as single or aggregated framboids or euhedral crystals, and can also occur as a replacement of organic matter and morphological proportions are relative to a particular sedimentary system (Wilkin et al., 1996). Framboids, formed as aggregates of iron monosulfide microcrysts (Bond and Wignall, 2010) may develop within the water column at the oxic-anoxic boundary under euxinic conditions if the initial reaction rate is fast enough. Euhedral pyrite forms within the top few centimeters of the sedimentary column where the rate of reaction is slow enough to allow sulfide to react with other elements in the sediment to form pyrite (Roychoudhury et al., 2003). Data from modern sediments shows that euxinic conditions result in smaller framboids size (less than 4% of framboids are > 10 µm in diameter) as framboids form in the water column and reach 5 - 6 µm causing them to fall out of the water column and below the Fe-reduction zone where they cease growing (Bond and Wignall, 2010). Non-euxinic conditions produce larger framboids (more than 10% of framboids are > than 10 µm) (Wilkin et al., 1996; Wang et al., 2012) where framboids form within the surface sediment. Further discrimination between

syngenetic framboids (primary) produced in the water column or surface sediment, and diagenetic sedimentary pyrites (secondary) can be done on the basis of the size and shape (Bond and Wignall, 2010; Wang et al., 2012). Diagenetic pyrite is typically euhedral or amorphous, while syngenetic framboids are typically small and retain a framboidal texture. In ancient rocks, it is common to observe a diagenetic overprint of framboids, which in some case may increase the difficulty of using pyrite as a paleoredox proxy. However, Wignall and Newton (1998) show that the co-existence of primary framboidal pyrite with non-framboidal pyrite does not necessarily hinder pyrite use as a paleoredox indicator since framboid size distribution is not significantly changed by a diagenetic overprint.

Pyrite distribution is relatively consistent throughout the samples collected from the Biri shale. Framboids are pervasive in each sample while larger diagenetic, anhedral to euhedral crystals are dispersed but also persistent, some samples containing more than others. Figure 15 shows framboid size distribution from 3 thin sections; average framboid size ranges between 3 and 7 microns.

Based on the work of multiple authors and specifically that of Bond and Wignall (2010), framboid size distribution in the Biri shale indicates deposition under weakly suboxic to anoxic bottom waters in which H_2S existed below the sediment-water interface (Table 5).

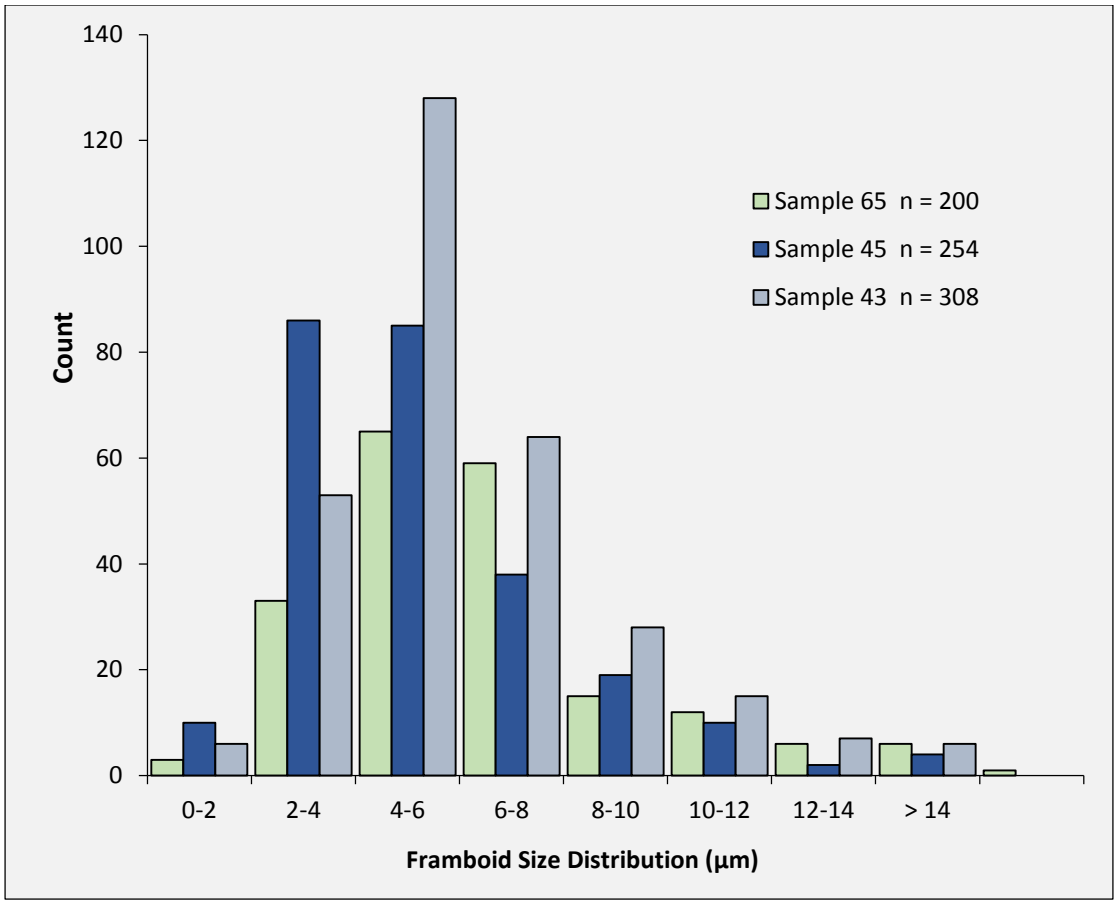

Figure 15. *Histogram of pyrite framboid size distribution from three samples. Sample 43 at .97 m, 45 at 1.87 m, and 65 at 36.52 m.*

Table 5. *Redox conditions and corresponding pyrite framboid size distribution. From Bond and Wignall (2010).*

Conditions	Framboid parameters	Sedimentary fabric
Euxinic (persistently sulfidic lower water column)	Small (mean 3–5 µm), abundant, with narrow size range. Framboids dominate pyrite fraction.	Finely laminated
Anoxic (no oxygen in bottom waters for long periods)	Small (mean 4–6 µm), abundant, with a few, larger framboids. Framboids dominate pyrite fraction.	Finely laminated
Lower dysoxic (weakly oxygenated bottom waters)	Mean 6–10 µm, moderately common, with a few, larger framboids and some crystalline pyrite.	Finely laminated with rare bioturbation
Upper dysoxic (partial oxygen restriction in bottom waters)	Moderately common to rare, broad range of sizes, only a small proportion <5 µm. Majority of pyrite as crystals.	Microburrowed. Bioturbation may obscure laminated fabric.
Oxic (no oxygen restriction)	No framboids, rare pyrite crystals.	Burrowed and/or massive

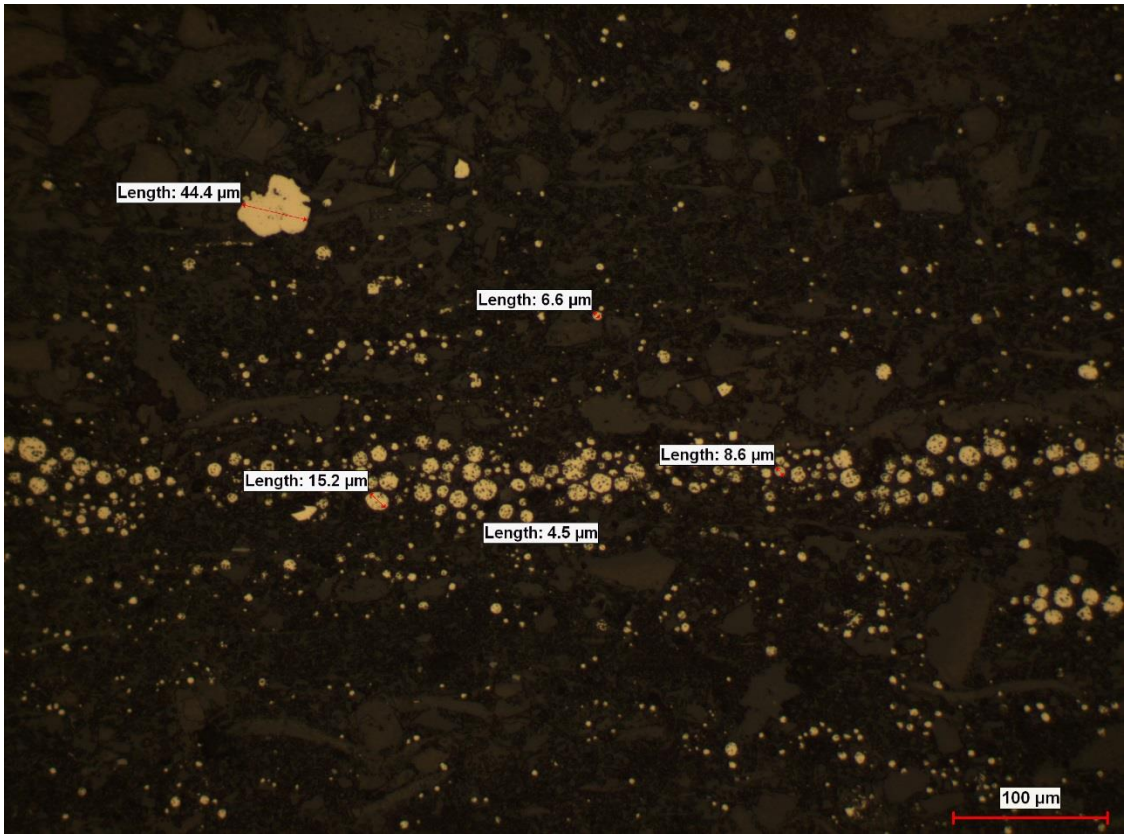

Figure 16. *Petrographic image of pyrite taken from sample 43 at 0.97 m depth showing the distribution of pyrite framboid sizes. A lamination with coarse framboids lies parallel to bedding. A diagenetic anhedral crystal is also pictured. Photo taken in PPL at 200x magnification.*

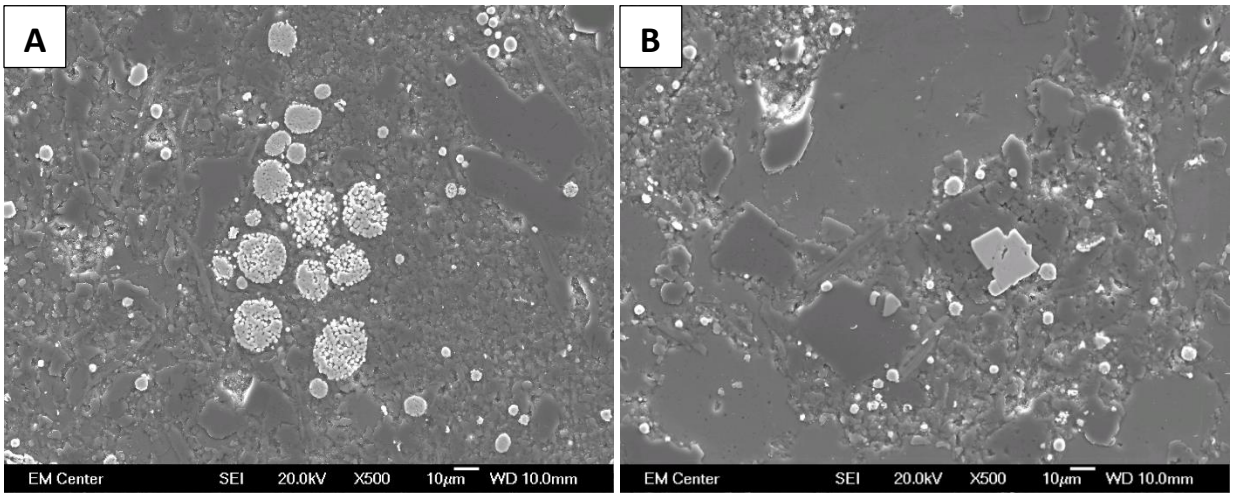

Figure 17. *SEM pictures of A.) Pyrite framboids and B.) Euhedral pyrite crystal surrounded by smaller framboids.*

5.8 CORRELATION WITH PREVIOUS WORK: HYDROGRAPHY AND DEPOSITIONAL SETTING

Mo shows the most promise as a paleoredox indicator in recent literature and in the Biri shale as well. It is likely that enough organic matter accumulated in the sediment to generate H_2S, establishing reducing conditions within the pore water that sequestered Mo (and U). Cruse and Lyons (2004) suggest that water column H_2S is not necessary for Mo enrichment in marine sediments. Biri Mo values are relatively low (Avg 4.5 ppm); Scott and Lyons (2012) suggest Mo values above crustal values of 1 – 2 ppm but below 25 ppm indicate an anoxic water column where the presence of sulfide is restricted to pore fluid. Low Mo enrichments may also be caused by basin restriction: such is the case in the Black Sea where TEs like Mo are subject to the "Basin Reservoir Effect" where depletion occurs due to strong euxinic conditions, in correlation with lack of TE replenishment from global marine waters (Tribovillard, 2006). Establishing the degree of water mass restriction or exchange in ancient marine basins necessitates a better hydrographic understanding of individual basins.

The Hedmark group formations have been well mapped and plausible restorations and inferences of the basin's original dimensions and hydrography have been done (Bjørlykke et al., 1976; Nystuen, 1981; Nystuen 1982; Morley, 1986). The Biri Formation itself contains large facies variation within limited distances of one another, indicative of a complex depositional setting: carbonate shelf facies transitions quickly to basinal facies. Continuous, outcropping sections are few, making detailed paleoenvironment reconstructions difficult (Bjørlykke et al., 1976).

The marine setting in which the Biri formation was deposited has been previously discussed by Bjørlykke et al. (1976), Tucker (1983), Nystuen (1987), and Vidal and Nystuen (1990). Bjørlykke et al. (1976) describe six distinct depositional settings from five different locations throughout southern Norway where the Biri Formation is exposed. Depositional settings include carbonate platform, platform margin and platform slope, intratidal to supratidal environment with tidal channels, protected environments, and deeper basin settings. Based on the lack of evidence for hypersaline conditions

except in the supratidal environment, the authors suggest the likelihood of unrestricted circulation of Hedmark basin and shelf environments with open marine waters to the west. From stratigraphically equivalent facies to the north containing gypsum and halite pseudomorphs, Vidal and Nystuen (1990) postulated that arid conditions prevailed for at least some time during deposition of the Biri Formation, giving credence to the idea that hypersaline conditions may have developed in some locations if the basin was restricted from circulation with marine waters to the west.

Tucker (1983) focused on the laminated, organic-rich limestone deposited around the basin margin in a shelf environment below storm wave base. He interpreted the deposition of the laminated limestone as taking place under suboxic to anoxic conditions brought about by increased productivity during the marine transgression, corresponding with the development of an oxygen minimum zone that allowed accumulation of organic rich sediment. He associated increased organic productivity with nutrients derived from flooding of the Precambrain basement during the transgression and by upwelling of deeper, nutrient-rich marine waters. Likewise, based on reconstructed basin morphology, Nystuen (1987) speculated that deposition of the Biri Formation took place where restricted circulation of bottom water created anoxic conditions at the sediment water interface.

Vidal and Nystuen (1990), offer two possible depositional scenarios for the Biri Formation based on micropaleontology and (apparent) absence of aerobic eukaryotic producers. The first agrees with that of Tucker (1983) in which cold, nutrient-rich marine waters upwelled from deeper parts of the basin creating plankton blooms and disrupting an otherwise oxygen-depleted water body. The second hypothesis suggests that deposition occurred in stratified suboxic basins with high concentrations of H_2S under a shallow chemocline. In this scenario, anoxygenic photosynthetic bacteria were the primary producers instead of oxygenic cyanobacterial phytoplankton.

Geochemical evidence from both the Djupdalsbekken locality and samples taken at Øvre Rendal generally support the hypothesis that during deposition of the upper member of the Biri Formation the

main graben of the Hedmark basin was fully connected to open marine waters to the west. Data from the two locations (Table 6) reveal distinct differences, notably in TOC content, and distinct similarities in Mo and other TE concentrations. The Djupdalsbekken locality in the Biri district lies within the main graben and shows geochemical similarities to modern continental margin upwelling zone analogs, specifically the Namibian shelf described by Algeo and Lyons (2006). The Namibian shelf and places with similar hydrography have unrestricted water mass circulation. Algeo and Lyons (2006) report low Mo/TOC ratios ($\sim 6 \pm 3$) reflecting low Mo removal per unit of organic content. The authors suggest that the low ratio, in an environment with unrestricted renewal of Mo, is caused by insufficient H_2S in the water column to reach the critical threshold of H_2S concentration necessary for conversion of molybdate to thiomolybdate. The Namibian shelf and similar environments, it is thought, are subject to enough upwelling and subsequent water mass exchange to prevent H_2S from building up in the water column. Although organic rich, the Namibian shelf exhibits mainly non-euxinic, anoxic to suboxic conditions (Algeo and Lyons, 2006).

There is no definitive evidence to determine whether or not the Hedmark basin was openly connected during the entirety of Biri deposition, or whether there was some degree of limited, periodic restriction. Biri Mo/TOC values at Djupdalsbekken average 7 ± 3, similar to that of the Namibian shelf, indicating free circulation with the open ocean to the west. Also in agreement are the geochemical indicators showing a suboxic to anoxic benthic water column with a chemocline at the sediment water interface and some amount of pore water H_2S. These results coincide with the previous work done by Bjørlykke et al. (1976), Tucker (1983), and Vidal and Nystuen (1990).

Geochemical data from the Biri Formation taken at Øvre Rendal is less conclusive. Paleogeographic reconstruction of the evolution of the Hedmark basin by Nystuen (1987) following on the work of Sæther and Nystuen (1981) and Nystuen (1982) shows evidence of subbasin development at Øvre Rendal and in the Bjørånes area (

Figure **18**). At Øvre Rendal, TOC is significantly higher while Mo values are consistent with those at Djupdalsbekken, with a resulting Mo/TOC on average ~ 2. Nystuen (1982) suggests that the ~ 10 km long sub basin at Øvre Rendal and ~ 25 km long Bjørånes subbasin were connected to some extent to one another and to the larger Hedmark graben, but that both were stagnant and anoxic as evidenced by the high TOC and the pyritic black shale found at both locations (Nystuen, 1982). Trace element geochemical evidence in these likely silled, restricted subbasins supports the outcrop evidence: low Mo/TOC values (~ 2) are likely a result of Mo drawdown into the sediment without adequate resupply from open ocean waters, the "Basin Reservoir Effect" best illustrated by the modern day Black Sea. The enrichment in pyrite at Øvre Rendal, clearly seen in hand sample, is likely indicative of strongly euxinic conditions, in which the counterintuitive relationship between increasingly sulfidic conditions and lower Mo sequestration was active (see Algeo and Lyons, 2006). Alternatively, if these subbasins were connected enough to sufficiently resupply Mo, low Mo per unit of organic content may be a result of sedimentary Mo dilution in a subbasin that saw high bioproductivity and underwent fast, tectonically controlled subsidence compared to the main Hedmark basin (Sæther and Nystuen, 1981).

Under these two different depositional settings, it seems plausible that both interpretations developed by Vidal and Nystuen (1990) are correct, one at Djupdalsbekken where oxygenic cyanobacterial phytoplankton were the primary producers, but were not preserved (see Vidal and Nystuen, 1990), and one at Øvre Rendal where anoxygenic photosynthetic bacteria were the primary producers in a sulfide-rich water column.

The possibility that Mo concentrations were low relative to modern values during the Neoproterozoic and during deposition of the Biri Formation may be a complicating factor (Scott et al., 2008). In this case, more caution may be needed when using Mo as a paleoredox indicator and when comparing the Mo/TOC relationship of the Biri to modern analogs like the Namibian shelf and Black Sea. Fike et al. (2006) show evidence that the Neoproterozoic ocean became increasingly oxygenated after

the Marinoan glaciation event (~ 635) and Scott et al. (2008) bracket deep ocean oxygenation between 662 and 551 Ma, with modern redox conditions established by 551 Ma. Deep ocean oxygenation created a decreased sink for marine Mo which correspondingly raised the global Mo concentration to modern values (100 nM) from earlier Proterozoic values (10 - 20% below modern values) (Scott et al., 2008). This time-span brackets deposition of the Biri Formation, suggesting that Mo concentrations in the Hedmark basin marine waters may have been lower compared to that of modern concentrations. In this case, the relatively low Mo values in the Biri shale at both locations may be a result of comparatively depleted marine concentrations in the late Neoproterozoic. The same may be said for the marine U budget in the Neoproterozoic ocean. Low U enrichment during the deposition of the Biri shale may be attributed to lower marine U values that resulted from widespread ocean anoxia (Partin et al., 2013). Sahoo et al. (2012) suggest a more precise time for the rise of ocean oxygen near the end of the Marinoan glaciation around 632 Ma. If this earlier date suggested by Sahoo et al. (2012) is accurate, at the time of Biri shale deposition oceanic oxygen conditions would have been similar to contemporary values, and thus Mo and U concentrations also. In any respect, a multitude of additional paleoredox proxies indicate deposition under sub-oxic to anoxic conditions at the Djupdalsbekken locality and under euxinic conditions in the Øvre Rendal subbasin.

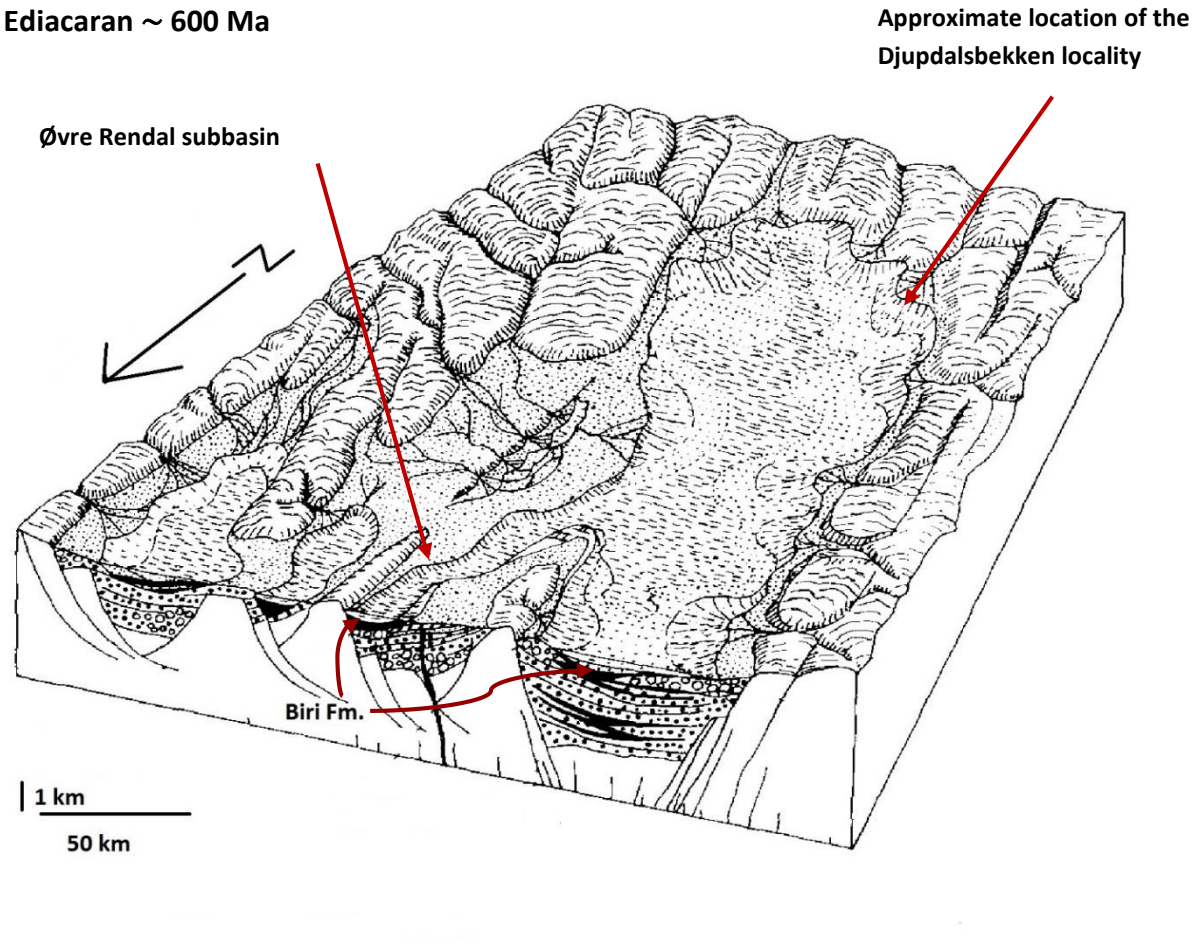

Figure 18. *Illustration of the Hedmark basin and emergence of subbasins during the mid-Ediacaran Period. After Nystuen (1987).*

Table 6. *Selected major and trace element data from the Biri shale at Djupdalsbekken and Øvre Rendal*

	Djupdalsbekken	Øvre Rendal 1	Øvre Rendal 2
TOC	0.68	2.68	2.59
Al_2O_3	11.91	21	19.79
MnO	0.07	0.04	0.07
Fe_2O_3	4.57	2.58	7.82
MgO	1.29	1.38	1.86
P_2O_5	0.01	0.05	0.29
CaO	16.6	0.02	0.37
S	2.35	0.56	3.02
Mo	4.92	< 5	6
U	6.86	< 10	< 10
V	85.03	115.5	119
Zn	96.08	36.17	62.5
Cu	28.7	< 10	23.5
Ni	24.3	6	34
Co	14.04	< 5	23
Cr	30.43	33.83	46
Pb	27.06	27	37.5
Ba	218.1	1273	1062
Th	17.31	26.7	19
Mo/TOC	7 ± 3	1.8	2.3

Finally, numerous authors recommend a degree of caution concerning the use of paleoredox indicators. Among the reasons perhaps the most important is that there may be more than one controlling factor on a given trace element enrichment. MacManus et al. (2006) show how enrichment of Mo and U are variably dependent on multiple variables including organic carbon cycling, sulfur burial rate and bottom water redox conditions. Assuming steady state redox conditions, authigenic accumulation of TEs is influenced by factors including the sedimentation rate of the siliciclastic fraction, the rain rate of organic matter to the seafloor which may include variation in organic matter type, and variation in intra-basinal hydrothermal TE sources (Algeo and Lyons, 2006). All may vary temporally and spatially within a single basin. Thus, a 1:1 correlation may be misleading. Similarly, correlation between two TEs may be a result of an indirect relationship, one that may be indicative of the host phase (e.g. similar depletion in carbonate-rich samples) (Georgiev et al., 2012) and thus, as used here, a multi-proxy

approach in conjunction with a knowledge of the geology and hydrography of the basin is suggested, helping to protect against potentially misleading correlations.

CHAPTER 6. DISTURBED RE-OS ISOTOPE SYSTEMATICS AND POST-DEPOSITIONAL TRACE ELEMENT MOBILIZATION

6.1 DATING THE MOELV TILLITE: GENESIS OF BIRI SHALE TRACE ELEMENT GEOCHEMISTRY

The Neoproterozoic geologic record documents (arguably) three distinct glacial events recorded by corresponding glacially-derived deposits, commonly tillite and diamictite. Debate regarding the extent of these glaciations remains, but recent work suggests that the Sturtian (~ 711-685 Ma) and Marinoan (~ 635 Ma) were likely global events – the "snowball earth" described by Schrag et al. (2002), while the latest, regionally correlated Gaskiers glaciation (~ 580 Ma) was likely smaller in extent (Knoll, 2000; Halverson, 2005; Hoffman and Li, 2009).

In southern Norway, the glacially derived Moelv tillite is thought to represent the Varanger glaciation and is generally correlated to the Gaskiers glaciation (Hannah et al., 2007). The age, however, is not well constrained, and some authors suggest the Varanger glaciation occurred as two discrete events (Kaufman et al., 1997). Bingen et al. (2005) obtained dates from detrital zircons within the underlying Rendalen Formation from paired U-Pb and Lu-Hf isotope studies, but the resulting dates ranging from 677 ± 15 to 620 ± 14 Ma are not well constrained. The youngest age (620 ± 14 Ma) places a maximum age for the overlying Moelv tillite, leaving open the possibility of a Gaskiers age for the glaciation. To refine this age, Hannah et al. (2007) dated the Biri formation at Djupdalsbekken using Re-Os isotope signatures which yielded a much younger, 560 ± 4 Ma maximum age. Additional Re-Os data collected near the contact with the overlying Ring Formation resulted in dates with much less precision: 665 ± 54 Ma. Here, I attempt to explain why some sections of the Biri shale yield well constrained dates and why some do not, using trace element (TE) geochemical signatures. Identification of post-depositional changes within redox-sensitive TE concentration profiles may indicate the reason for disturbed and undisturbed Re-Os isotope systematics in the Biri shale. Ultimately, this work provides a

background to constrain the age of the Moelv tillite in an attempt to refine our understanding of regional and globally correlated Neoproterozoic glaciations.

6.2 POST-DEPOSITIONAL MOBILIZATION OF REDOX-SENSITIVE TRACE ELEMENTS

The discussion on the depositional setting of the Biri Formation given above is predicated on TOC and TE data representing depositional conditions without post-depositional disturbance. In this case, trace elements remain immobile in a closed system and offer an accurate signature of their distribution and concentration in the sediment at the time of deposition and early diagenesis. If post-depositional disturbance occurs through re-oxygenation of the sediment, once sequestered (reduced) TEs become mobile (oxidized). This may occur relatively soon after deposition (e.g. via turbidite/gravity flows), long after deposition similar to conditions that produce roll-front uranium deposits or Mississippi Valley type deposits, or ultimately during weathering upon exposure at the earth's surface (e.g. Georgiev et al., 2012). The degree and depth to which oxidizing agents penetrate determines the level to which redox-sensitive elements are remobilized. Uranium is particularly susceptible to remobilization and is dependent on the O_2 concentration (Zheng et al., 2002) while V, Cd and Mo are susceptible to a lesser degree (Morford, 2001).

Undisturbed Re and Os in the system act as a high precision geochronometer, and indicate the timing of organic-rich sediment deposition. If re-oxygenation occurs the geochronometer may be disturbed, resulting in Re-Os dates that do not reflect the timing of deposition, but the timing of remobilization and subsequent fixation, if it occurs. Similarly, other remobilized TEs may be lost to the overlying water column if early oxygenation occurs, or to any later, oxygen-rich fluid moving through the sediment. Vertical redistribution within the sediment column can result in concentration profiles with peaks at the interface between oxidizing and reducing sediment (Thomson et al., 1998).

The same TEs useful in identifying paleoredox conditions are often those that can be remobilized. Individual elements behave uniquely based on their valency in the sediment during re-

oxygenation; oxidized or reduced forms show differential aptitude for adsorption or precipitation reactions with sulfides and/or Fe-Mn oxyhydroxides (Colodner et al., 1992). This results in a diagenetic redistribution of varying magnitude and spatial arrangement between elements (Thomson et al., 1993). Commonly used indicators of active or relict oxidation fronts include Mn, Re, Mo, U, Cd, Se, Ag, Ba, and also TOC.

Most of the work done on post-depositional mobility with these redox-sensitive trace elements has been done with cores taken from deep sea sediments and turbidite sequences in such locations as the Cape Verde Abyssal plain (Colley et al., 1984) the Madeira abyssal plane (MAP) turbidite (Colley and Thomson, 1985; Cowie et al., 1995; Rosenthal et al., 1995; De Lange et al., 1998 (ODP); Crusius and Thomson, 2000, 2003), the Southern Nares abyssal plain (Buckley and Cranston, 1998) and the eastern Mediterranean sapropels (Higgs et al., 1994; Thompson et al., 1995; Rinna et al., 2003). As a result, the studies are based on relatively young re-oxygenation in (sometimes unconsolidated) sediment; the oldest section studied reveals post-depositional mobility of TEs in a 14 m.y. old turbidite (De Lange, 1998). Alternatively, remobilization during subaerial weathering may also result in TE patterns similar to those found in turbidites (Jaffe et al., 2002). Here, an attempt is made to identify a relict oxidation front in the ancient marine Biri shale (~ 560 Ma) based on TE patterns described by various authors as they have been found in much younger marine sediments.

6.3 TRACE ELEMENT DATA FROM THE BIRI SHALE

TE data gathered from the Biri shale at the Djupdalsbekken locality appear to show a relict oxidation front, based on the distribution of major and minor elements and subsequent, identifiable patters of enrichment and depletion. Unlike the discussion above on the paleoredox setting of the Biri shale, data presented here include data for the first three samples. One of the hurdles to identifying a relict oxidation front in the Biri shale is the varying CO_3 content between samples. Unless otherwise

noted, the data presented here have been corrected for variable CO_3 contents using the methods given in section 3.8.

6.4 MAJOR AND TRACE ELEMENT CONCENTRATION PROFILES

Figure 19 shows the concentration profiles for Mn, Fe, U, Mo, Re and TOC over the sampled section. Fe and Mn are presented as unmodified data (not normalized) and show the position of the dolomitized, Mn-rich zone at the top of the Biri shale, indicated by blue shading. Fe concentrations (~ 2 wt. %) are depleted in this zone, as are S concentrations (~ 0.65 wt. %) compared to samples above and below and as a result, this zone contains correspondingly little pyrite. Relatively constant TOC concentrations show that variations in Mo and U concentrations are not due to variations in TOC content. Enrichment of Mn at the top is discussed at length below.

Of interest are the distributions of U and Mo which are both susceptible to being remobilized by re-oxygenation of the host rock, U more than Mo (Tribovillard et al., 2006; McManus et al., 2006). Overlain on the concentration profiles in Figure 19 is an approximation of the extent to which a redox front penetrated through the Biri shale, indicated by the gray shading. The oxidation front remobilized formerly sequestered U and Mo and re-deposited them near meters 6 and 7 as the reducing capacity of the Biri shale increased. Re-deposition at the lower extent of the oxidation front as it penetrated through the rock created concentration peaks for both U and Mo at this depth in the sediment, while conditions deeper in the sediment remained reducing.

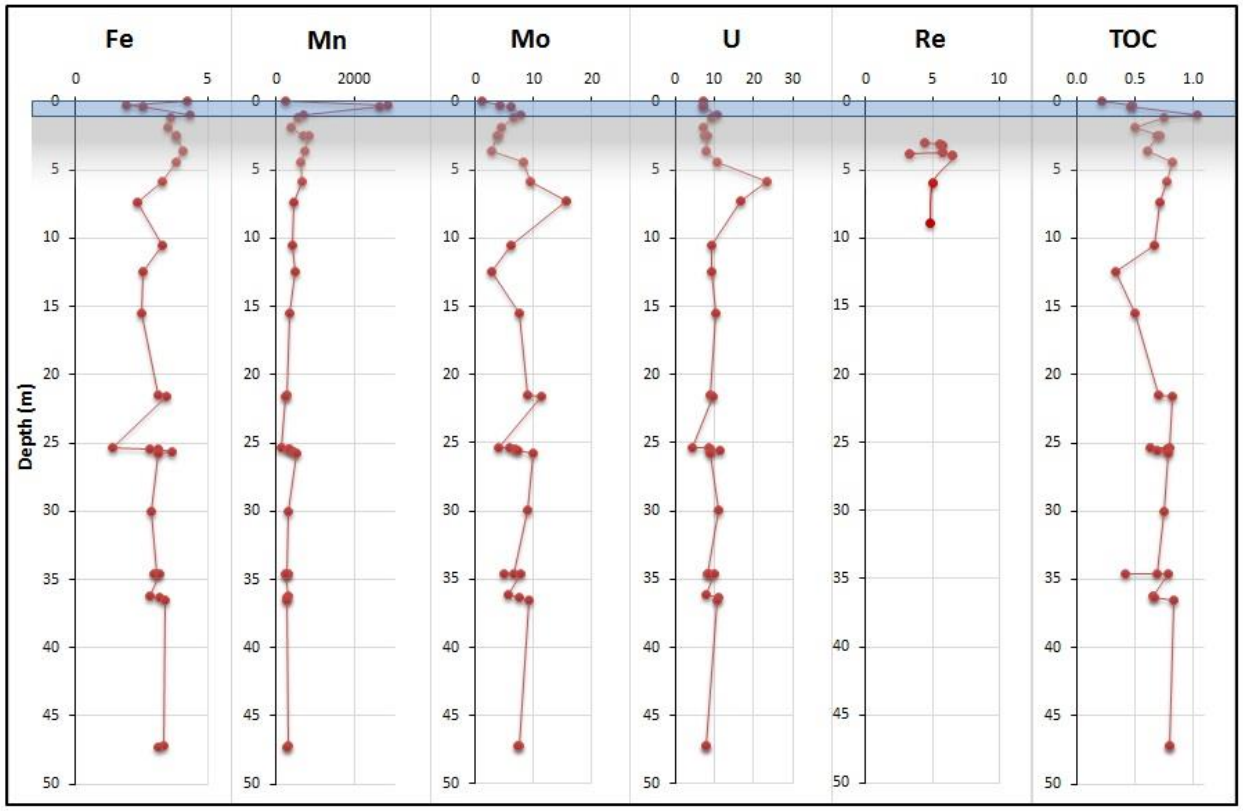

Figure 19. *Concentration profiles for select major and minor trace elements, as well as TOC. Fe, Mn and Re are presented as unmodified data, while Mo and U have been normalized to the CO_3 content. Fe and TOC are in wt. %, Mn, Mo, U are in ppm, and Re in ppb. Blue shaded area indicates dolomitized zone and gray shaded area represents the approximate extent of oxidation.*

The high CO_3 (~ 70 %) samples 41 and 42 at 0.22 m and 0.37 m, respectively, compared to an average of ~ 34 wt. % for other samples, may be categorized not as shale but as an argillaceous limestone. The enrichment of Mn in these surface samples likely resulted from a purification process of Mn within the sediment. This process occurs as particulate Mn and Fe oxyhydroxides accumulate at the sediment water interface (under a relatively oxic water column) where they are subsequently buried in the sediment. Bacterially-mediated oxidation of the organic matter in the sediment causes conditions within the upper horizon to become reducing, and Mn-Fe-oxyhydroxides are reduced to form free Mn^{2+} and Fe^{2+} species in the sediment pore water (Okita et al., 1988). Mn^{2+} and Fe^{2+} anions migrate through the sediment until they encounter an oxidation front where they may be recrystallized as oxyhydroxides

and become fixed in the sediment once again. Fe species are likely to be removed from solution by precipitation of pyrite (Force and Maynard, 1991) and so compared to Mn species, less Fe makes its way back to the surface horizon resulting in much larger Mn concentrations in surface oxyhydroxides. In this way "zone refining" concentrates Mn at the top while depletion occurs at greater depth (Calvert and Pederson, 1996). This effect was likely in place to some extent during formation of the Biri shale and was effectively stopped when deposition of the overlying Ring Formation conglomerate began. As a result, Mn concentrations in the surface horizon are 5 to 6 times greater than average concentrations in the underlying horizons. A closer look at the Mn profile given as the Mn enrichment factor in Figure 20 reveals a statistically significant change in Mn enrichment near meters 6 and 7. This may be indicative of an oxidation front that lost its oxidative quality as it penetrated deeper in the sediment, resulting in precipitation of Mn oxyhydroxides (Thomson et al., 1995).

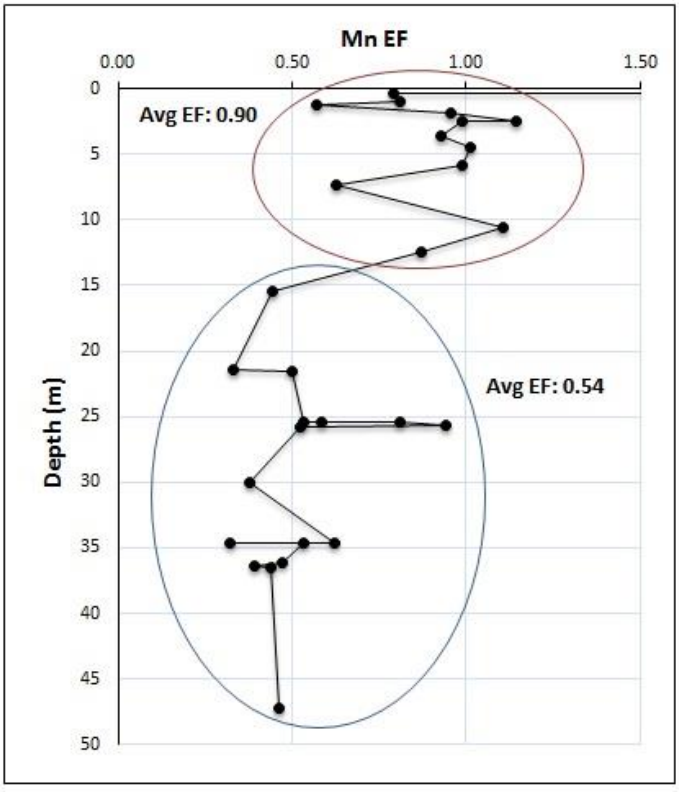

Figure 20. *Mn enrichment factors show average values near 1 in the upper section of the Biri shale.*

6.5 PLACEMENT OF THE OXIDATION FRONT: EVIDENCE FROM PYRITE, MANGANESE AND $\delta^{13}C$

Pyrite morphology, manganese concentrations and $\delta^{13}C$ values provide the evidence for the placement and thus timing of a mechanism which caused oxidation in the upper meters of the Biri shale. The previously described shale, carbonate, and siltstone horizons, as well as the Ring Formation are shown in Figure 21 which illustrate this evidence.

Ring Formation

Ring Formation Siltstone

Biri Formation: Carbonate-rich portion at the top overlying black shale.

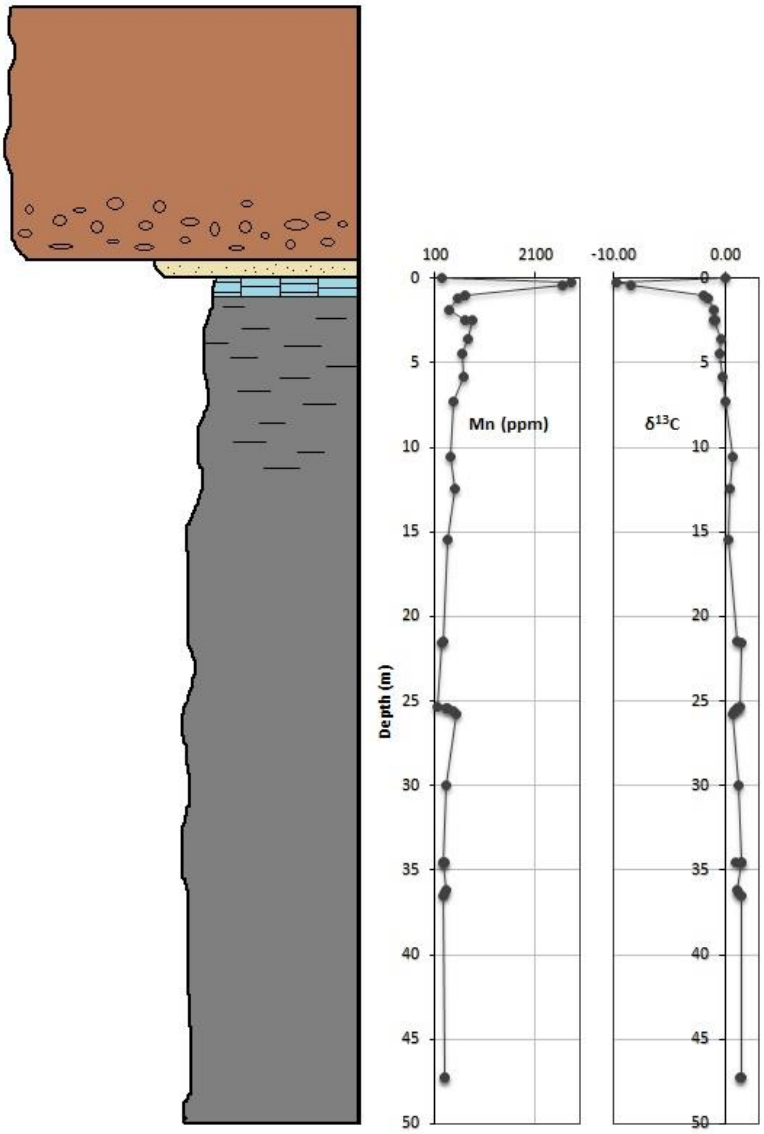

Figure 21. *Sketch of a stratigraphic column with Mn and $\delta^{13}C_{inorg}$ profiles.*

Primary carbonate precipitated from normal marine waters contain $\delta^{13}C_{inorg}$ values near 0 ‰, whereas organic carbon in the sediment is significantly depleted in $\delta^{13}C$ (Okita et al., 1988). Organic carbon from the Biri shale has typical low $\delta^{13}C_{org}$ values, averaging ~ - 32 ‰. $\delta^{13}C_{inorg}$ (CO_3 carbon) values obtained from the Biri shale hover around 0 ‰ (± 2 ‰) except in samples 41 and 42 with values of - 8 ‰ and -9 ‰ respectively. These values represent mixing of organically derived C ($\delta^{13}C_{org}$ ~ - 32 ‰) and inorganic C ($\delta^{13}C_{inorg}$ ~ 0 ‰). This indicates oxidation, remineralization and contribution of C_{org} to the inorganic CO_3 with roughly one fourth of the C (as CO_2) contributed by organic carbon. This can occur by Mn, Fe, or sulfate reduction-oxidation reactions with C_{org} or by O_2 penetration and oxidation, though Canfield et al. (1993) show that oxidation by O_2 penetration occurs only to a limited extent. With the (relatively) small amount of Fe and S (bound in pyrite) in these samples, it is more likely that C_{org} was oxidized by the reduction of $MnO_2 \rightarrow Mn^{2+}$, though oxidation by sulfate reduction can't be ruled out. Mn-oxides that were accumulating in the first centimeters of the sediment were available for this redox reaction with organic matter which occurs by the reaction:

$$CH_2O + 2MnO_2 + 3CO_2 + H_2O \rightarrow 2Mn^{2+} + HCO_3^- \text{ (Okita et al., 1998)}$$

The resulting formation of Mn^{2+} and isotopically light HCO_3^- allowed these species to become available to either be flushed from the system and/or re-deposited: Mn as Mn-oxides or, both Mn^{2+} and HCO_3^- to be incorporated into the CO_3 found in these samples. The relatively small amount of Mn in these samples (~ 0.3 wt. %) compared to concentrations found in manganese ore (~ 30 wt. %), and manganese carbonate (~ 8 - 10 wt %) (Okita et al., 1988) means that the high CO_3 content was not a result of supersaturation of Mn^{2+} in pore waters and subsequent diagenetic precipitation of Mn carbonate (Calvert and Pederson, 1996). More likely, the high carbonate content was a result of the transition from outer shelf deposition to shallower conditions and the deposition of CO_3-rich muds where available Mn was diagenitcally substituted into the lattice structure of the calcite as $Ca(Mn)CO_3$. Although not unequivocal, results from SEM-EDS elemental mapping show that the Mn content

corresponds to the carbonate fraction of these samples (41 & 42). In addition, there is very strong inverse correlation between the Mn concentration and the $\delta^{13}C_{inorg}$ values throughout the Biri shale (r^2 = 0.92) as illustrated in Figure 21, similar to that shown by Okita et al. (1988) and Force and Maynard (1991). The decreasing $\delta^{13}C_{inorg}$ values observed in the upper meters of the Biri shale plausibly indicate an increasing contribution of CO_2 from the MnO_2 redox reaction with C_{org}.

These reactions occur under reducing conditions which places a syndepositional chemocline at the sediment water interface, as indicated previously. The presence of pyrite framboids in both the CO_3-rich samples and also in the overlying siltstone is further indication that these upper sediments were deposited in conditions that quickly became anoxic and reducing within the sediment, but beneath a relatively oxygen-rich water column. These lines of evidence indicate that re-oxidation of the sediment must have occurred post-deposition. The overlying, likely well-oxygenated Ring Formation is the most plausible source of oxygen-rich fluid, interpreted to be deposition of submarine and subaerial prograding marine fan deltas (Bjørlykke et al., 1976). Thus, reoxdiation of the Biri shale may have occurred syn-depositionaly to the Ring Formation, or at some time afterward.

6.6 DEVELOPMENT OF AN OXIDATION FRONT

The oxidation front may have formed either syn-depositionally with oxic sediments of the Ring Formation, or post-depositionally from oxic waters in the Ring Formation and overlying sedimentary units. Here it is argued that the post-depositional possibility occurred during the Caledonian orogeny. Because it is likely that deposition of the Ring Formation occurred by oxygen-rich, prograding conglomeratic sediment, deposition of the Ring Formation provides a viable source for oxygen. Alternatively, if fluids were expelled from the overlying sediment during the Caledonian orogeny, it is plausible that those fluids had been hydraulically recharged in the overlying sedimentary units from meteoric waters and were oxygen-rich. Fluids expelled during orogenic events have been postulated where sediments are buried beneath thrust sheets (Oliver, 1986), and orogenic fluid expulsion

(dewatering) has been linked to the development of Mississippi Valley-type lead-zinc deposits during convergent tectonism (Cathles and Smith, 1983; Leach and Rowan, 1986).

6.7 EVIDENCE FOR LATER FLUID FLOW: DOLOMITIZATION IN THE BIRI SHALE

In the northern and eastern margin of the basin, dolomite found at the top of the Biri Formation is interpreted as early diagenetic: Nystuen (1982) suggested that the dolomite at the top of the Øvre Rendal section was formed under a shallowing basin near the end of the depositional period of the Biri Formation. Paleo-reconstruction of the basin indicates this may be the case (arid climactic conditions are also indicated) by deposition in a shallow tidal flat (epeiric platform) during the marine regression that marks the end of Biri deposition. In the western and southern margin of the basin at the Djupdalsbekken locality, deposition of the Biri shale was likely in a lower, open shelf environment that transitioned to a shallower shelf setting toward the end of Biri deposition (Figure 22). This is supported by petrographic evidence that shows a lower energy setting deeper in the section, contrasted with a higher energy setting in the upper 1-2 meters under the contact with the Ring Formation. Interpretation of the Ring Formation as deposition of coarse clastics by prograding marine fan deltas by Nystuen (2008) yields a plausible interpretation of the observed lenticular laminations (Figure 23) as deposition under current flow (Schieber et al., 2010) in a delta front environment.

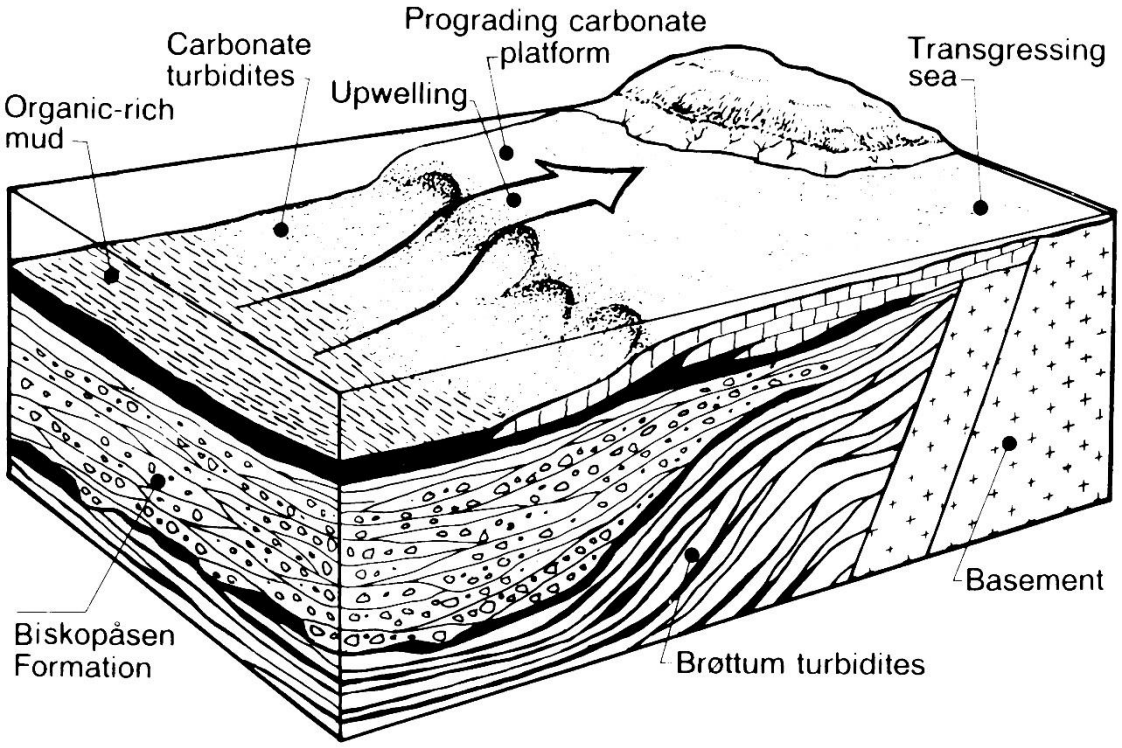

Figure 22. *Sketch showing the depositional setting of the Biri shale in the southwestern portion of the Hedmark basin where the Djupdalsbekken outcrop is located. From Vidal and Nystuen (1990).*

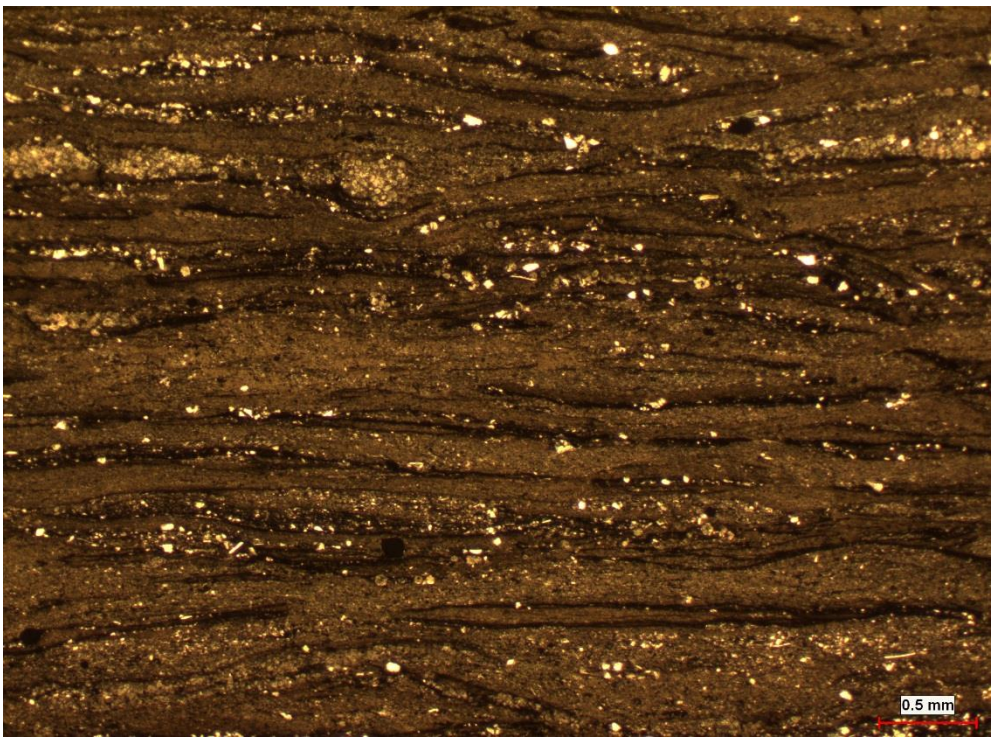

Figure 23. *Petrographic image from sample 45 (1.87 m) showing apparent lenticular fabric indicating deposition under current flow (Schieber et al., 2010). 25x, PPL.*

Textures in thin section show diagenetic replacive dolomite in the first meter of the Biri shale indicating later fluid flow. The dolomite is interpreted to be of diagenetic origin based on its replacive texture, replacing original calcite and calcareous mud (Figure 24), and rimming, in some places causing a sucrosic texture that represent multiple generations of formation (Figure 25). In addition, deposition of the overlying Ring Formation is interpreted to be by gravity flow of prograding marine fan deltas oriented in steeply dipping clinoforms (Nystuen, 2008). This depositional interpretation of the Ring Formation largely precludes primary dolomite formation in the Biri Formation at the Djupdalsbekken locality by modern analogs e.g. hypersaline or mixing zone models, as does the interpreted depositional model for the Biri shale given elsewhere (e.g. Bjørlykke et al., 1976; Vidal and Nystuen, 1990).

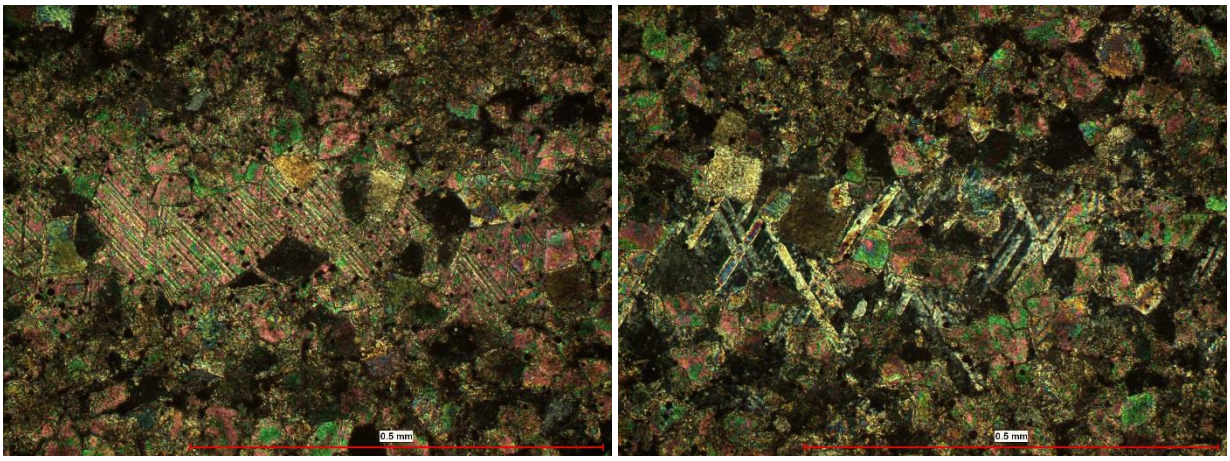

Figure 24. *Petrographic images from sample 42 (0.37 m) showing dolomite replacing calcite.*

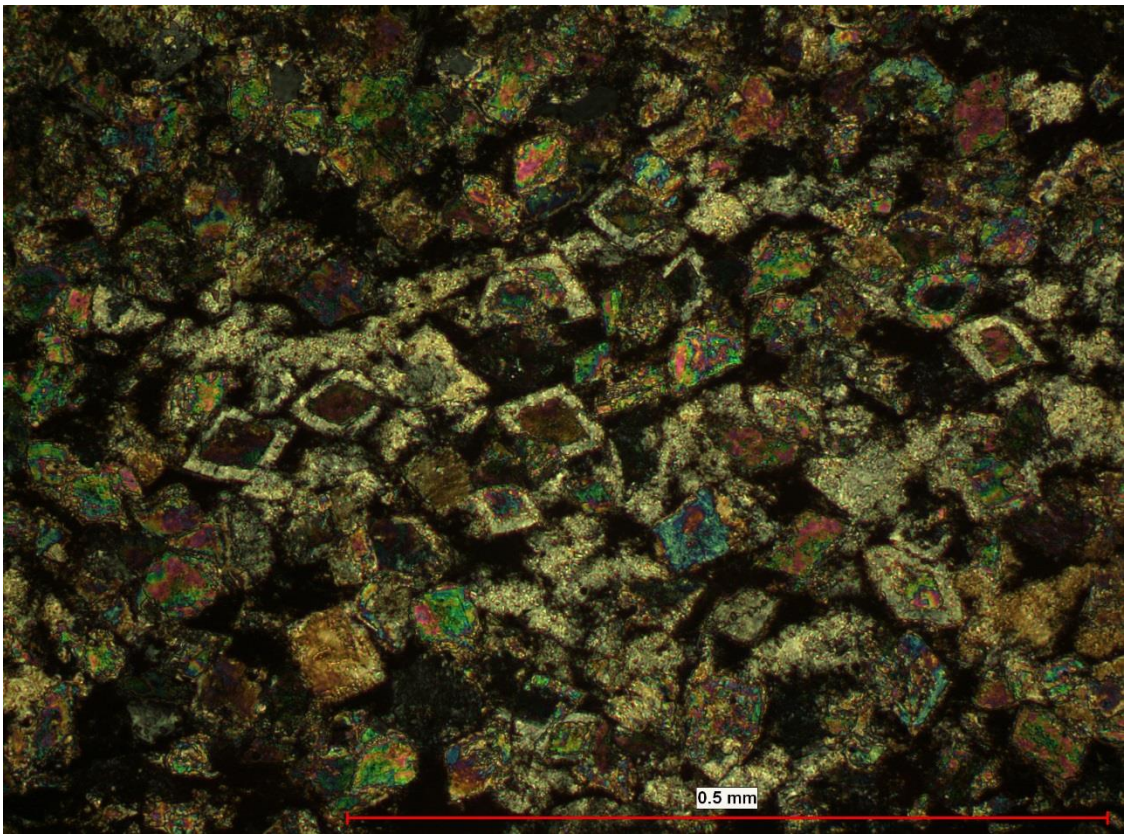

Figure 25. *Petrographic image from sample 42 (0.37 m) showing sucrosic dolomite.*

$\delta^{18}O$ values in the Biri shale may also provide evidence for later fluid flow through the upper horizons of the Biri shale. Based on the depositional models given above, the very negative $\delta^{18}O$ values throughout the Biri shale (average ~ - 13 ‰) are likely not indicative of mixing with isotopically light meteoric water at high latitudes or high altitude snowmelt runoff into the Hedmark basin. More likely they indicate a diagenetic overprint of originally higher values; alternatively, the $\delta^{18}O$ of the oceans has changed through time, as shown by Veizer et al. (1999) and thus Biri samples are representative of Precambrian values (Fauer and Mensing, 2009). Most importantly for this discussion, the dolomitized horizon (samples 41 and 42), shows a positive shift in $\delta^{18}O$ values to - 9.61 ‰ (sample 42) and - 6.68 ‰ (sample 41) from the underlying samples (average - 13 ‰). This positive shift can be reasonably accounted for by a handful of mechanisms. Veizer et al. (1999) show that Phanerozoic $\delta^{18}O$ values

oscillated through time on a scale of ~ 150 M.y., with a positive shift concurrent with the onset of major glaciations and in close proximity to glacially-derived rocks. Such is the case with the Biri shale and its proximity to the overlying Moelv Tillite. In this case, the dolomite inherited its $\delta^{18}O$ values from the original calcite it replaced. Additionally, as shown by Ferry et al., (2011) dolomitization in a channelized system where oxygen isotope exchange equilibrium is achieved may result in remineralization without any significant change in $\delta^{18}O$. Again, as a result, $\delta^{18}O$ values in the dolomitized samples of the Biri shale indicate values that were present in the original calcite and thus reflect Precambrian values and the positive shift shown by Veizer et al. (1999) that proceeds major glacial events. The relatively large increase from the calcite sample 43 ($\delta^{18}O$ = - 15.84 ‰) at 97 cm to the - 9.61 $\delta^{18}O$ ‰ value of the dolomitized sample 42 at 37 cm can also indicate dolomitization by a colder fluid and subsequent fractionation of $\delta^{18}O$ during recrystallization. To achieve this however, the dolomitizing fluid must have been colder than the marine water from which the original calcite precipitated. Alternatively, if dolomitization occurred by fluids expelled from overlying sediments during the Caledonian orogeny, it is possible that that $\delta^{18}O$ values are representative of later, higher Paleozoic $\delta^{18}O$ values. Fluids emplaced by hydraulic recharge of overlying sediment would reflect the higher $\delta^{18}O$ values in the Paleozoic, and thus the dolomitic horizons as well.

These details are useful, for the most part, to indicate the lack of definitive evidence to argue that an oxic front developed in the Biri Shale either during deposition of the Ring Formation (or soon afterward), or much later during the Caledonian orogeny. Dolomitization is possible in both instances, the main point being that evidence exists for later fluid flow and re-oxygenation of the Biri shale. In both cases, the oxygen-rich fluid would have flowed relatively easily through the (likely) porous conglomerate of the Ring Formation, but would have had more difficulty flowing through the tighter, less porous Biri shale. Pathways for later fluid flow developed through the fractures and imbrications that resulted from the Caledonian orogeny are also likely. As dolomitization of the top 0.5 meters occurred, it increased the

porosity in the upper horizon and provided a place for oxygen-rich fluid to collect, and from which oxygen penetration into lower horizons to occur.

6.8 IMPLICATIONS FOR RE – OS GEOCHRONOLOGY OF THE BIRI SHALE

Hannah et al. (2007) show that Re-Os data in the upper horizons (1-8 m) of the Biri shale is disturbed. The data and discussion presented above indicate that disturbed Re-Os isotope systematics were the result of post-depositional emplacement of an oxygen rich fluid in the uppermost horizons of the Biri shale. Subsequent penetration of an oxidation front resulted in remobilization of redox sensitive TEs, including Re. Colodner et al. (1992) demonstrated the mobilization of Re by a penetrating oxidation front, but also found that Re wasn't necessarily re-immobilized. Likewise, Crusius and Thomson (2000) show oxygen penetration in a turbidite (from piston cores) that mobilized Mo, U and Re, with corresponding re-immobilized concentration peaks that can be relatively wide (0.5 – 3 m). They found that Re maximums are located centimeters to meters below the depth to which the oxidation front penetrated.

Figure 26 shows the concentration profiles of U, Mo, and Re in the Biri shale. Re data were obtained from different samples at a prior date and are presented in Hannah et al. (2007). With limited Re data in the section, U and Mo are used as a proxies since the redox behavior of Re has been shown to closely resemble both elements (Crusius et al., 1996; Crusius and Thomson, 2000; Helz and Dolor, 2012).

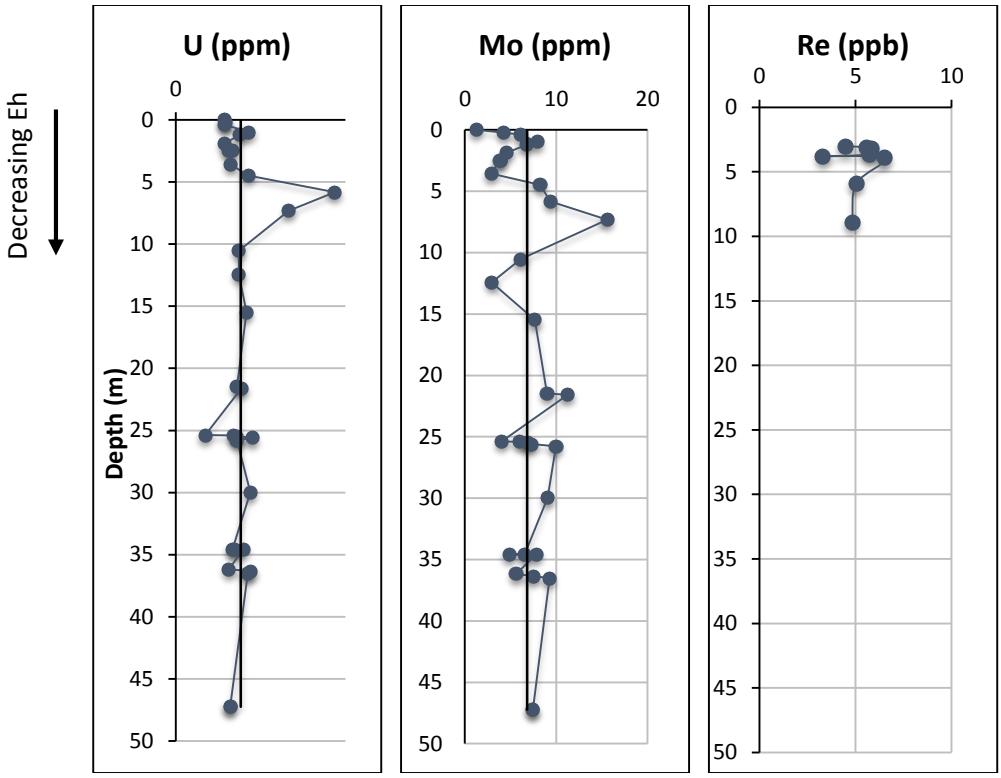

Figure 26. *Concentration profiles for U, Mo, and Re. The black line indicates average concentration in the section.*

Below a depth of 10 meters, U and Mo hover about an average value. In the top 10 m, both U and Mo show some depletion in meters 1 to 4 with re-immobilized concentration peaks between 5 and 8 m. The disturbed Re data from Hannah et al. (2007) were taken from samples at depths between 3 to 9 m. Using U and Mo as proxies for Re, the evidence from Colodner (1992) and Crusius and Thomson (2000) suggests that Re was remobilized in the uppermost few meters of the Biri Formation by an oxidizing fluid and variably re-immobilized further down section as conditions became increasingly reducing (lower Eh).

Determining Eh values (redox potential) for U, Mo and Re species quantitatively in the Biri shale would better predict where (in what order) U, Mo and Re would be re-immobilized as they encounter reducing conditions. However, since variables including how Re is held in the sediment, and the nature of the oxidizing fluid are unknown, Eh values cannot be precisely defined. On the other hand,

concentration profiles of U and Mo in Figure 26 show a striking similarity to the distribution and order of these trace elements in roll-front uranium deposits, illustrated in Figure 27 (Maynard, 1983; Dahlkamp, 2009). As the reducing capacity of the sediment increase (lower Eh value), U is precipitated first at a higher Eh value, Mo next at a lower Eh value, and finally Re at a lower Eh value than either U or Mo. In roll-front uranium deposits worldwide, Re is found at the nose of the roll where the reducing character of the rock is strong enough to re-immobilize Re (low Eh value) (Dahlkamp, 2009). Re persists in dissolved form after both U and Mo have precipitated from solution under less reducing conditions. As a result, Re is either carried further into the reducing section and re-immobilized, or if conditions are not reducing enough, may be flushed out of the system entirely.

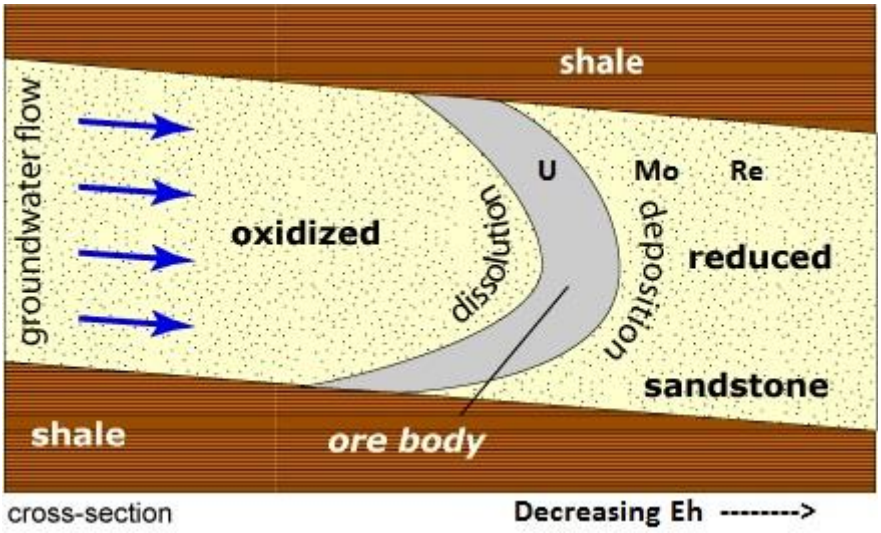

Figure 27. *Cross-section view of an idealized roll-front uranium deposit. After Myers (2010).*

Using the uranium roll-front deposit mechanism as an analog for trace element behavior in the Biri shale gives further evidence that U, Mo and Re were redistributed according to their redox potential. The resulting conclusion remains that the disturbed Re-Os isotope systematics found by Hannah et al. (2007) may have been a result of this behavior in the context of a re-oxygenating event within the Biri shale.

6.9 CONSIDERATION OF OTHER FACTORS

Notwithstanding the evidence given above, the possibility remains that disturbed Re-Os data are simply a matter of sampling from outcrop. Subsequent complications from differential weathering through subaerial exposure or through differential, unseen, fractures between samples that allowed fluids to leach and remobilize Re and Os from the samples cannot be entirely ruled out. For example, the undisturbed Re-Os data came from samples that were relatively better indurated (higher CO_3 content) than the more friable samples where the disturbed data were observed. It is reasonable to assume that the better indurated samples would have undergone less weathering than the more friable samples, and thus produce the undisturbed (preserved) and disturbed (weathered) Re-Os data. However, this difference is not observed in any of the geochemical data nor does it correlate with the placement of the oxidation front; depletion or enrichment of TEs exist apart from carbonate content. Furthermore, concentration peaks do not correlate with TOC content, and so it is reasonable to assume that the visible concentration peaks are not related to depositional flux during periods of elevated or declining productivity and associated TOC–TE accumulation.

Finally, it must be noted that the timing of oxidative burndown is not constrained; oxidation may have accompanied deposition of the Ring Formation or occurred during a later fluid flow event. However, disturbed Re-Os isotope systematics may only be explained by remobilization of Re (and Os) during a later time period, the most likely candidate for this being the Caledonian orogeny. If remobilization occurred during deposition of the Ring Formation, there would be no effect on dates generated by Re-Os data because, within uncertainty of the isotopic age, deposition of the Biri and Ring sediments were synchronous. Deposition of these units occurred around 560 Ma based on current dating, and were subsequently thrust towards the east during the Caledonian orogeny around 440 Ma. Resetting of the parent-daughter isotopic relationship near 440 Ma can plausibly generate the dates

given by Hannah et al. (2007), but the dates cannot be generated by a parent-daughter isotopic reset at the synchronous time of deposition for the Ring and Biri Formations near 560 Ma.

CHAPTER 7: CONCLUSIONS

The overarching goal of this thesis is to provide a framework for understanding disturbed Re-Os isotope systematics in the Biri shale through a detailed trace element (TE) chemistry investigation. Part of this framework is to understand the initial redox conditions during deposition of the Biri shale through TE geochemical proxies, and to identify how those TEs may have been subsequently disturbed by post-depositional reoxidation of the sediment. Deposition under sub-oxic to anoxic marine waters with free H_2S in pore waters is indicated for the Biri shale in meters 1- 47 by a multi-proxy approach, with pyrite morphology and size distribution, along with molybdenum and uranium concentrations showing the most value as paleoredox proxies. Low TOC values and weak TOC-TE correlation suggest suboxic bottom water, as do moderate enrichments of Mo and U, and the average EF_{Mo}/EF_U ratio of one. Pyrite morphology corroborates the other redox proxy evidence indicating suboxic to anoxic water column with a chemocline at the sediment water interface.

Petrographic textures indicating secondary dolomitization in the first meter of the Biri shale, along with $\delta^{13}C$ and $\delta^{18}O$ stable isotope data provide evidence for the placement, timing and presence of later fluid flow in the Biri shale. Geochemical evidence supports the theory that emplacement of an oxygen-rich fluid in the upper section of the Biri shale caused remobilization of TEs by oxygen penetration in meters $\sim$ 0 through 10. The depth to which the oxic front penetrated the Biri shale is documented by relative depletion of redox sensitive elements near the top of the section and concentration peaks for both U and Mo at about 6 and 7 meters downsection. Lack of Re data, and previous work (e.g. Crusius and Thomson, 2000; 2003) showing variable re-immobilization of Re make it impossible at this point to be precise in calculating the degree to which Re was mobilized or re-immobilized. Nonetheless, U and Mo can be used as well-established proxies for Re and allow us to

conclude that Re was at least remobilized post-deposition. This remobilization is likely the cause of disturbed Re-Os isotope systematics given by Hannah et al. (2007).

There are two plausible explanations for the TE distribution but only one explanation for the disturbed Re-Os isotope systematics results. The geochemical data may be explained by re-oxygenation of the Biri shale either at the time of deposition of the Ring Formation, or at later time. Disturbed Re-Os data, however, can only be explained by a later event, likely by fluid expulsed from overlying sediment during the Caledonian orogeny

LIST OF REFERENCES

Algeo, T. J., Lyons, T. W., Blakey, R. C., & Over, D. J. (2007). Hydrographic conditions of the Devono–Carboniferous North American Seaway inferred from sedimentary Mo–TOC relationships. *Palaeogeography, Palaeoclimatology, Palaeoecology*, *256*(3–4), 204–230. doi:10.1016/j.palaeo.2007.02.035

Algeo, T. J., & Maynard, J. B. (2004). Trace-element behavior and redox facies in core shales of Upper Pennsylvanian Kansas-type cyclothems. *Chemical Geology*, *206*(3-4), 289–318. doi:10.1016/j.chemgeo.2003.12.009

Algeo, T. J., & Maynard, J. B. (2008). Trace-metal covariation as a guide to water-mass conditions in ancient anoxic marine environments. *Geosphere*, *4*(5), 872. doi:10.1130/GES00174.1

Algeo, T. J., & Tribovillard, N. (2009). Environmental analysis of paleoceanographic systems based on molybdenum–uranium covariation. *Chemical Geology*, *268*(3-4), 211–225. doi:10.1016/j.chemgeo.2009.09.001

Aller, R. (1994). The sedimentary Mn cycle in Long Island Sound: Its role as intermediate oxidant and the influence of bioturbation, O2, and Corg flux on diagenetic reaction balances. *Journal of Marine Research*.

Berner, R. A. (1970). Sedimentary pyrite formation. *American Journal of Science*. doi:10.2475/ajs.268.1.1

Bingen, B., Griffin, W. L., Torsvik, T. H., & Saeed, A. (2005). Timing of Late Neoproterozoic glaciation on Baltica constrained by detrital zircon geochronology in the Hedmark Group, south-east Norway. *Terra Nova*, *17*(3), 250–258. doi:10.1111/j.1365-3121.2005.00609.x

Bingen, B., & Solli, A. (2009). Geochronology of magmatism in the Caledonian and Sveconorwegian belts of Baltica: synopsis for detrital zircon provenance studies. *Norwegian Journal of Geology*, *89*, 267–290.

Bjørlykke, A. (1979). Gjøvik and Dokka. Description of the geological maps 1816 I and 1816 IV – 1:50 000. *Norges geol. Unders*. 344, 1 – 48.

Bjørlykke, K., Elvsborg, A., & Høy, T. (1976). Late Precambrian sedimentation in the central sparagmite basin of South Norway. *Norsk Geologisk Tidsskrift. Supplement*, *56*(3), 233–290

Bohacs, K. (1998). Introduction: Mudrock Sedimentology and Stratigraphy - Challenges at the Basin and Local Scales. In *Shales and Mudstones I,* J. Schieber, P. Sethi, & W. Zimmerle (Eds.), (pp. 33–78). Stuttgart: E. Schweizerbart'sche Verlagsbuchhandlung.

Bond, D. P. G., & Wignall, P. B. (2010). Pyrite framboid study of marine Permian-Triassic boundary sections: A complex anoxic event and its relationship to contemporaneous mass extinction. *Geological Society of America Bulletin*, *122*(7-8), 1265–1279. doi:10.1130/B30042.1

Bowring, S. (2002). Geochronological constraints on terminal Neoproterozoic events and the rise of metazoans. *Astrobiology*, *2*(4), 457.

Breit, G. N., & Wanty, R. B. (1991). Vanadium accumulation in carbonaceous rocks: A review of geochemical controls during deposition and diagenesis. *Chemical Geology*, *91*(2), 83–97. doi:10.1016/0009-2541(91)90083-4

Brumsack, H. J. (1989). Geochemistry of Recent TOC-rich sediment from the Gulf of California and the Black Sea. *Geologische Rundschau*, *78*(3), 851–882. Brumsack, H. J. (2006). The trace metal content of recent organic carbon-rich sediments: Implications for Cretaceous black shale formation. *Palaeogeography, Palaeoclimatology, Palaeoecology*, *232*(2-4), 344–361. doi:10.1016/j.palaeo.2005.05.011

Buckley, D. ., & Cranston, R. (1988). Early diagenesis in deep sea turbidites: The imprint of paleo-oxidation zones. *Geochimica et Cosmochimica Acta*, *52*(12), 2925–2939. doi:10.1016/0016-7037(88)90158-5

Calvert, S. E., & Pedersen, T. F. (1996). Sedimentary geochemistry of manganese; implications for the environment of formation of manganiferous black shales. *Economic Geology*, *91*(1), 36–47. doi:10.2113/gsecongeo.91.1.36

Canfield, D., Jørgensen, B., Fossing, H., Glud, R., Gundersen, J., Ramsing, N., Hall, P. O. (1993). Pathways of organic carbon oxidation in three continental margin sediments. *Marine Geology*, *113*(1-2), 27–40. doi:10.1016/0025-3227(93)90147-N

Cathles, L. M., & Smith, A. T. (1983). Thermal constraints on the formation of mississippi valley-type lead-zinc deposits and their implications for episodic basin dewatering and deposit genesis. *Economic Geology and the Bulletin of the Society of Economic Geologists*, *78*(5), 983–1002.

Chappaz, A., Gobeil, C., & Tessier, A. (2008). Sequestration mechanisms and anthropogenic inputs of rhenium in sediments from Eastern Canada lakes. *Geochimica et Cosmochimica Acta*, *72*(24), 6027–6036. doi:10.1016/j.gca.2008.10.003

Colley, S., & Thomson, J. (1985). Recurrent uranium relocations in distal turbidites emplaced in pelagic conditions. *Geochimica et Cosmochimica Acta*, *49*(11), 2339–2348. doi:10.1016/0016-7037(85)90234-0

Colley, S., Thomson, J., Wilson, T. R. ., & Higgs, N. (1984). Post-depositional migration of elements during diagenesis in brown clay and turbidite sequences in the North East Atlantic. *Geochimica et Cosmochimica Acta*, *48*(6), 1223–1235. doi:10.1016/0016-7037(84)90057-7

Collier, R. W. (1984). Particulate and dissolved vanadium in the North Pacific Ocean. *Nature*, *309*(5967), 441–444. doi:10.1038/309441a0

Colodner, D. C., Boyle, E. A., Edmond, J. M., & Thomson, J. (1992). Post-depositional mobility of platinum, iridium and rhenium in marine sediments. *Nature*, *358*(6385), 402–404. doi:10.1038/358402a0

Cowie, G. L., Hedges, J. I., Prahl, F. G., & de Lange, G. J. (1995). Elemental and major biochemical changes across an oxidation front in a relict turbidite: An oxygen effect. *Geochimica et Cosmochimica Acta*, *59*(1), 33–46. doi:10.1016/0016-7037(94)00329-K

Cruse, A. M., & Lyons, T. W. (2004). Trace metal records of regional paleoenvironmental variability in Pennsylvanian (Upper Carboniferous) black shales. *Chemical Geology*, *206*(3–4), 319–345. doi:10.1016/j.chemgeo.2003.12.010

Crusius, J., Calvert, S., Pedersen, T., & Sage, D. (1996). Rhenium and molybdenum enrichments in sediments as indicators of oxic, suboxic and sulfidic conditions of deposition. *Earth and Planetary Science*, (96), 65–78.

Crusius, J., & Thomson, J. (2000). Comparative behavior of authigenic Re, U, and Mo during reoxidation and subsequent long-term burial in marine sediments. *Geochimica et Cosmochimica Acta*, *64*(13), 2233–2242. doi:10.1016/S0016-7037(99)00433-0

Crusius, J., & Thomson, J. (2003). Mobility of authigenic rhenium, silver, and selenium during postdepositional oxidation in marine sediments. *Geochimica et Cosmochimica Acta*, *67*(2), 265–273.

Dahlkamp, F. J. (Ed.). (2009). *Uranium Deposits of the World*. Berlin, Heidelberg: Springer. doi:10.1007/978-3-540-78558-3

Dolor, M. K., Gilmour, C. C., & Helz, G. R. (2009). Distinct Microbial Behavior of Re Compared to Tc: Evidence Against Microbial Re Fixation in Aquatic Sediments. *Geomicrobiology Journal*, *26*(7), 470–483. doi:10.1080/01490450903060822

Erickson, B. E., & Helz, G. R. (2000). Molybdenum(VI) speciation in sulfidic waters: *Geochimica et Cosmochimica Acta*, *64*(7), 1149–1158. doi:10.1016/S0016-7037(99)00423-8

Emerson, S. R., & Huested, S. (1991). Ocean anoxia and the concentrations of molybdenum and vanadium in seawater. *Marine Chemistry*, *34*(3-4), 177–196.

Faure, G., & Mensing, T. M. (2009). *Isotopes: Principles and Applications*. (Vol. 3, p. 897). Wiley.

Fike, D. A., Grotzinger, J. P., Pratt, L. M., & Summons, R. E. (2006). Oxidation of the Ediacaran ocean. *Nature*, *444*(7120), 744–7. doi:10.1038/nature05345

Georgiev, S., Stein, H. J., Hannah, J. L., Bingen, B., Weiss, H. M., & Piasecki, S. (2011). Hot acidic Late Permian seas stifle life in record time. *Earth and Planetary Science Letters*, *310*(3-4), 389–400. doi:10.1016/j.epsl.2011.08.010

Georgiev, S., Stein, H. J., Hannah, J. L., Weiss, H. M., Bingen, B., Xu, G., Piasecki, S. (2012). Chemical signals for oxidative weathering predict Re–Os isochroneity in black shales, East Greenland. *Chemical Geology*, *324-325*, 108–121. doi:10.1016/j.chemgeo.2012.01.003

Gradstein, F. M., Ogg, J. G., Schmitz, M. D., & Ogg, G. M. (Eds.). (2012). *The Geologic Time Scale 2012,* (First, Vol. 1, p. 435). Elsevier : Amsterdam, Netherlands.

Halverson, G. P., Hoffman, P. F., Schrag, D. P., Maloof, A. C., & Rice, a. H. N. (2005). Toward a Neoproterozoic composite carbon-isotope record. *Geological Society of America Bulletin*, *117*(9), 1181. doi:10.1130/B25630.1

Hannah, J. L., Bekker, A., Stein, H. J., Markey, R. J., & Holland, H. D. (2004). Primitive Os and 2316 Ma age for marine shale: implications for Paleoproterozoic glacial events and the rise of atmospheric oxygen. *Earth and Planetary Science Letters*, *225*(1-2), 43–52. doi:10.1016/j.epsl.2004.06.013

Hannah, J. L., & Stein, H. J. (2013). Re-Os Istope Geochemistry. In *Reading the Archive of Earth's Oxygenation,* V. A. Melezhik, A. R. Prave, E. J. Hanski, A. E. Fallick, A. Lepland, L. R. Kump, & H. Strauss (Eds.), (pp. 1506–1514). Berlin, Heidelberg: doi:10.1007/978-3-642-29670-3

Hannah, J. L., Yang, G., Bingen, B., Stein, H. J., & Zimmerman, A. (2007). ~560 Ma and ~300 Ma Re-Os ages constrain Neoproterozoic glaciation and record Variscan hydrocarbon migration on extension of Oslo rift. *Goldschmidt Conference Abstracts*.

Helz, G. R., Bura-Nakić, E., Mikac, N., & Ciglenečki, I. (2011). New model for molybdenum behavior in euxinic waters. *Chemical Geology*, *284*(3-4), 323–332. doi:10.1016/j.chemgeo.2011.03.012

Helz, G. R., & Dolor, M. K. (2012). What regulates rhenium deposition in euxinic basins? *Chemical Geology*, *304-305*, 131–141. doi:10.1016/j.chemgeo.2012.02.011

Helz, G. R., Miller, C. V., Charnock, J. M., Mosselmans, J. F. W., Pattrick, R. A. D., Garner, C. D., & Vaughan, D. J. (1996). Mechanism of molybdenum removal from the sea and its concentration in black shales: EXAFS evidence. *Geochimica et Cosmochimica Acta*, *60*(19), 3631–3642. doi:10.1016/0016-7037(96)00195-0

Higgs, N. C., Thomson, J., Wilson, T. R. S., & Croudace, I. W. (1994). Modification and complete removal of eastern Mediterranean sapropels by postdepositional oxidation. *Geology*, *22*(5), 423. doi:10.1130/0091-7613(1994)022<0423:MACROE>2.3.CO;2

Hoffman, P. F., & Li, Z.-X. (2009). A palaeogeographic context for Neoproterozoic glaciation. *Palaeogeography, Palaeoclimatology, Palaeoecology*, *277*(3–4), 158–172. doi:10.1016/j.palaeo.2009.03.013

Holtedahl, O. (1922). A tillite-like conglomerate in the Eocambrian Sparagmite of southern Norway. *American Journal of Science*, *s5-4*(20), 165–173. doi:10.2475/ajs.s5-4.20.165

Huerta-Diaz, M. A., & Morse, J. W. (1992). Pyritization of trace metals in anoxic marine sediments. *Geochimica et Cosmochimica Acta*, *56*(7), 2681–2702. doi:10.1016/0016-7037(92)90353-K

Jaffe, L., Peucker-Ehrenbrink, B., & Petsch, S. (2002). Mobility of rhenium, platinum group elements and organic carbon during black shale weathering. *Earth and Planetary Science*, *198*, 339–353.

Kaufman, a J., Knoll, a H., & Narbonne, G. M. (1997). Isotopes, ice ages, and terminal Proterozoic earth history. *Proceedings of the National Academy of Sciences of the United States of America*, *94*(13), 6600–5.

Klinkhammer, G. ., & Palmer, M. (1991). Uranium in the oceans: Where it goes and why. *Geochimica et Cosmochimica Acta*, *55*(7), 1799–1806. doi:10.1016/0016-7037(91)90024-Y

Knoll, a H. (2000). Learning to tell Neoproterozoic time. *Precambrian Research*, *100*(1-3), 3–20.

Kumpulainen, R., & Nystuen, J. P. (1985). Late Proterozoic basin evolution and sedimentation in the westernmost part of Baltoscandia (pp. 213–232). Uppsala, Sweden: John Wiley & Sons : Chichester, United Kingdom.

Lange, D. (1998). 33. Oxic vs. anoxic diagenetic alteration of turbidite sediments in the Madeira Abyssal Plain, eastern North Atlantic. *Weaver, Schmincke, Firth and Duffileld (Eds.): Proceedings of the Ocean Drilling Program, Scientific Results*, *157*, 573–579.

Leach, D. L., & Rowan, E. L. (1986). Genetic link between Ouachita foldbelt tectonism and the mississippi valley-type lead-zinc deposits of the Ozarks. *Geology [Boulder]*, *14*(11), 931–935.

Leventhal, J.S. (1998). Metal-rich black shales: formation, economic geology and environmental considerations. In *Shales and Mudstones* II, J. Schieber, W. Zimmerle, and P. Sethi, (Eds.), (pp. 255-282). Stuttgart, E. Schweizerbart'sche Verlagsbuchhandlung.

Li, Z. X., Bogdanova, S. V., Collins, A. S., Davidson, A., De Waele, B., Ernst, R. E., Vernikovsky, V. (2008). Assembly, configuration, and break-up history of Rodinia: A synthesis. *Precambrian Research*, *160*(1-2), 179–210. doi:10.1016/j.precamres.2007.04.021

Maynard, J. B. (1983). *Geochemistry of sedimentary ore deposits*. New York: Springer-Verlag.

MacQuaker, J. H. S., Keller, M. A., & Davies, S. J. (2010). Algal Blooms and "Marine Snow": Mechanisms That Enhance Preservation of Organic Carbon in Ancient Fine-Grained Sediments. *Journal of Sedimentary Research*, *80* (11), 934–942. doi:10.2110/jsr.2010.085

McLennan, S. (2001). Relationships between the trace element composition of sedimentary rocks and upper continental crust. *Geochemistry, Geophysics, Geosystems*, *4*(2).

McManus, J., Berelson, W. M., Klinkhammer, G. P., Hammond, D. E., & Holm, C. (2005). Authigenic uranium: Relationship to oxygen penetration depth and organic carbon rain. *Geochimica et Cosmochimica Acta*, *69*(1), 95–108. doi:10.1016/j.gca.2004.06.023

McManus, J., Berelson, W. M., Severmann, S., Poulson, R. L., Hammond, D. E., Klinkhammer, G. P., & Holm, C. (2006). Molybdenum and uranium geochemistry in continental margin sediments: Paleoproxy potential. *Geochimica et Cosmochimica Acta*, *70*(18), 4643–4662. doi:10.1016/j.gca.2006.06.1564

Meunier, J. D. (1994). The composition and origin of vanadium-rich clay minerals in Colorado Plateau Jurassic sandstones. *Clays and Clay Minerals*, *42*(4), 391.

Meyers, J.D. (2010). Uranium - Roll Front Deposits, Lecture Activity – Geologic Time A Correlation Exercise. University of Wyoming: www.gg.uwyo.edu.

Miller, C. A., Peucker-Ehrenbrink, B., Walker, B. D., & Marcantonio, F. (2011). Re-assessing the surface cycling of molybdenum and rhenium. *Geochimica et Cosmochimica Acta*, *75*(22), 7146–7179. doi:10.1016/j.gca.2011.09.005

Mongenot, T., Tribovillard, N.-P., Desprairies, A., Lallier-Vergès, E., & Laggoun-Defarge, F. (1996). Trace elements as palaeoenvironmental markers in strongly mature hydrocarbon source rocks: the Cretaceous La Luna Formation of Venezuela. *Sedimentary Geology*, *103*(1-2), 23–37. doi:10.1016/0037-0738(95)00078-X

Morford, J. L. (2001). Trace metal evidence for changes in the redox environment associated with the transition from terrigenous clay to diatomaceous sediment, Saanich Inlet, BC. *Marine Geology*, *174*(1-4), 355.

Morford, J. L., & Emerson, S. (1999). The geochemistry of redox sensitive trace metals in sediments. *Geochimica et Cosmochimica Acta*, *63*(11–12), 1735–1750. doi:10.1016/S0016-7037(99)00126-X

Morford, J. L., Martin, W. R., & Carney, C. M. (2009a). Uranium diagenesis in sediments underlying bottom waters with high oxygen content. *Geochimica et Cosmochimica Acta*, *73*(10), 2920–2937. doi:10.1016/j.gca.2009.02.014

Morford, J. L., Martin, W. R., & Carney, C. M. (2012). Rhenium geochemical cycling: Insights from continental margins. *Chemical Geology*, *324-325*, 73–86. doi:10.1016/j.chemgeo.2011.12.014

Morford, J. L., Martin, W. R., François, R., & Carney, C. M. (2009b). A model for uranium, rhenium, and molybdenum diagenesis in marine sediments based on results from coastal locations. *Geochimica et Cosmochimica Acta*, *73*(10), 2938–2960. doi:10.1016/j.gca.2009.02.029

Morley, C. K. (1994). Fold-generated imbricates: examples from the Caledonides of Southern Norway. *Journal of Structural Geology*, *16*(5), 619–631. doi:10.1016/0191-8141(94)90114-7

Morse, J. W. (1994). Interactions of trace metals with authigenic sulfide minerals: implications for their bioavailability. *Marine Chemistry*, *46*(1–2), 1–6. doi:10.1016/0304-4203(94)90040-X

Narbonne, G. M., Xiao, S., Shields, G. A., & Gehling, J. G. (2012). Chapter 18 - The Ediacaran Period. In F. M. Gradstein, J. G. Ogg, M. D. Schmitz, & G. Ogg (Eds.), The Geologic Time scale 2012, (pp. 413–435). Boston: Elsevier. doi:10.1016/B978-0-444-59425-9.00018-4

Nystuen, J. P. (1981). The late Precambrian “sparagmites” of southern Norway; a major Caledonian allochthon; the Osen-Roa nappe complex. *American Journal of Science*, *281*(1), 69–94. doi:10.2475/ajs.281.1.69

Nystuen, J. P. (1982). Late Proterozoic basin evolution on the Baltoscandian Craton; the Hedmark Group, Southern Norway. *Norges Geol. Unders.*, (375), 1–74.

Nystuen, J. P. (1987). Synthesis of the tectonic and sedimentological evolution of the late Proterozoic-Early Cambrian Hedmark Basin, the Caledonian thrust belt, southern Norway. *Norsk Geologisk Tidsskrift*, *67*(4), 395–418.

Nystuen, J. P., Andresen, A., Kumpulainen, R. A., & Siedlecka, A. (2008). Neoproterozoic basin evolution in Fennoscandia, East Greenland and Svalbard. *Episodes*, *31*(1), 35–43.

Nystuen, J. P. (2008). Neoproterozoic Moelv Tillite and the Hedmark Basin, the Mjøsa Area, South Norway. 33 IGC Excursion No. 101.

Okita, P. M., Maynard, J. B., Spiker, E. C., & Force, E. R. (1988). Isotopic evidence for organic matter oxidation by manganese reduction in the formation of stratiform manganese carbonate ore. *Geochimica et Cosmochimica Acta*, *52*(11), 2679–2685. doi:10.1016/0016-7037(88)90036-1

Partin, C. A., Bekker, A., Planavsky, N. J., Scott, C. T., Gill, B. C., Li, C., Lyons, T. W. (2013). Large-scale fluctuations in Precambrian atmospheric and oceanic oxygen levels from the record of U in shales. *Earth and Planetary Science Letters*, *369-370*, 284–293. doi:10.1016/j.epsl.2013.03.031

Peucker-Ehrenbrink, B., & Hannigan, R. (2000). Effects of black shale weathering on the mobility of rhenium and platinum group elements. *Geology*, *28*(5), 475–478.

Piper, D. Z., & Calvert, S. E. (2009). A marine biogeochemical perspective on black shale deposition. *Earth-Science Reviews*, *95*(1-2), 63–96. doi:10.1016/j.earscirev.2009.03.001

Quinby-Hunt, M. S., P. Wilde, C. J. Orth, and W.B.N. Berry. (1989) Elemental Geochemistry of Black Shales-Statistical Comparison of Low-Calcic Shales with Other Shales. In *Metalliferous Black Shales and related Ore Deposits*, R. I. Grauch and J. S. Leventhal (eds.), U. S. Geological Survey Circular 1037, p. 8-15.

Raiswell, R., & Berner, R. A. (1987). Organic carbon losses during burial and thermal maturation of normal marine shales. *Geology [Boulder]*, *15*(9), 853–856.

Raiswell, R., & Buckley, F. (1988). Degree of pyritization of iron as a paleoenvironmental indicator of bottom-water oxygenation. *Journal of Sedimentary Petrology*, *58*(5), 812–819.

Rimmer, S. M. (2004). Geochemical paleoredox indicators in Devonian–Mississippian black shales, Central Appalachian Basin (USA). *Chemical Geology*, *206*(3-4), 373–391. doi:10.1016/j.chemgeo.2003.12.029

Rinna, J., Warning, B., Meyers, P. A., Brumsack, H.-J., & Rullkötter, J. (2002). Combined organic and inorganic geochemical reconstruction of paleodepositional conditions of a Pliocene sapropel from the eastern Mediterranean Sea. *Geochimica et Cosmochimica Acta*, *66*(11), 1969–1986. doi:10.1016/S0016-7037(02)00826-8

Riquier, L., Tribovillard, N., Averbuch, O., Devleeschouwer, X., & Riboulleau, A. (2006). The Late Frasnian Kellwasser horizons of the Harz Mountains (Germany): Two oxygen-deficient periods resulting from different mechanisms. *Chemical Geology*, *233*(1-2), 137–155. doi:10.1016/j.chemgeo.2006.02.021

Roberts, D. (2003). The Scandinavian Caledonides: event chronology, palaeogeographic settings and likely modern analogues. *Tectonophysics*, *365*(1-4), 283–299. doi:10.1016/S0040-1951(03)00026-X

Ross, D. J. K., & Bustin, R. M. (2009). Investigating the use of sedimentary geochemical proxies for paleoenvironment interpretation of thermally mature organic-rich strata: Examples from the Devonian–Mississippian shales, Western Canadian Sedimentary Basin. *Chemical Geology*, *260*(1-2), 1–19. doi:10.1016/j.chemgeo.2008.10.027

Sahoo, S. K., Planavsky, N. J., Kendall, B., Wang, X., Shi, X., Scott, C., Jiang, G. (2012). Ocean oxygenation in the wake of the Marinoan glaciation. *Nature*, *489*(7417), 546–9. doi:10.1038/nature11445

Schieber, J. (1994). Evidence for high-energy events and shallow-water deposition in the Chattanooga Shale, Devonian, central Tennessee, USA. *Sedimentary Geology*, *93*(3–4), 193–208. doi:10.1016/0037-0738(94)90005-1

Schieber, J., & Zimmerle, W. (1998). Introduction and overview; the history and promise of shale research. In *Shales and Mudstones I,* J. Schieber, W. Zimmerle, & P. S. Sethi (Eds.), (pp. 1–10). E. Schweizerbart'sche Verlagsbuchhandlung Naegele u. Obermiller : Stuttgart, Germany

Schieber, J., & Southard, J. B. (2009). Bedload transport of mud by floccule ripples--Direct observation of ripple migration processes and their implications. *Geology*, *37*(6), 483–486. doi:10.1130/G25319A.1

Schieber, J., Southard, J. B., & Schimmelmann, A. (2010). Lenticular shale fabrics resulting from intermittent erosion of water-rich muds--Interpreting the rock record in the light of recent flume experiments. *Journal of Sedimentary Research*, *80*(1), 119–128. doi:10.2110/jsr.2010.005

Schrag, D. P., Berner, R. A., Hoffman, P. F., & Halverson, G. P. (2002). On the initiation of a snowball Earth. *Geochemistry, Geophysics, Geosystems*, *3*(6). doi:10.1029/2001GC000219

Schröder, S., & Grotzinger, J. (2007). Evidence for anoxia at the Ediacaran–Cambrian boundary: the record of redox-sensitive trace elements and rare earth elements in Oman. *Journal of the Geological Society*, *164*, 175–187.

Schultz, R. B. (1989). Geochemical characteristics and inferred depositional environments of Upper Pennsylvanian (Virgilian) black shales in eastern Kansas. *The Compass*, *67*(1), 47.

Scott, C., & Lyons, T. W. (2012). Contrasting molybdenum cycling and isotopic properties in euxinic versus non-euxinic sediments and sedimentary rocks: Refining the paleoproxies. *Chemical Geology*, *324–325*(0), 19–27. doi:10.1016/j.chemgeo.2012.05.012

Scott, C., Lyons, T. W., Bekker, A., Shen, Y., Poulton, S. W., Chu, X., & Anbar, A. D. (2008). Tracing the stepwise oxygenation of the Proterozoic ocean. *Nature*, *452*(7186), 456–9. doi:10.1038/nature06811

Sæther, T., & Nystuen, J. P. (1981). Tectonic framework, stratigraphy, sedimentation and volcanism of the late Precambrian Hedmark Group, Oesterdalen, South Norway. *Norsk Geologisk Tidsskrift*, *61*(3-4), 193–211.

Taylor, S. R., & McLennan, S. M. (1995). The geochemical evolution of the continental crust. *Reviews of Geophysics*, *33*(2), 241–265. doi:10.1029/95RG00262

Thomson, J., & Higgs, N. (1995). Redistribution and geochemical behaviour of redox-sensitive elements around S1, the most recent eastern Mediterranean sapropel. *Geochimica et Cosmochimica Acta*, *59*(17), 3487–3501.

Thomson, J., Higgs, N. C., Croudace, I. W., Colley, S., & Hydes, D. J. (1993). Redox zonation of elements at an oxic/post-oxic boundary in deep-sea sediments. *Geochimica et Cosmochimica Acta*, *57*(3), 579–595. doi:10.1016/0016-7037(93)90369-8

Thomson, J. Jarvis, I., Green, D.R.H., Green, D. (1998). Oxidation fronts in Madeira abyssal plain turbidites: Persistence of early diagenetic trace-element enrichments during burial, SITE 950. In P. P. E. Weaver Schmincke, H.-U., Firth, J.V., Duffield,W. (Ed.), *Proceedings of the Ocean Drilling Program, Scientific Results* (Vol. 157, pp. 559–571). Ocean Drilling Program.

Tissot, L. H., Dauphas, N., Reinhard, C. T., Lyons, T. W., Asael, D., & Rouxel, O. (2013). Reading the Archive of Earth's Oxygenation. In V. A. Melezhik, A. R. Prave, E. J. Hanski, A. E. Fallick, A. Lepland, L. R. Kump, & H. Strauss (Eds.), (Vol. 3, pp. 1500–1506). Berlin, Heidelberg: Springer Berlin Heidelberg. doi:10.1007/978-3-642-29670-3

Tourtelot, H. (1979). Black shale—its deposition and diagenesis. *Clays and Clay Minerals*, *27*(5), 313–321

Tribovillard, N., Algeo, T. J., Lyons, T., & Riboulleau, A. (2006). Trace metals as paleoredox and paleoproductivity proxies: An update. *Chemical Geology*, *232*(1-2), 12–32. doi:10.1016/j.chemgeo.2006.02.012

Tribovillard, N., Bout-Roumazeilles, V., Algeo, T., Lyons, T. W., Sionneau, T., Montero-Serrano, J. C., Baudin, F. (2008). Paleodepositional conditions in the Orca Basin as inferred from organic matter and trace metal contents. *Marine Geology*, *254*(1–2), 62–72. doi:10.1016/j.margeo.2008.04.016

Tribovillard, N., Riboulleau, A., Lyons, T., & Baudin, F. (2004). Enhanced trapping of molybdenum by sulfurized marine organic matter of marine origin in Mesozoic limestones and shales. *Chemical Geology*, *213*(4), 385–401. doi:10.1016/j.chemgeo.2004.08.011

Tucker, M. E. (1983). Sedimentation of organic-rich limestones in the late Precambrian of Southern Norway. *Precambrian Research*, *22*(3-4), 295–315. doi:10.1016/0301-9268(83)90053-0

Tuttle, B. M. L. W., Breit, G. N., & Goldhaber, M. B. (2003). Geochemical Data from New Albany Shale, Kentucky : A Study in Metal Mobility During Weathering of Black Shales.

Veizer, J., Ala, D., Azmy, K., Bruckschen, P., Buhl, D., Bruhn, F., Strauss, H. (1999). $^{87}Sr/^{86}Sr$, $\delta^{13}C$ and $\delta^{18}O$ evolution of Phanerozoic seawater. *Chemical Geology*, *161*(1-3), 59–88. doi:10.1016/S0009-2541(99)00081-9

Vidal, G., & Nystuen, J. P. (1990). Lower Cambrian acritarchs and the Proterozoic-Cambrian boundary in Southern Norway. *Norsk Geologisk Tidsskrift*, *70*(4), 191–222.

Vine, J. D., & Tourtelot, E. B. (1970). Geochemistry of black shale deposits; a summary report. *Economic Geology*, *65* (3), 253–272. doi:10.2113/gsecongeo.65.3.253

Vorlicek, T. P., Kahn, M. D., Kasuya, Y., & Helz, G. R. (2004). Capture of molybdenum in pyrite-forming sediments: role of ligand-induced reduction by polysulfides. *Geochimica et Cosmochimica Acta*, *68*(3), 547–556. doi:10.1016/S0016-7037(03)00444-7

Wedepohl, K. H. (1971). Environmental influences on the chemical composition of shales and clays. *Physics and Chemistry of the Earth*, *8*, 305–333. doi:10.1016/0079-1946(71)90020-6

Weijden, C. H. Van der. (2002). Pitfalls of normalization of marine geochemical data using a common divisor. *Marine Geology*, *184*, 167–187.

Wignall, P. B. (1991). Model for transgressive black shales? *Geology*, *19* (2), 167–170. doi:10.1130/0091-7613(1991)019<0167:MFTBS>2.3.CO;2

Wignall, P. B., & Newton, R. (1998). Pyrite framboid diameter as a measure of oxygen deficiency in ancient mudrocks. *American Journal of Science*, *298*(7), 537–552. doi:10.2475/ajs.298.7.537

Wilkin, R. T., Barnes, H. L., & Brantley, S. L. (1996). The size distribution of framboidal pyrite in modern sediments: An indicator of redox conditions. *Geochimica et Cosmochimica Acta*, *60*(20), 3897–3912. doi:10.1016/0016-7037(96)00209-8

Xu, G., Hannah, J. L., Bingen, B., Georgiev, S., & Stein, H. J. (2012). Digestion methods for trace element measurements in shales: Paleoredox proxies examined. *Chemical Geology*, *324-325*, 132–147. doi:10.1016/j.chemgeo.2012.01.029

Zheng, Y., Anderson, R. F., van Geen, A., & Fleisher, M. Q. (2002). Remobilization of authigenic uranium in marine sediments by bioturbation. *Geochimica et Cosmochimica Acta*, *66*(10), 1759–1772. doi:10.1016/S0016-7037(01)00886-9

APPENDIX I

Table 7. *Major and trace element chemical analysis results.*

Analyte Symbol		Li	Na	Mg	Al	K	Ca	Cd	V	Cr	Mn	Fe	Hf	Hg	Ni	Er	Be
Unit Symbol		ppm	%	%	%	%	%	ppm	ppm	ppm	ppm	%	ppm	ppb	ppm	ppm	ppm
Detection Limit		0.5	0.01	0.01	0.01	0.01	0.01	0.1	1	0.5	1	0.01	0.1	10	0.5	0.1	0.1
Analysis Method	Depth (m)	TD-MS	TD-MS	TD-MS	TD-MS	TD-MS	TD-MS	TD-MS	TD-MS	TD-MS	TD-MS	TD-MS	TD-MS	TD-MS	TD-MS	TD-MS	TD-MS
BIRI-40	0	68.4	1.48	2.02	9.07	4.48	0.33	< 0.1	68	25.7	241	4.26	4.9	< 10	23.7	2.4	5.6
BIRI-41	0.22	63.1	0.27	7.54	1.74	0.15	22.3	< 0.1	26	13.2	2830	1.93	0.4	< 10	12.3	2.3	0.9
BIRI-42	0.37	91.9	0.19	7.03	2.16	0.12	22	< 0.1	31	14.5	2640	2.56	0.7	< 10	13.4	2.3	1
BIRI-43	0.97	42.2	1.59	1.35	9.3	3.76	4.13	0.3	128	37	706	4.36	3	< 10	29	4.5	4.8
BIRI-44	1.21	33	1.13	1.07	7.27	2.13	6.94	0.2	99	27.9	565	3.63	2.2	< 10	24.7	3.6	3.4
BIRI-45	1.87	32.5	1.57	0.99	7.05	2.15	1.88	< 0.1	84	35.9	388	3.52	2.3	< 10	24.5	3	3.8
BIRI-46A	2.47	36	1.44	1.03	7.76	1.32	5.26	0.1	85	60.9	713	3.8	2.6	< 10	25.5	3.8	3.7
BIRI-46B	2.47	37.7	1.35	1.05	7.81	1.96	7.37	< 0.1	86	29.6	858	3.83	2.6	< 10	26	4.4	3.6
BIRI-47	3.57	33.6	1.42	1.02	7.82	2.19	8.19	< 0.1	80	19	745	4.06	2.6	< 10	25.7	4.8	3.3
BIRI-48	4.47	38.8	1.49	0.94	7.18	2.89	10.6	< 0.1	97	33.2	642	3.8	2.5	< 10	26.7	3.8	3.1
BIRI-49	5.82	28.9	1.13	0.85	6.82	2.47	14.2	0.1	88	28.8	663	3.29	2.7	< 10	23.5	3.2	2.6
BIRI-50	7.32	17.1	0.88	0.68	4.91	1.97	18.9	< 0.1	79	25.6	466	2.36	1.4	< 10	21.9	2.5	2.1
BIRI-51	10.5	30.4	1.39	0.77	6.91	1.91	10.7	< 0.1	86	29.7	417	3.31	2.3	< 10	24.5	3.6	3.2
BIRI-52	12.4	26.1	1.11	0.55	4.61	1.39	19.9	< 0.1	47	18.7	490	2.54	1.5	< 10	19.6	2.8	2
BIRI-53	15.5	22.1	1.06	0.49	4.31	1.21	21.5	< 0.1	69	23.9	361	2.5	1.6	< 10	21.2	4.1	1.9
BIRI-54	21.5	32.3	1.58	0.63	6.28	1.78	14.3	< 0.1	93	25.6	268	3.11	2.1	< 10	24.8	3.6	2.7
BIRI-55	21.6	37.2	1.68	0.75	7.68	1.74	10.7	0.2	116	29	245	3.44	2.5	< 10	26.4	3.5	3.1
BIRI-56	25.4	13.6	0.78	0.32	3.12	0.92	6.36	< 0.1	41	15.5	150	1.41	1	< 10	11.3	1.5	1.1
BIRI-57	25.4	26.1	1.52	0.65	6.21	1.74	15	< 0.1	80	30.9	317	2.81	2.1	< 10	23.9	3.3	2.6
BIRI-58	25.5	33.3	1.53	0.77	6.4	1.87	14.1	< 0.1	84	32.4	361	3.15	2.4	< 10	23.1	3.5	2.8
BIRI-59	25.6	39	1.34	0.84	5.88	1.68	15.9	0.1	75	29.1	458	3.64	2.3	< 10	27.3	3.7	2.9
BIRI-60	25.8	21.6	1.35	0.75	5.76	2.12	12.8	< 0.1	87	31.9	521	3.12	2.5	< 10	26.9	2.3	3.2
BIRI-61	30	25.3	1.83	0.62	6.19	1.41	13.7	< 0.1	87	32	313	2.9	2	< 10	33.3	3.1	2.5
BIRI-62A	34.6	25.7	1.98	0.65	7.28	1.67	9.68	< 0.1	92	30.5	264	3.06	2.2	< 10	25.2	3.4	3.2
BIRI-62B	34.6	33.7	1.48	0.65	5.02	1.14	16.9	0.1	60	18	301	2.96	1.6	< 10	21.2	3.8	2.1
BIRI-62C	34.6	26.1	2.17	0.66	7.99	1.94	8.24	< 0.1	96	29.9	248	3.19	2.4	< 10	25.2	3.1	3.2
BIRI-63	36.2	27.5	1.68	0.68	5.98	1.59	16.2	0.1	81	25.2	307	2.8	2.3	< 10	22.2	3.6	2.7
BIRI-64	36.4	36.3	1.82	0.75	6.26	1.57	14	< 0.1	85	33.4	283	3.19	2.3	< 10	22.7	3.8	2.6
BIRI-65	36.5	30.5	1.99	0.74	7.28	2.08	9.92	0.1	99	31.6	275	3.39	3	< 10	23.9	3.3	3.4
BIRI-66	47.2	32.4	1.93	0.8	7.12	2.03	11.8	< 0.1	92	29.5	302	3.37	2.6	< 10	24.4	2.5	3.5
BIRI-67	47.2	27.4	1.79	0.72	6.66	1.92	13	< 0.1	85	57.5	296	3.15	2.6	< 10	25.8	2.7	3.2

Ho	Ag	Cs	Co	Eu	Bi	Se	Zn	Ga	As	Rb	Y	Sr	Zr	Nb	Mo	In	Sn	Sb
ppm	ppm	ppm	ppm	ppm	ppm	ppm	ppm	ppm	ppm	ppm	ppm	ppm	ppm	ppm	ppm	ppm	ppm	ppm
0.1	0.05	0.05	0.1	0.05	0.02	0.1	0.2	0.1	0.1	0.2	0.1	0.2	1	0.1	0.1	0.1	1	0.1
TD-MS	TD-MS	TD-MS	TD-MS	TD-MS	TD-MS	TD-MS	TD-MS	TD-MS	TD-MS	TD-MS	TD-MS	TD-MS	TD-MS	TD-MS	TD-MS	TD-MS	TD-MS	TD-MS
0.8	0.71	6.14	14	1.18	0.35	< 0.1	64	27.9	9.1	227	19.7	82	171	27	1.1	< 0.1	3	8.8
0.9	0.13	0.25	3.6	1.39	0.11	< 0.1	40.9	4.7	5.6	8.5	31.9	302	30	4.1	1	< 0.1	< 1	3
0.9	0.15	0.23	4.3	0.93	0.12	< 0.1	48.2	6	7.6	6.3	27.2	375	27	4.6	1.6	< 0.1	< 1	1.1
1.6	0.47	5.5	19	2.1	0.43	0.9	177	25.5	25.3	206	39.1	187	103	17.1	6.4	< 0.1	3	2.2
1.3	0.4	3.74	12.1	1.88	0.36	0.4	103	19.8	19.9	145	31.1	364	74	13.2	5.2	< 0.1	2	0.9
1.1	0.41	4.34	15.7	1.28	0.38	< 0.1	104	21.7	16.7	138	23.5	138	80	15.9	4	< 0.1	3	0.8
1.4	0.42	4.32	16	1.73	0.4	< 0.1	111	21.7	19	111	34.2	254	84	15.1	3.3	< 0.1	3	0.9
1.6	0.4	4.15	15.2	1.99	0.38	0.6	114	20.8	19.8	138	40.1	342	86	14.9	3.1	< 0.1	2	0.8
1.7	0.4	3.49	15.7	1.93	0.39	0.5	91.8	20.9	16.9	144	41.5	358	87	15.6	2.4	< 0.1	2	0.8
1.4	0.37	3.24	14.3	1.63	0.37	0.7	95.7	18.9	25	141	33.1	491	86	13.5	6	< 0.1	2	0.6
1.1	0.51	2.34	12.1	1.53	0.38	0.1	107	17.8	18.1	139	27.1	670	93	18.6	6.4	< 0.1	2	0.7
0.9	0.28	2.53	8.6	0.93	0.3	0.5	62.7	12.3	17.2	106	21.3	545	47	8.7	7.3	< 0.1	1	0.4
1.3	0.42	2.57	14.6	1.45	0.33	0.3	81.9	18.1	18.1	117	30.3	417	74	13.5	4.8	< 0.1	2	0.6
1	0.24	1.28	9.2	1.4	0.22	< 0.1	73.6	11.3	10.5	73.7	24.8	874	50	8.9	1.7	< 0.1	1	0.3
1.5	0.33	1.47	9.4	1.58	0.24	0.7	68.8	10.9	14.7	67.6	39.5	> 1000	54	9.1	4.8	< 0.1	1	0.5
1.3	0.35	1.94	13.6	1.48	0.32	0.4	92.4	16.8	16.6	97.1	32	812	67	12.1	6.4	< 0.1	2	0.7
1.3	0.66	2.34	15.6	1.44	0.38	0.7	118	20.2	21.6	106	29.7	561	76	14.3	8.5	< 0.1	2	0.6
0.5	0.19	0.9	7.3	0.56	0.16	< 0.1	40.5	8.1	7.3	48.3	13.8	374	33	5.6	2.5	< 0.1	< 1	0.3
1.2	0.32	1.83	17.4	1.3	0.32	0.5	81.9	15.9	16	95.2	29.5	898	66	11.4	4.6	< 0.1	2	0.5
1.2	0.35	1.89	13.9	1.39	0.47	0.4	110	16.6	15.5	99.5	30.1	841	76	12.7	4.8	< 0.1	2	0.5
1.3	0.33	1.69	12.9	1.6	0.33	0.6	123	15.5	13.2	90.9	32.6	895	73	12.7	4.5	< 0.1	2	0.5
0.8	0.48	2.16	16	0.85	0.35	< 0.1	92.6	18.1	18.3	111	23	756	84	14.7	6	< 0.1	2	0.7
1.1	0.32	1.78	14.5	1.05	0.35	0.3	76.4	15.5	15.3	78.9	26.2	840	62	11.4	5.3	< 0.1	2	0.6
1.2	0.34	2.24	18.2	1.35	0.38	0.3	95.4	19.2	16.9	99.1	28.7	638	69	12.6	5.1	< 0.1	2	0.5
1.4	0.23	1.27	9.8	1.92	0.27	0.3	129	11.1	11.3	62.1	33.2	> 1000	49	8.6	3.4	< 0.1	1	0.3
1.1	0.38	2.4	18.3	1.28	0.41	0.4	84.4	19.6	18.2	111	25.8	569	72	13.5	5.6	< 0.1	2	0.5
1.3	0.34	1.51	12.4	1.48	0.31	0.3	99.8	14.3	14.9	85.5	32.1	940	74	12.3	4.3	< 0.1	2	0.5
1.4	0.35	1.56	12.9	1.49	0.32	0.6	83.7	15.2	14.7	83.7	32.5	863	75	13	4.9	< 0.1	2	0.5
1.2	0.45	1.97	17	1.13	0.4	0.1	96.1	19.7	17.6	111	26.9	636	89	16.7	6.3	< 0.1	2	0.6
0.9	0.41	2.02	16	0.91	0.38	< 0.1	81	18.4	17.7	106	22.2	706	79	14.3	5.3	< 0.1	2	0.6
0.9	0.37	1.9	15.5	1	0.36	< 0.1	95.6	17.4	15.5	101	23.8	803	81	13.1	5.1	< 0.1	2	0.6

Te	Ba	La	Ce	Pr	Nd	Sm	Gd	Tb	Dy	Cu	Ge	Tm	Yb	Lu	Ta	W	Re	Tl
ppm	ppm	ppm	ppm	ppm	ppm	ppm	ppm	ppm	ppm	ppm	ppm	ppm	ppm	ppm	ppm	ppm	ppm	ppm
0.1	1	0.1	0.1	0.1	0.1	0.1	0.1	0.1	0.1	0.2	0.1	0.1	0.1	0.1	0.1	0.1	0.001	0.05
TD-MS	TD-MS	TD-MS	TD-MS	TD-MS	TD-MS	TD-MS	TD-MS	TD-MS	TD-MS	TD-MS	TD-MS	TD-MS	TD-MS	TD-MS	TD-MS	TD-MS	TD-MS	TD-MS
< 0.1	94	105	179	22.7	71.6	9.2	6.4	0.7	4	26	0.4	0.4	2.3	0.4	1.4	0.8	< 0.001	1.52
< 0.1	43	24.6	53.3	7.1	28.3	5.6	5.9	0.9	5	9.3	0.2	0.3	1.3	0.2	0.1	0.3	< 0.001	0.09
< 0.1	36	27.1	56	5.9	20.8	3.9	4.1	0.7	4.1	10.9	0.1	0.3	1.5	0.2	0.2	0.2	< 0.001	0.08
< 0.1	110	91	180	22.3	79.5	13.5	11.2	1.5	8.6	40.6	0.3	0.7	3.9	0.6	1	0.8	0.001	1.87
< 0.1	247	94.8	183	22.4	77.3	12.3	9.6	1.3	7	31.3	0.3	0.5	3	0.5	0.7	0.7	< 0.001	1.75
< 0.1	552	66.1	136	16.2	56.1	9.2	7.1	1	5.4	32.4	0.3	0.5	2.8	0.4	1	0.7	< 0.001	1.87
< 0.1	99	75.3	141	18	62.6	10.3	8.6	1.2	7	33.8	0.2	0.6	3.2	0.5	0.9	0.6	< 0.001	2.1
< 0.1	171	81.8	156	20.1	70.4	11.8	10	1.4	8.3	33.9	0.3	0.6	3.6	0.6	0.9	0.6	< 0.001	2.21
< 0.1	130	83.1	165	20.3	72.1	12.3	10.5	1.5	8.9	30.9	0.3	0.7	3.8	0.6	0.9	0.5	< 0.001	2.21
< 0.1	151	73.9	146	18	63.3	10.6	8.9	1.2	7.2	33.7	0.3	0.5	3.2	0.5	0.8	0.5	< 0.001	2.13
< 0.1	182	68.9	134	16.1	55.4	9	7.4	1	5.6	28	0.3	0.5	2.7	0.4	1.1	0.4	< 0.001	2.07
< 0.1	192	49.1	95	11.7	40.8	6.7	5.4	0.8	4.6	24	0.2	0.4	2.1	0.3	0.5	0.4	< 0.001	1.68
< 0.1	144	75	145	18	62.6	10.2	8.6	1.2	6.6	28.5	0.2	0.5	3	0.5	0.8	0.4	< 0.001	1.95
< 0.1	286	57.9	111	13.9	48.4	7.7	6.3	0.9	5.2	16.8	0.2	0.4	2.2	0.3	0.6	0.3	< 0.001	0.93
< 0.1	297	56.3	123	13.6	49.5	9	8.5	1.3	7.5	19.9	0.2	0.6	3.3	0.5	0.5	0.5	< 0.001	0.87
< 0.1	179	66.8	128	15.9	55.9	9.4	8.1	1.2	6.7	28.3	0.2	0.5	2.9	0.5	0.7	0.6	< 0.001	0.97
< 0.1	160	78.3	150	18.7	65.6	10.6	8.5	1.2	6.7	36.4	0.2	0.5	3	0.5	0.8	0.6	< 0.001	1.16
< 0.1	114	30.3	58.2	6.9	24	3.8	3.2	0.5	2.7	13.2	< 0.1	0.2	1.3	0.2	0.3	0.1	< 0.001	0.46
< 0.1	251	64.3	126	15.7	55	9	7.2	1	6.2	34.9	0.2	0.5	2.7	0.4	0.7	0.8	< 0.001	0.87
< 0.1	257	68.8	132	16.3	56.5	9.3	7.6	1.1	6.4	27.6	0.2	0.5	2.9	0.5	0.8	0.6	< 0.001	0.93
< 0.1	210	73	138	17.4	61.2	10.1	8.3	1.2	6.9	23.2	0.2	0.5	3.1	0.5	0.8	0.5	< 0.001	0.83
< 0.1	290	58.3	94.6	12.2	38.9	5.7	4.9	0.7	4	31.9	0.2	0.4	2	0.3	1	0.7	< 0.001	1.01
< 0.1	249	58.2	106	13	44.8	7.3	6.2	0.9	5.4	26.2	0.2	0.5	2.7	0.4	1	0.6	< 0.001	0.88
< 0.1	166	71.6	133	15.9	54.6	9.1	7.8	1.1	6.4	29.9	0.2	0.5	2.8	0.4	0.7	0.5	< 0.001	1.02
< 0.1	249	60.2	128	16.6	62.7	11.5	9.6	1.4	7.7	18.6	0.2	0.5	3	0.5	0.6	0.3	< 0.001	0.61
< 0.1	239	78.9	140	16.6	55.1	8.9	7.7	1.1	5.9	32.4	0.2	0.4	2.7	0.4	0.8	0.6	< 0.001	1.08
< 0.1	313	66.7	129	16.3	58.2	10.1	8.2	1.2	6.8	26.9	0.2	0.5	3	0.5	0.8	0.4	< 0.001	0.78
< 0.1	320	67.7	126	16	56.9	9.8	8.5	1.2	7.2	25.3	0.2	0.5	3.1	0.5	0.8	0.5	< 0.001	0.8
< 0.1	141	75.4	133	16.4	54.4	8.9	7.3	1.1	6.2	33.4	0.2	0.5	2.8	0.4	1	0.6	< 0.001	1
< 0.1	236	59.9	99.1	12.9	42.7	6.3	5.3	0.7	4.5	31.8	0.1	0.4	2.2	0.3	1	0.6	< 0.001	0.98
< 0.1	172	59.8	103	13.2	44.3	6.8	5.6	0.8	4.9	30	0.1	0.4	2.4	0.4	1	0.8	0.002	0.9

Pb	Sc	Th	U	Ti	P	S
ppm	ppm	ppm	ppm	%	%	%
0.5	1	0.1	0.1	0.0005	0.001	0.01
TD-MS	TD-ICP	TD-MS	TD-MS	TD-ICP	TD-ICP	TD-ICP
78.2	13	23.9	6.4	0.544	0.101	2.8
22.9	3	4.5	1.7	0.0625	0.209	0.58
27.5	3	5.8	1.9	0.0774	0.053	0.72
91.1	15	21.4	8.7	0.376	0.052	3.02
49.4	12	19.4	7.3	0.278	0.041	2.56
29.2	14	18.6	6.3	0.325	0.05	2.76
29.1	14	18.8	6.5	0.331	0.051	2.77
27.9	13	19.1	6.7	0.307	0.049	2.59
29.1	12	19.3	6.7	0.312	0.051	2.99
26.7	12	18.4	7.8	0.292	0.043	2.61
23.6	10	17.8	16	0.246	0.043	2.42
18	8	13.1	7.8	0.193	0.034	1.96
24.3	11	17.3	7.3	0.279	0.042	2.53
15.6	7	12.8	5.4	0.181	0.033	1.79
17.2	9	12.5	6.5	0.176	0.058	1.9
23.6	10	17	6.4	0.248	0.037	2.26
27.9	12	20.1	7.3	0.308	0.041	2.45
11.3	10	8.1	2.7	0.279	0.037	2.3
22.5	10	16.7	6.5	0.246	0.034	2.09
24.5	10	17.5	6.3	0.28	0.041	2.24
20.9	9	17.2	7	0.258	0.043	2.55
25.3	7	17.8	5.4	0.27	0.038	2.18
23.2	9	16.6	6.4	0.234	0.035	2.12
26.2	12	18.4	6.5	0.276	0.034	2.33
16.8	8	13	6	0.181	0.034	1.81
30	11	21	7.1	0.297	0.037	2.56
21.7	10	16.4	6	0.252	0.041	1.8
22.6	10	17.9	7.2	0.253	0.061	1.9
29.1	11	20.5	7.2	0.309	0.041	2.65
26.7	9	19.8	5.7	0.301	0.04	2.45
24.3	9	18.4	5.5	0.284	0.04	2.37

Table 8. *XRF data and calculated concentrations of select major and trace elements in the non-carbonate fraction. Fe and S (wt %), TEs (ppm).*

Sample	Evolved gases [%]	Calculated Co3 [wt%]	CO_3 + Ca + Mg	% non-carbonate fraction	Fe	S	Mo	U	Mn	V	Cr	Se	Ba	Cd	Ag	Co	Zn	Pb	Ni	Cu
BIRI-40	6.15	8.36	11.18	0.89	4.80	3.2	1.2	7.2	271	76.6	28.9	0.00	105.8	0.00	0.80	15.8	72.1	88.0	26.7	29.3
BIRI-41	34.90	47.46	76.61	0.23	8.25	2.5	4.3	7.3	12099	111.2	56.4	0.00	183.8	0.00	0.56	15.4	174.9	97.9	52.6	39.8
BIRI-42	33.30	45.29	73.66	0.26	9.72	2.7	6.1	7.2	10023	117.7	55.0	0.00	136.7	0.00	0.57	16.3	183.0	104.4	50.9	41.4
BIRI-43	8.89	12.09	18.95	0.81	5.38	3.7	7.9	10.7	871	157.9	45.7	1.11	135.7	0.37	0.58	23.4	218.4	112.4	35.8	50.1
BIRI-44	10.10	13.74	22.63	0.77	4.69	3.3	6.7	9.4	730	128.0	36.1	0.52	319.2	0.26	0.52	15.6	133.1	63.8	31.9	40.5
BIRI-45	6.59	8.96	12.76	0.87	4.04	3.2	4.6	7.2	445	96.3	41.2	0.00	632.8	0.00	0.47	18.0	119.2	33.5	28.1	37.1
BIRI-46A	7.53	10.24	15.64	0.84	4.50	3.3	3.9	7.7	845	100.8	72.2	0.00	117.4	0.12	0.50	19.0	131.6	34.5	30.2	40.1
BIRI-46B	9.13	12.42	19.29	0.81	4.75	3.2	3.8	8.3	1063	106.6	36.7	0.74	211.9	0.00	0.50	18.8	141.2	34.6	32.2	42.0
BIRI-47	7.56	10.28	16.59	0.83	4.87	3.6	2.9	8.0	893	95.9	22.8	0.60	155.9	0.00	0.48	18.8	110.1	34.9	30.8	37.0
BIRI-48	12.50	17.00	27.10	0.73	5.21	3.6	8.2	10.7	881	133.1	45.5	0.96	207.1	0.00	0.51	19.6	131.3	36.6	36.6	46.2
BIRI-49	14.00	19.04	31.72	0.68	4.82	3.5	9.4	23.4	971	128.9	42.2	0.15	266.5	0.15	0.75	17.7	156.7	34.6	34.4	41.0
BIRI-50	23.60	32.10	53.18	0.47	5.04	4.2	15.6	16.7	995	168.7	54.7	1.07	410.0	0.00	0.60	18.4	133.9	38.4	46.8	51.3
BIRI-51	9.80	13.33	21.49	0.79	4.22	3.2	6.1	9.3	531	109.5	37.8	0.38	183.4	0.00	0.53	18.6	104.3	31.0	31.2	36.3
BIRI-52	18.40	25.02	41.93	0.58	4.37	3.1	2.9	9.3	844	80.9	32.2	0.00	492.5	0.00	0.41	15.8	126.7	26.9	33.8	28.9
BIRI-53	16.60	22.58	37.44	0.63	4.00	3.0	7.7	10.4	577	110.3	38.2	1.12	474.8	0.00	0.53	15.0	110.0	27.5	33.9	31.8
BIRI-54	13.30	18.09	28.75	0.71	4.36	3.2	9.0	9.0	376	130.5	35.9	0.56	251.2	0.00	0.49	19.1	129.7	33.1	34.8	39.7
BIRI-55	11.00	14.96	24.67	0.75	4.57	3.3	11.3	9.7	325	154.0	38.5	0.93	212.4	0.27	0.88	20.7	156.6	37.0	35.0	48.3
BIRI-56	16.90	22.98	37.69	0.62	2.26	3.7	4.0	4.3	241	65.8	24.9	0.00	183.0	0.00	0.30	11.7	65.0	18.1	18.1	21.2
BIRI-57	11.00	14.96	23.59	0.76	3.68	2.7	6.0	8.5	415	104.7	40.4	0.65	328.5	0.00	0.42	22.8	107.2	29.4	31.3	45.7
BIRI-58	13.00	17.68	29.60	0.70	4.47	3.2	6.8	8.9	513	119.3	46.0	0.57	365.0	0.00	0.50	19.7	156.2	34.8	32.8	39.2
BIRI-59	16.90	22.98	38.18	0.62	5.89	4.1	7.3	11.3	741	121.3	47.1	0.97	339.7	0.16	0.53	20.9	199.0	33.8	44.2	37.5
BIRI-60	17.80	24.21	39.90	0.60	5.19	3.6	10.0	9.0	867	144.8	53.1	0.00	482.6	0.00	0.80	26.6	154.1	42.1	44.8	53.1
BIRI-61	18.40	25.02	41.59	0.58	4.96	3.6	9.1	11.0	536	148.9	54.8	0.51	426.3	0.00	0.55	24.8	130.8	39.7	57.0	44.9
BIRI-62A	9.86	13.41	22.08	0.78	3.93	3.0	6.5	8.3	339	118.1	39.1	0.39	213.1	0.00	0.44	23.4	122.4	33.6	32.3	38.4
BIRI-62B	13.40	18.22	29.82	0.70	4.22	2.6	4.8	8.5	429	85.5	25.6	0.43	354.8	0.14	0.33	14.0	183.8	23.9	30.2	26.5
BIRI-62C	13.20	17.95	28.49	0.72	4.46	3.6	7.8	9.9	347	134.2	41.8	0.56	334.2	0.00	0.53	25.6	118.0	42.0	35.2	45.3
BIRI-63	10.50	14.28	23.16	0.77	3.64	2.3	5.6	7.8	400	105.4	32.8	0.39	407.4	0.13	0.44	16.1	129.9	28.2	28.9	35.0
BIRI-64	15.40	20.94	34.70	0.65	4.89	2.9	7.5	11.0	433	130.2	51.1	0.92	490.0	0.00	0.54	19.8	128.2	34.6	34.8	38.7
BIRI-65	14.00	19.04	31.94	0.68	4.98	3.9	9.3	10.6	404	145.5	46.4	0.15	207.2	0.15	0.66	25.0	141.2	42.8	35.1	49.1
BIRI-66	13.00	17.68	28.95	0.71	4.74	3.4	7.5	8.0	425	129.5	41.5	0.00	332.2	0.00	0.58	22.5	114.0	37.6	34.3	44.8
BIRI-67	13.70	18.63	31.29	0.69	4.58	3.4	7.4	8.0	431	123.7	83.7	0.00	250.3	0.00	0.54	22.6	139.1	35.4	37.5	43.7

APPENDIX II

Table 9. *Source Rock Analysis Results*

		Percent	Leco	Rock-Eval	Rock-Eval	Rock-Eval	Tmax	Hydrogen	Oxygen	S2/S3	S1/TOC	Production
		Carbonate	TOC	S1	S2	S3		Index	Index	Conc.	Norm. Oil	Index
Sample	Depth (m)	(wt%)	(wt% HC)	(mg HC/g)	(mg HC/g)	(mg CO2/g)	(°C)	(S2x100/TOC)	(S3x100/TOC)	(mg HC/mg CO2)	Content	(S1/(S1+S2)
BIRI-40	0	1.92	0.22	0.03	0.01	0.07	0	4	31	0	13	0.75
BIRI-41	0.22	77.04	0.48	0.02	0.02	0.51	0	4	107	0	4	0.50
BIRI-42	0.37	68.26	0.46	0.01	0.01	0.29	0	2	63	0	2	0.50
BIRI-43	0.97	9.59	1.04	0.08	0.01	0.23	0	1	22	0	8	0.89
BIRI-44	1.21	17.17	0.75	0.03	0.02	0.04	0	3	5	1	4	0.60
BIRI-45	1.87	5.69	0.51	0.02	0.01	0.02	0	2	4	1	4	0.67
BIRI-46A	2.47	14.95	0.72	0.02	0.01	0.08	0	1	11	0	3	0.67
BIRI-46B	2.47	18.14	0.70	0.07	0.03	0.06	0	4	9	1	10	0.70
BIRI-47	3.57	21.31	0.61	0.04	0.01	0.13	0	2	21	0	7	0.80
BIRI-48	4.47	26.83	0.83	0.04	0.02	0.16	0	2	19	0	5	0.67
BIRI-49	5.82	32.83	0.78	0.05	0.01	0.05	0	1	6	0	6	0.83
BIRI-50	7.32	46.71	0.72	0.08	0.01	0.04	0	1	6	0	11	0.89
BIRI-51	10.52	27.38	0.68	0.07	0.02	0.04	0	3	6	1	10	0.78
BIRI-52	12.42	51.66	0.34	0.05	0.03	0.05	0	9	15	1	15	0.63
BIRI-53	15.48	55.42	0.51	0.09	0.01	0.10	0	2	20	0	18	0.90
BIRI-54	21.48	33.27	0.71	0.10	0.02	0.05	0	3	7	0	14	0.83
BIRI-55	21.58	27.50	0.83	0.08	0.01	0.04	0	1	5	0	10	0.89
BIRI-56	25.38	32.84	0.80	0.04	0.03	0.07	0	4	9	0	5	0.57
BIRI-57	25.4	37.21	0.64	0.03	0.01	0.26	0	2	41	0	5	0.75
BIRI-58	25.45	35.89	0.78	0.06	0.01	0.19	0	1	24	0	8	0.86
BIRI-59	25.6	37.49	0.69	0.04	0.02	0.11	0	3	16	0	6	0.67
BIRI-60	25.78	33.97	0.80	0.07	0.01	0.03	0	1	4	0	9	0.88
BIRI-61	29.98	34.47	0.75	0.05	0.03	0.04	0	4	5	1	7	0.63
BIRI-62A	34.58	24.19	0.70	0.07	0.04	0.13	0	6	19	0	10	0.64
BIRI-62B	34.58	42.07	0.42	0.05	0.01	0.23	0	2	55	0	12	0.83
BIRI-62C	34.58	18.76	0.80	0.11	0.02	0.22	0	3	28	0	14	0.85
BIRI-63	36.18	39.09	0.66	0.08	0.01	0.06	0	2	9	0	12	0.89
BIRI-64	36.35	33.07	0.67	0.07	0.03	0.12	0	4	18	0	10	0.70
BIRI-65	36.52	24.39	0.83	0.05	0.02	0.12	0	2	14	0	6	0.71
BIRI-66	47.22	28.90	0.80	0.05	0.01	0.07	0	1	9	0	6	0.83
BIRI-67	47.24	31.47	0.80	0.05	0.02	0.04	0	2	5	1	6	0.71

Table 10. *Sulphur-34 Analysis Results of Untreated Sample. Duplicate analysis results shown in* ***BOLD****. Method: EA-IRMS*

Sample	*Elemental S	Result $\delta^{34}S_{V\text{-}CDT}$	Mean $\delta^{34}S_{V\text{-}CDT}$
	(%)	**(‰)**	**(‰)**
40	**2.64**	**9.72**	
"	**2.73**	**9.45**	**9.58**
41	0.49	-18.33	
42	0.33	-20.14	
43	**2.73**	**-20.22**	
"	**2.95**	**-20.15**	**-20.18**
44	2.61	-15.73	
45	2.89	-17.20	
46A	2.69	-17.48	
46B	2.42	-17.52	
47	**2.89**	**-13.29**	
"	**2.86**	**-13.38**	**-13.33**
48	2.50	-16.56	
49	2.09	-16.40	
50	1.39	-14.71	
51	1.92	-15.43	
52	**1.49**	**-8.33**	
"	**1.04**	**-8.41**	**-8.37**
53	1.20	-13.78	
54	2.35	-16.74	
55	2.68	-19.64	
56	2.47	-19.39	
57	**2.30**	**-19.60**	
"	**2.39**	**-19.77**	**-19.68**
58	2.53	-19.10	
59	**2.50**	**-4.19**	
"	**2.46**	**-4.69**	
60	2.11	-19.91	
61	2.49	-18.37	
62A	**2.60**	**-21.80**	
"	**2.17**	**-21.39**	**-21.60**
62B	1.92	-8.84	
62C	2.88	-21.24	
63	1.40	-20.97	
64	1.99	-15.93	
65	**2.44**	**-20.16**	
"	**2.58**	**-20.46**	**-20.31**
66	2.64	-19.69	
67	2.55	-16.48	

*Not acid washed, measured untreated.

Table 11. Carbon-13 Analysis Results of Carbonate Free Fraction (acid washed). Method: EA-IRMS

Sample	*Elemental Carbon	Result $\delta^{13}C_{V\text{-}PDB}$	Mean $\delta^{13}C_{V\text{-}PDB}$
	(%)	**(‰)**	**(‰)**
40	0.2	-30.52	
41	2.1	-33.51	
42	**1.5**	**-32.84**	
"	**1.6**	**-32.53**	**-32.68**
43	1.1	-32.52	
44	0.9	-32.82	
45	0.6	-32.60	
46A	0.9	-32.37	
46B	**0.9**	**-32.69**	
"	**0.9**	**-32.71**	**-32.70**
47	0.8	-32.93	
48	1.3	-32.63	
49	1.2	-33.06	
50	1.4	-33.67	
51	**1.0**	**-32.48**	
"	**1.0**	**-32.70**	**-32.59**
52	0.8	-31.57	
53	1.3	-31.62	
54	1.1	-32.61	
55	1.2	-32.77	
56	**1.2**	**-32.42**	
"	**1.3**	**-32.43**	**-32.42**
57	1.1	-32.55	
58	1.3	-32.24	
59	1.2	-32.33	
60	1.2	-32.75	
61	**1.3**	**-32.16**	
"	**1.2**	**-32.40**	**-32.28**
62A	1.0	-32.31	
62B	0.8	-30.98	
62C	1.1	-31.82	
63	1.2	-32.36	
64	**1.1**	**-32.36**	
"	**1.1**	**-32.35**	**-32.36**
65	1.1	-32.67	
66	1.2	-32.68	
67	1.2	-32.23	

*Acid washed to remove inorganic carbon (TOC will therefore be higher where significant carbonate was present).

Table 12. *Carbon-13 & Oxygen-18 Analysis of Inorganic Carbon (Carbonate). Method: Acid-CF-IRMS*

Sample	Result $\delta^{13}C_{V\text{-}PDB}$	Mean $\delta^{13}C_{V\text{-}PDB}$	Result $\delta^{18}O_{V\text{-}PDB}$	Mean $\delta^{18}O_{V\text{-}PDB}$
	(‰)	**(‰)**	**(‰)**	**(‰)**
40	-		-	
41	-9.81		-6.68	
42	-8.41		-9.61	
43	-1.98		-15.84	
44	**-1.53**		**-15.80**	
"	**-1.44**	**-1.48**	**-15.91**	**-15.85**
45	-0.97		-16.00	
46A	-0.95		-16.09	
46B	-1.02		-15.99	
47	-0.43		-15.17	
48	**-0.47**		**-15.79**	
"	**-0.46**	**-0.47**	**-15.80**	**-15.80**
49	-0.19		-15.60	
50	0.05		-14.89	
51	0.66		-14.58	
52	0.40		-13.82	
53	**0.22**		**-12.91**	
"	**0.21**	**0.21**	**-12.88**	**-12.89**
54	1.00		-12.49	
55	1.41		-12.65	
56	1.26		-12.65	
57	1.19		-12.45	
58	**1.00**		**-12.42**	
"	**1.03**	**1.02**	**-12.46**	**-12.44**
59	0.86		-12.44	
60	0.73		-12.45	
61	1.21		-12.32	
62A	1.41		-12.49	
62B	**0.96**		**-12.42**	
"	**0.97**	**0.96**	**-12.42**	**-12.42**
62C	1.47		-12.86	
63	1.01		-12.21	
64	1.22		-12.25	
65	1.44		-12.62	
66	**1.40**		**-12.30**	
"	**1.43**	**1.42**	**-12.20**	**-12.25**
67	**1.37**		**-12.21**	
"	**1.47**	**1.42**	**-12.16**	**-12.18**

Nb. No CO_2 was produced for sample 40 which indicates that it did not contain any carbonate

APPENDIX III

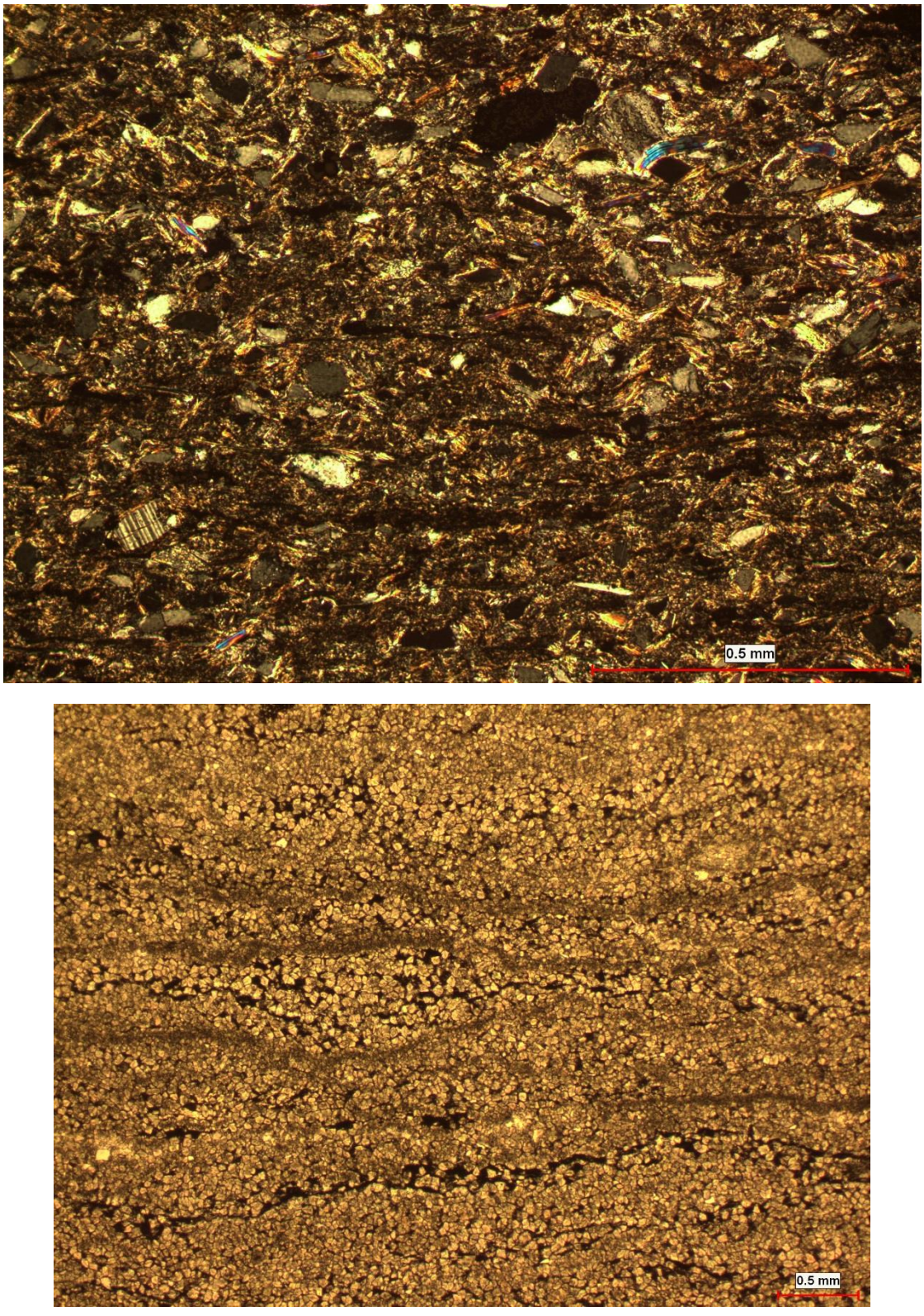

Figure 28. *Top: Sample 40 (0 m) siltstone with quartz, muscovite and potassiium feldspar, among other grains. Bottom: Sample 41 (0.22 m) dolomite with micro crystalline dolomite in darker bands.*

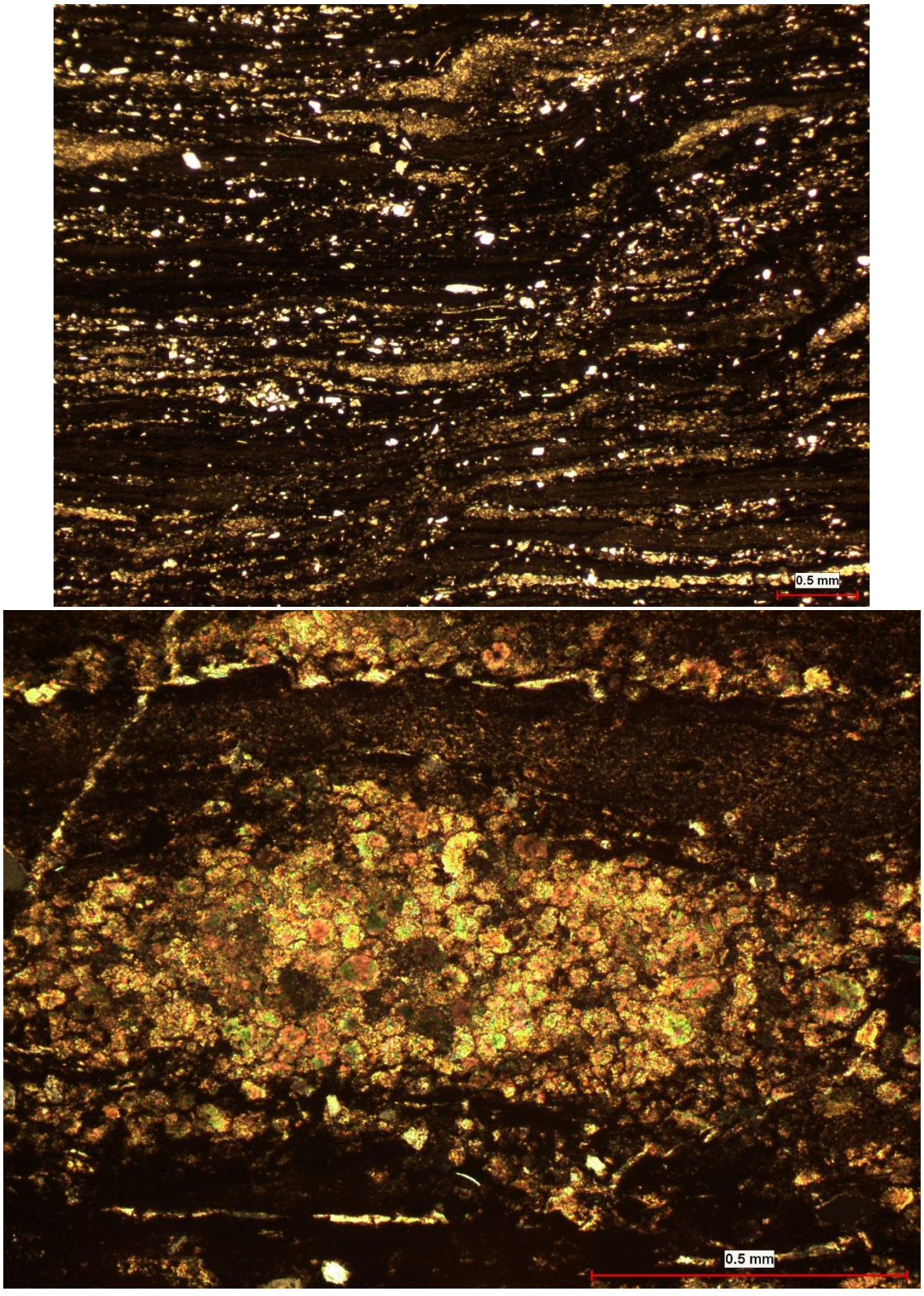

Figure 29. *Top: sample 43 (0.97 m). Bottom: sample 47 (3.57 m) showing round, radial calcite. This feature was also noted by Tucker (1983).*

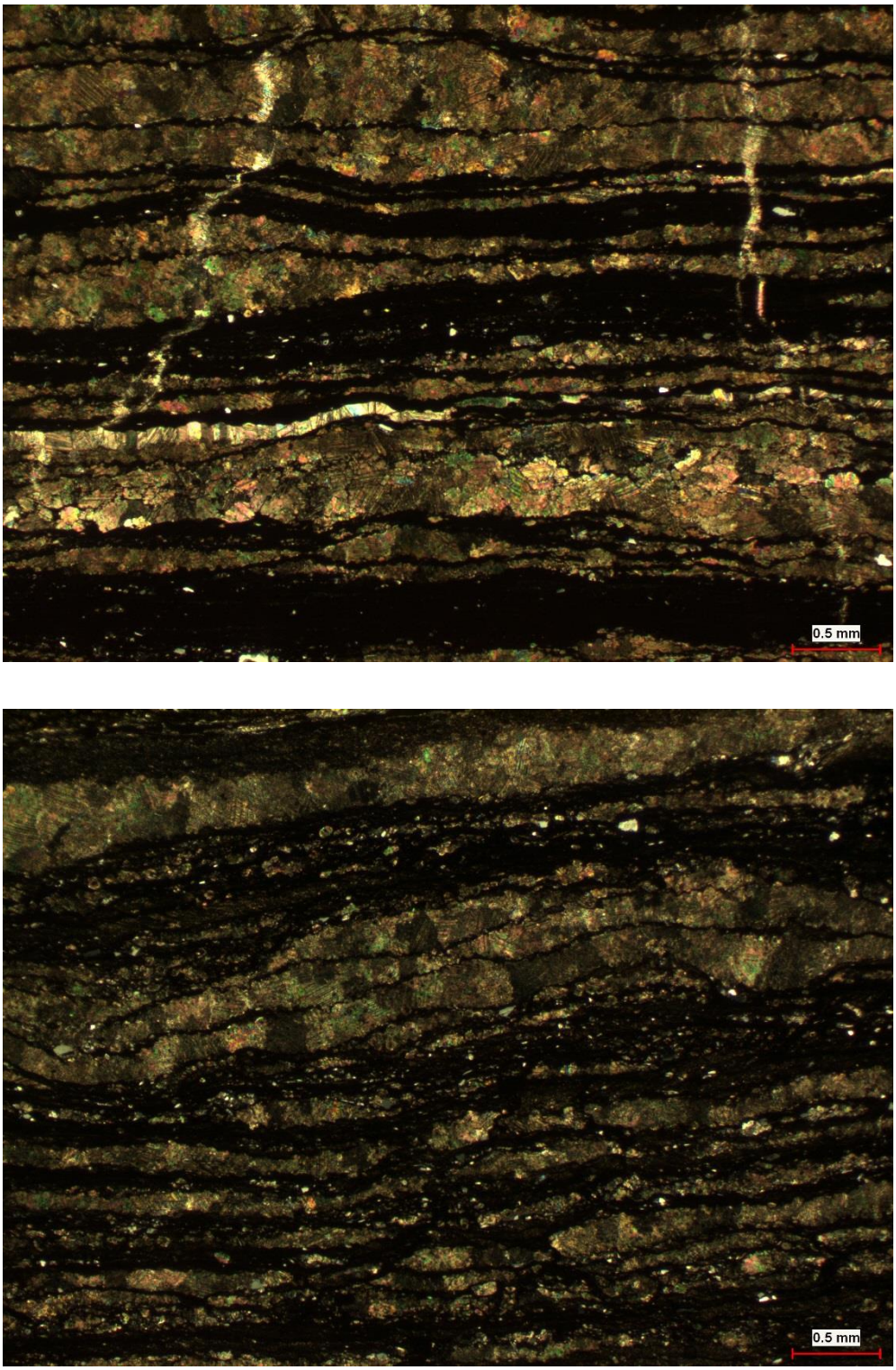

Figure 30. *Top: sample 50 (7.32 m). Bottom: sample 57 (25.4 m).*

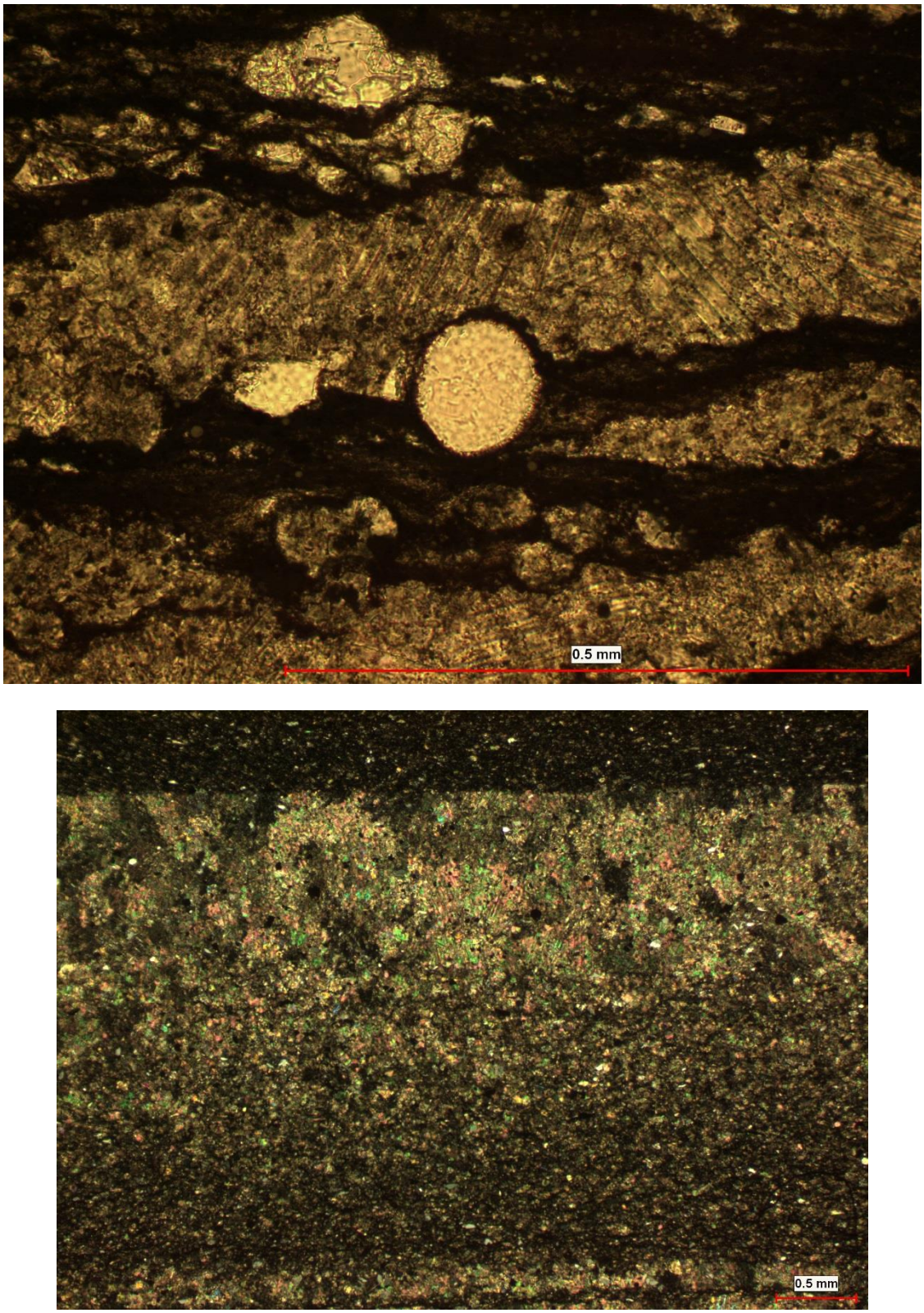

Figure 31. *Top: Sample 57 (25.4 m) - presumed Acritarch composed of calcium phosphate (EDS). Bottom: sample 62b (34.58 m)*

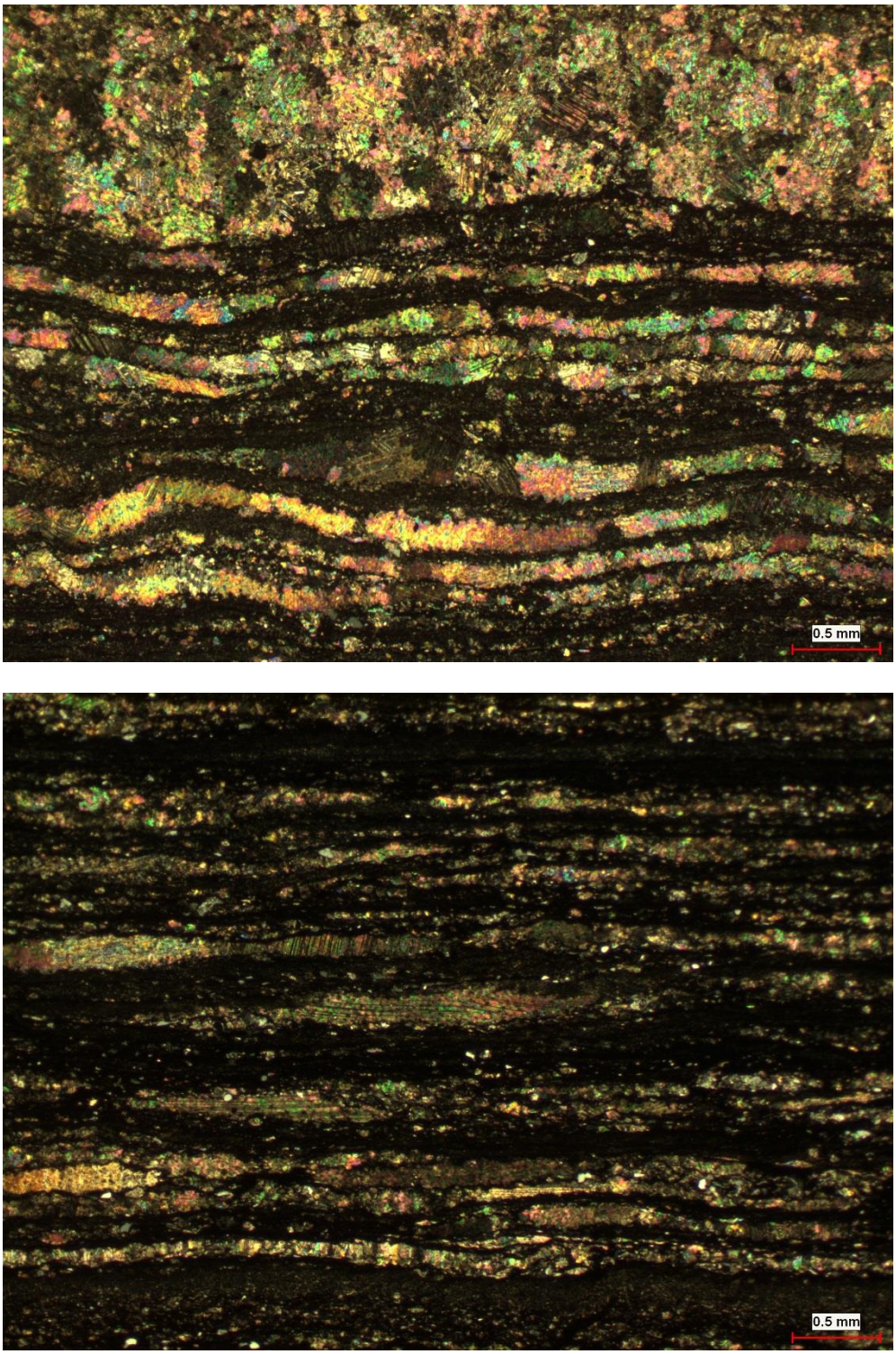

Figure 32. *Top: sample 62b (34.58 m). Bottom: sample 67 (47.24 m)*